STUDY OF OSCILLATING LIQUID FLOW AS A THERMAL MANAGEMENT SOLUTION

by

Bader Abdullah Al Nifay

BS, Mechanical Engineering, University of Pittsburgh, 2013

Submitted to the Graduate Faculty of

Swanson School of Engineering in partial fulfillment

of the requirements for the degree of

Master of Science

University of Pittsburgh

2015

UNIVERSITY OF PITTSBURGH

SWANSON SCHOOL OF ENGINEERING

This thesis was presented

by

Bader Abdullah Al Nifay

It was defended on

April 14, 2015

and approved by

Jeffrey S. Vipperman, Ph.D., Professor
Department Mechanical Engineering and Materials Science

Sung Kwon Cho, Ph.D., Associate Professor
Department Mechanical Engineering and Materials Science

Mark L. Kimber, Ph.D., Assistant Professor
Department Mechanical Engineering and Materials Science

Thesis Advisor: Mark L. Kimber, Ph.D., Assistant Professor
Department Mechanical Engineering and Materials Science

STUDY OF OSCILLATING LIQUID FLOW AS A THERMAL MANAGEMENT SOLUTION

Bader Abdullah Al Nifay, M.S.

University of Pittsburgh, 2015

For many electronic devices where air cooling is the norm, heat loads continue to increase and are projected to soon require a transition to liquid cooling, where more efficient thermal energy transport is achievable due to better fluid properties. In most scenarios, a liquid cooled solution entails a bulk fluid motion traveling past a heated surface, but flows that oscillate back and forth also show promise. However, before this is realized, some fundamental performance models must be extended. This paper focuses on characterizing the dynamics of the flow inside a U-tube manometer under continuous oscillation. For oscillating flow, the dimensionless parameter of interest is the Womersley number (W_0) or the Valensi number (V_a) (one can simply be expressed in terms of the other), and can be used to predict velocity profiles of oscillating flow. In this study, an air blower is utilized to force the fluid to move inside a U-tube manometer by providing an oscillating pressure signal. The dynamic response is the key metric of interest in this work, and is characterized by experimentally measuring the resonance frequency (ω_n) and the damping ratio (ζ), the latter of which is dependent on frictional losses. When the working fluid is under continuous oscillation, additional sources of frictional losses exist, and a non-standard analysis is needed to adequately predict the damping. The dynamic response is measured for different amounts of fluid in a range of tube sizes and empirical correlations are

developed to better predict the observed data. Results suggest that the velocity profiles under continuous oscillation are not parabolic and hence quantifying the damping based on the theoretical damped oscillation analysis is not applicable. The results of this study are conceptually applied to a microchannel heat sink, where oscillating flows show promise in handling large heat fluxes.

Keywords: Oscillating manometer, forced oscillation, damping ratio, thermal, internal flow

TABLE OF CONTENTS

LIST OF TABLES

LIST OF FIGURES

NOMENCLATURE

English

A	Cross section area of the tube
D	Diameter of the tube
D_h	Hydraulic Diameter of a cross section area
g	Gravitation force
h_c	Height of a microchannel heat sink
KC	Keulegan-Carpenter number
l_c	Length of a microchannel heat sink
L	Length of fluid inside the U-tube
n_c	Number of channels in microchannel heat sink
N	Number of oscillating cycles
P	Pressure
R	Radius of the tube
Re_D	Reynolds number
V_a	Valensi number
w_c	Width of a microchannel heat sink
W_0	Womersley number

$x_{fd,h}$	Hydrodynamic entry length
X	Magnitude of fluid displacement
X_1	Amplitude of fluid displacement for N = 1
X_{N+1}	Amplitude of fluid displacement of the following cycle N

Greek

δ	Logarithmic ratio between amplitudes
δ_{st}	Static displacement of fluid inside the U-tube manometer
ζ	Damping ratio
ν	Kinematic viscosity of the fluid
ρ	Density of the fluid
ω_o	Oscillating Frequency
ω_n	Natural Frequency

1.0 INTRODUCTION

Although both gases and liquids can be used as working fluids across a wide range of thermal management techniques, liquid cooling is far superior due much higher thermal conductivity and specific heat. For example, the specific heat and thermal conductivity of water are $4.181\,\frac{kJ}{kg\cdot K}$ and $0.606\,\frac{W}{m\cdot K}$, respectively, which are greater than the corresponding values for air ($1.007\,\frac{kJ}{kg\cdot K}$ and $0.0263\,\frac{W}{m\cdot K}$) [1].

In many applications where air cooling is the standard, heat loads continue to rise because of increased functionality and power dissipation. In the field of electronics cooling for example, thermal management solutions must continually become more creative with each new device generation due to an increase in processing power. For many devices, heat loads are projected to soon require a transition to liquid cooling in order to best exploit efficient thermal energy transport properties of the working fluid. Various liquid-based thermal management solutions exist (e.g., cold plates and microchannel heat sinks), but most of them employ bulk fluid transport to carry away the heat. Low profile cooling (e.g., processing unit in tablets and/or phones) can be particularly challenging from a thermal management perspective due to the tight restrictions on available volume. As the required parts decrease in size, the cost of the thermal solution typically increases. A compromise between efficiency and cost is sought in order to develop an adequate thermal management solution.

For many of these low profile devices, natural convection is the primary thermal management approach. As the forecasted heat loads would require a transition from natural to forced convection, investigators have offered multiple potential low power solutions, including piezoelectric fans [2-4], synthetic jets [5-6], and ionic winds [7-8], to name a few. In this work, a miniature piezoelectric pump, or air blower [9], is investigated as an additional potential solution. The pump produces relatively high pressure (~ 2 kPa) and low flow rates which make it an ideal candidate for microchannel heat sink applications [9], or any other low flow situation where relatively large pressure drops are expected. The high pressures generated with the low profile air pump could potentially be used to actuate liquid flow through a microchannel heat sink. Specifically, the feasibility of using this air blower to drive the liquid back and forth through a microchannel heat sink is investigated. As a first step in gauging its usefulness as thermal management solution in this fashion, it is imperative to be able to predict the dynamics of oscillation.

1.1 BACKGROUND

Oscillating flow studies have a rich history that arguably began in 1955 with Womersley, who developed a modeling methodology for oscillating flow in arteries [10]. In his analysis, Womersley modeled the artery as a circular pipe or diameter *D* whose fluid is incompressible and subject to an oscillating pressure force. Solving the equation of motion for this scenario yields expressions for velocity profiles and flow rates as a function of the oscillating pressure driving the flow. Through his analysis, Womersley identifies a non-dimensional parameter, which is now known as the Womersley number (W_0), defined as [10]:

$$W_0 = \frac{D}{2}\sqrt{\frac{\omega_0}{\nu}} \quad \textbf{(1)}$$

where D is the characteristic length (defined as the diameter for circular tubes), ω_0 is the oscillation frequency and, ν is the fluid viscosity. Womersley has concluded that W_0 for typical human arteries are approximately equal to that of other biological creatures such as dogs, cats, and rats, suggesting the similarity across these scales is adequately captured by W_0. Since W_0 can influence the velocity profile, it also has an impact on the volumetric flow rate. For a rapid driving pressure gradient with constant amplitude [10, 11], the flow rate oscillates more frequently but at a cost of low amplitude because of high values of Womersley number ($W_0 > 1$). Although the assumption of a Newtonian fluid is inconsistent with the application of blood flow, the Womersley number provides qualitative insight into the behavior and response of such biological systems. When Womersley conducted his analysis on oscillating flow, he considered the flow to be on a horizontal plane and thus the flow is independent from gravitational force, which can play a significant role in the dynamic response, as will be discussed in the next sections.

With the advantage of modern day computing and analysis resources, additional studies have revealed a broader role of the Womersley number and how it impacts the nature of the flow regardless of the geometry. One of the studies is conducted by Loudon and Tordesillas in which they have summarized evidence of how the magnitude of the Womersley number influences the flow and the velocity profile [11]. These authors consider the simplest possible internal flow geometry, namely one dimensional flow between two parallel horizontal flat plates with no-slip conditions at the walls. It should be noted that their analysis is also independent of the gravitational force effect. The mathematical solution indicates that there exist relationships between the velocity profiles, the volumetric flow rate and the Womersley number. For $W_0 < 1$,

the fluid maintains a parabolic velocity profile because the flow is laminar. For $1 < W_0 < 10$, the velocity profile of the fluid begins to deviate from the parabolic shape because of the transition of flow from laminar to turbulent, but the maximum velocity still occurs at the center of the channel or tube. For $W_0 > 10$, the velocity of the fluid near the center of the channel is lower than that in a layer of flow near the walls and the parabolic velocity shape is completely lost. Loudon and Tordesillas have concluded that the abrupt change from laminar to turbulent flow is captured when $W_0 \approx 5$.

One scenario where oscillating flow is of importance is the dynamic response of U-tube manometers. Unlike the conditions explored by Womersley [10] and Loudon and Tordesillas [11] which are driven by an external pressure gradient, the oscillating flow in a U-tube manometer is at least partially driven by a gravitational force, and opportunities exist to exploit resonance conditions. The standard analysis reveals equations of motion that predict fluid behavior in a fashion similar to a standard second order response. The resulting analytical solution assumes the velocity profile as parabolic where the maximum velocity occurs at the farthest point from the wall (i.e. neutral of axis the tube). Experiments were conducted by Biery [14, 15] on Newtonian fluids to observe and examine the different behaviors of several liquids. Significant differences are observed between analytical and experimental results. Since the modeling approach relies on a standard second order dynamic response, the two parameters that describe this response are the damping ratio (ζ) and the natural frequency (ω_n). Theoretically, the natural frequency (ω_n) and the damping ratio (ζ) are defined according the following expressions [13, 18]:

$$\omega_n = \sqrt{\frac{2g}{L}} \tag{2}$$

$$\zeta = \frac{8\nu L\omega_n}{(gD^2)} \quad \textbf{(3)}$$

where g is the gravitational force and L is the length of the liquid inside the manometer.

Valensi [14] is the first to thoroughly examine the behavior of fluids undergoing damped oscillation flow. Based on his findings, the Valensi Number (V_a) is defined according the following expression:

$$V_a = \frac{D^2}{4}\frac{\omega_n}{\nu} \quad \textbf{(4)}$$

It is important to note the relationship between W_0 (Eq. (1)) and V_a (Eq. (4)). Although each is developed under different conditions, both arrive at essentially the same dimensionless number that describes the flow physics. In other words, the relationship between W_0 and V_a is simply:

$$W_0 = \sqrt{V_a} \quad \textbf{(5)}$$

Many studies utilize these two dimensionless numbers interchangeably since they share the same parameters [11, 14-15]. The velocity profile can be expressed in terms of W_0 or V_a, depending on one's preference, but for oscillating manometers, in order to fully predict the dynamic behavior of the fluid, one must also be able to quantify the natural frequency (ω_n) and damping ratio (ζ) of the system. The former is straightforward, but the latter has proven to be a difficult task, especially in the presence of complex fluid forces that cannot be quantified mathematically in the governing equations of motion.

Biery has conducted different experimental trials regarding the damped oscillations in U-tube manometers and has confirmed the discrepancy of the damping ratio (ζ) and velocity profile between the analytical results that are based on parabolic laminar flow assumptions and empirical data [14-15]. It should be noted that Biery's experimental results regarding the damping ratio (ζ) are based on the log decrement method. In other words, the fluid would be given an initial displacement and then released, after which the oscillations damped out with

time. By extracting and comparing peak fluid displacements of two separate oscillation cycles, the damping ratio can be calculated. In his findings, Biery discovered that the damping ratio (ζ) varied with each half cycle due to the fact that the initial velocity profile is not repeated, and for the first several cycles the damping ratio (ζ) varies with each half cycle until the damping ratio (ζ) reaches a steady value [14]. There are other secondary effects that caused the discrepancy in damping ratio (ζ) results which will be discussed in detail in the following sections. In order to match analytical results to the experimental results, Biery modified the driving force in the equation of motion due to secondary effects such as falling films, surface tension, and flow reversal effects [14-15].

There are numerous forces and fluid effects worth mentioning that help explain the discrepancies between experimental and analytical results. For example, if the contact angles between the liquid and the wetting manometer tube are not equal at the ascending and descending ends of the manometer tube, then a force due to surface tension can impact the results. The contact angles in Biery's trials are 0° at the ends of the manometer and thus the force is zero, but the same result cannot be achieved with a non-wetting tube as the contact angles are non-zero [15]. Another effect worth noting is that of a falling film. A liquid film is created by the ascending and descending of liquid on the manometer tube walls. This film is carried by the ascending liquid on the return stroke. Consequently, falling films cause a reduction in the mass of the system for a short time and change the instantaneous equilibrium position of the manometer tube [14-15]. Effects due to surface tension and falling films are minimal because of low viscosity fluids such as water and glycerin and manometers made of soft glass tubing [15]. Most of the deviation between the computer-generated model and the empirical results is attributed to the flow reversal effect which occurs when the velocity profiles of the fluid at the

ends of the tube do not maintain a parabolic shape and become extremely distorted while the velocity profile of the main body fluid maintains its parabolic shape. During the ascending and descending of the fluid at the ends of the tube, the velocity profiles have to adjust to the sudden change of velocity caused by the driving force. This causes the stationary fluid at the ends of the tube to abruptly accelerate and flow along the wall into the high-velocity region in the center of the stream. As a result, the fluid rotates in a large toroidal shape (vortex rings) [15]. This ends up causing an increase in the damping ratio (ζ) values [14-15]. Biery models the flow reversal effect as a force which is a function of an arbitrary constant, cross section area of the tube (A), radius of the tube (R), and the kinematic viscosity of the fluid (ν) [15]. This arbitrary constant is then modified to minimize the percentage error between the mathematical solution and empirical results. The general trend of the velocity profiles that are simulated by the mathematical solution indicated that the parabolic velocity profile assumption is invalid. Such assumption is only valid for highly viscous fluids and/or with manometers with small diameter (D < 2 mm) [12, 14-15]. In other words, the velocity profile assumption is only validated for small V_a (similar conclusion reached by Loudon and Tordesillas [11] for a non-gravity driven flow).

Correlations between the Valensi number and the empirical damping ratio (ζ) results are first developed by Valensi in 1947, the result of which is shown in Eq. (6) for V_a < 20 [14]:

$$\zeta = \frac{2.892}{V_a} \tag{6}$$

Valensi has recognized three different flow regimes in the oscillatory flow based on the magnitude of V_a [14, 16]. For V_a < 20, the inertial term in the governing equation of motions is small enough such that the velocity profile can be assumed to be parabolic [16]. For values of V_a between 20 and 70, the velocity profile becomes non-parabolic and complex. For values of V_a > 70, a central core of the fluid exists and this core is unaffected by the viscous forces [16].

Comparison of these numbers with the W_0 transition values again illustrates the consistency between the two scenarios.

In 1948, Valensi and Korman have applied the boundary layer theory to attain a solution [14, 16] for small damping ratio (ζ) values and for 100 < V_a < 1000:

$$\zeta = \frac{1}{\sqrt{2}\sqrt{V_a}} \tag{7}$$

Eq. (7) is found to agree well with the analytical solution as V_a number approaches 1000 [14]. Even with Eq. (7), empirical values of damping are 20-30% higher than the predicted model. Chan and Baird have explained the various factors that might affect the U-tube manometer. The first factor is the error in measuring the amplitude due to the wetting of the tube wall which is a result of the fluid movement [16]. Another factor is the hydrodynamic end effect which involved the toroidal circulations at each end of the free surface. Another possible issue is the curvature of the U-tube and how it affects the flow. [16]

In the early 1960s, an attempt to characterize the manometer problem based on the mechanical energy balance and an assumption of time varying parabolic velocity profile was conducted by Bird [20]. Bird solved his equation for V_a < 10 as shown below.

$$\zeta = \frac{\sqrt{12}}{V_a} \tag{8}$$

From an analytical stand point, the damping ratio (ζ) and the natural frequency (ω_n) of the manometer can be determined based on the momentum balance of the system. At rest, a change in pressure (ΔP) is enforced across the columns of the manometer. The assumption of the flow is laminar, incompressible, and parabolic. The solution will indicate the displacement of fluid (Z) as a function of time. The momentum balance on the fluid inside the U-tube manometer from a dynamic stand point is the following [18, 19]

$$\left(\frac{L}{2g}\right)\ddot{Z} + \left(\frac{16L\nu}{D^2 g}\right)\dot{Z} + Z = \frac{\Delta P}{\rho g} \quad \textbf{(9)}$$

rearranging the above equation to the general second order response

$$\ddot{Z} + (2\zeta\omega_n)\dot{Z} + \omega_n^2 Z = \omega_n^2 F(t) \quad \textbf{(10)}$$

then is it clear that $\omega_n = \sqrt{\frac{2g}{L}}$ and

$$\zeta = 4\left[\frac{4\nu}{D^2\omega_n}\right] = \frac{4}{V_a} \quad \textbf{(11)}$$

These expressions that predict damping have shown fairly good agreement for moderate to large values of W_0, but when W_0 is small (as is the case for a potential solution for thermal management of electronics), the expression provided in Eq. (6) leaves much to be desired. Others have found the same level of apprehension [14-16], but little headway has been made. One of the goals of this study is to quantify the damping and develop predictive correlations for conditions in the expected range for thermal management applications. We consider both a damped sinusoid response as well as a steady driving force whose frequency is near or within the bandwidth of the resonance frequency of the U-tube manometer. Results are shown to drastically differ depending on which method in employed. Trusted correlations for damping are needed in order to truly assess the potential of using flow oscillations through a microchannel heat sink.

The remainder of this thesis will proceed with three major chapters. In chapter 2.0 of the thesis, the central focus is on the physical assembly of the experimental setup and the procedures followed for data collection. Data is characterized using two different approaches to quantify the damping: (i) frequency response from an oscillating pressure and (ii) damped sinusoid from an initial displacement. Chapter 3.0 includes detailed analysis and comparison of the two types of damping data mentioned above, and is included in sections 3.1 and 3.23.1. Chapter 0 provides a summary which consists of the core findings in the thesis. A section of chapter 4.0 contains

details about the possibility and applicability of oscillating flow as a thermal management solution in the field of electronic and what other new parameters must be taken into consideration that impact the fluid flow inside the manometers.

2.0 EXPERIMENTAL SETUP AND PROCEDURE

As previously mentioned, the oscillation of liquid inside U-tube manometers is considered as a second order response where the natural frequency (ω_n) and damping ratio (ζ) are defined according to Eq. (2) and Eq. (3), respectively [13]. Two separate testing methods are employed to measure the quantities of interest. First, a frequency sweep procedure is used where the frequency of the driving pressure signal is tested at multiple points on either side of the natural frequency of the U-tube. Second, the log decrement method is conducted in order to quantify the difference between the two approaches. The same experimental facility is used for both sets of experiments. It will first be described, followed by procedures for each type of test. A detailed discussion of experimental uncertainty is also provided.

2.1 EXPERIMENTAL SETUP

The data collection of the oscillation of liquid in a U-tube is achieved through the use of four primary components: a standard digital camera (Cannon PowerShot A700), a piezoelectric blower, a custom-made supporting apparatus, and a function generator (Tektronix AFG3102). The experimental setup is illustrated in Figure 1. The custom-made supporting apparatus consists of three components: a top plate, a middle plate, and two triangular legs. The top plate contains two holes for barbed tube fittings. The air blower is placed on one of the holes of the top plate. A

set of screws and nuts are used to eliminate the space between the surfaces of the blower and the top plate. This ensures that the liquid column only oscillates due to the pressure exerted by the sinusoidal pressure from the air blower. The other tube end is exposed to atmospheric pressure. The blower itself is provided by Murata Manufacturing Co., Ltd and makes use of a piezoelectric element whose actuation is provided by the function generator. The frequency of actuation is tuned to the second resonance mode of the piezoelectric disk. This particular blower is traditionally used for low profile cooling applications by directing air towards a heated target. In this study, the blower is essentially used as a pressurizer, which then drives the liquid flow through the tube. For more details on the blower, see [9]. Tube clamps are placed in the middle plate to maintain the U-shape for the tube. A precision ruler is placed next to the liquid column to measure the displacement during the oscillation of the fluid. The digital camera is placed in front of the custom-made supporting apparatus ready to capture the liquid column oscillation due to the air blower. Figure 2 illustrates a side view of the experimental setup, where the digital camera can record a video of the damped oscillation of the liquid column for a range of frequencies. This setup allows for testing different tube sizes. A digital photo of the setup is shown in Figure 3. The top board of the apparatus consists of two threaded holes enabling quick interchanging of tube fittings when testing different tube sizes. The different tube sizes that are used in the setup and the different fluid lengths are listed in Table 1. The fluid used in all of the trials is water with a kinematic viscosity (ν) of $1.084 \times 10^{-6} m^2/s$ at 20 °C.

Table 1: Tube sizing and fluid length range for experimentation

Tube Inside Diameter, in (mm)	0.125, 0.170, 0.1875, 0.250, and 0.375 (3.175, 4.318, 4.762, 6.35, and 9.525)
Fluid Length Range, in (cm)	15.75 – 78.75 (40 – 200)

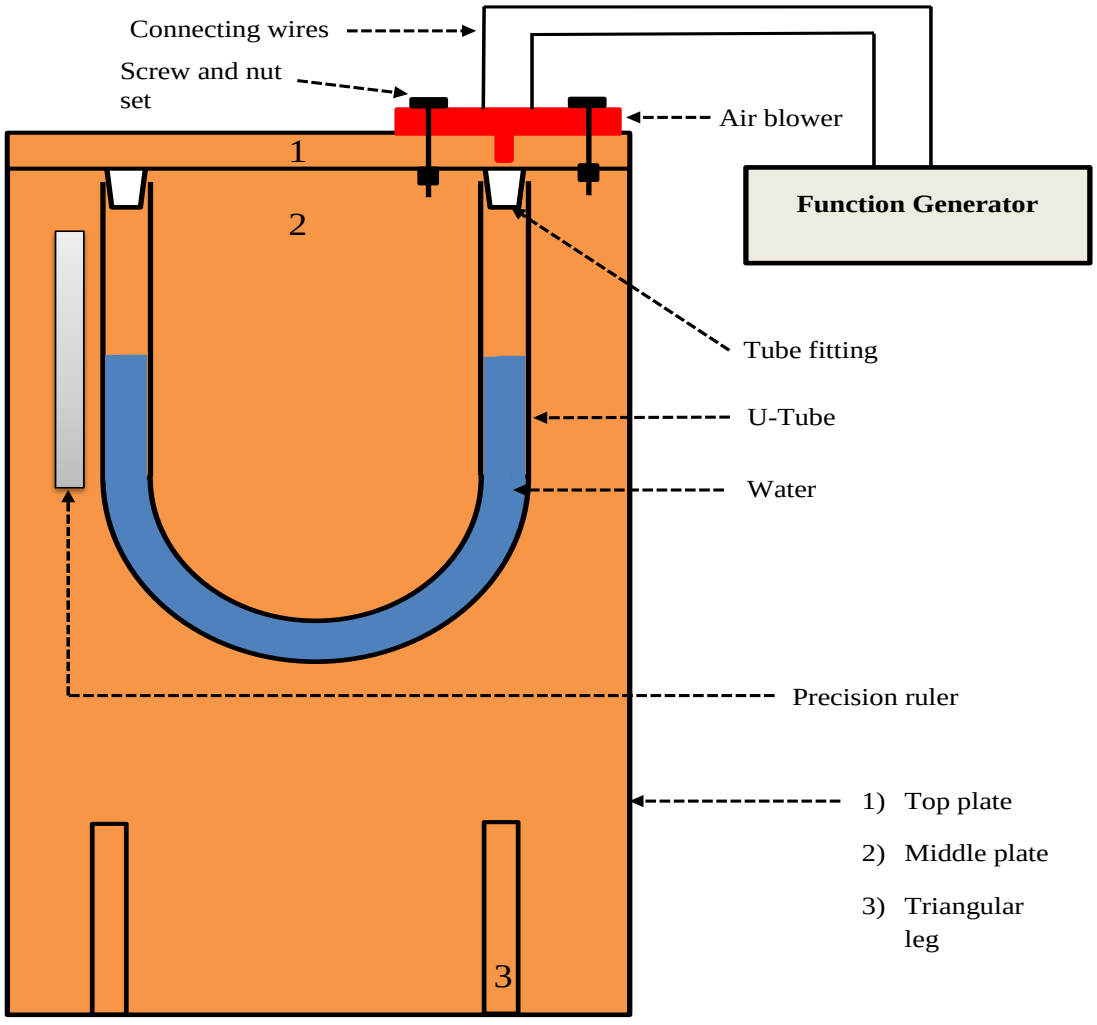

Figure 1: A front view of how the components of the test are oriented

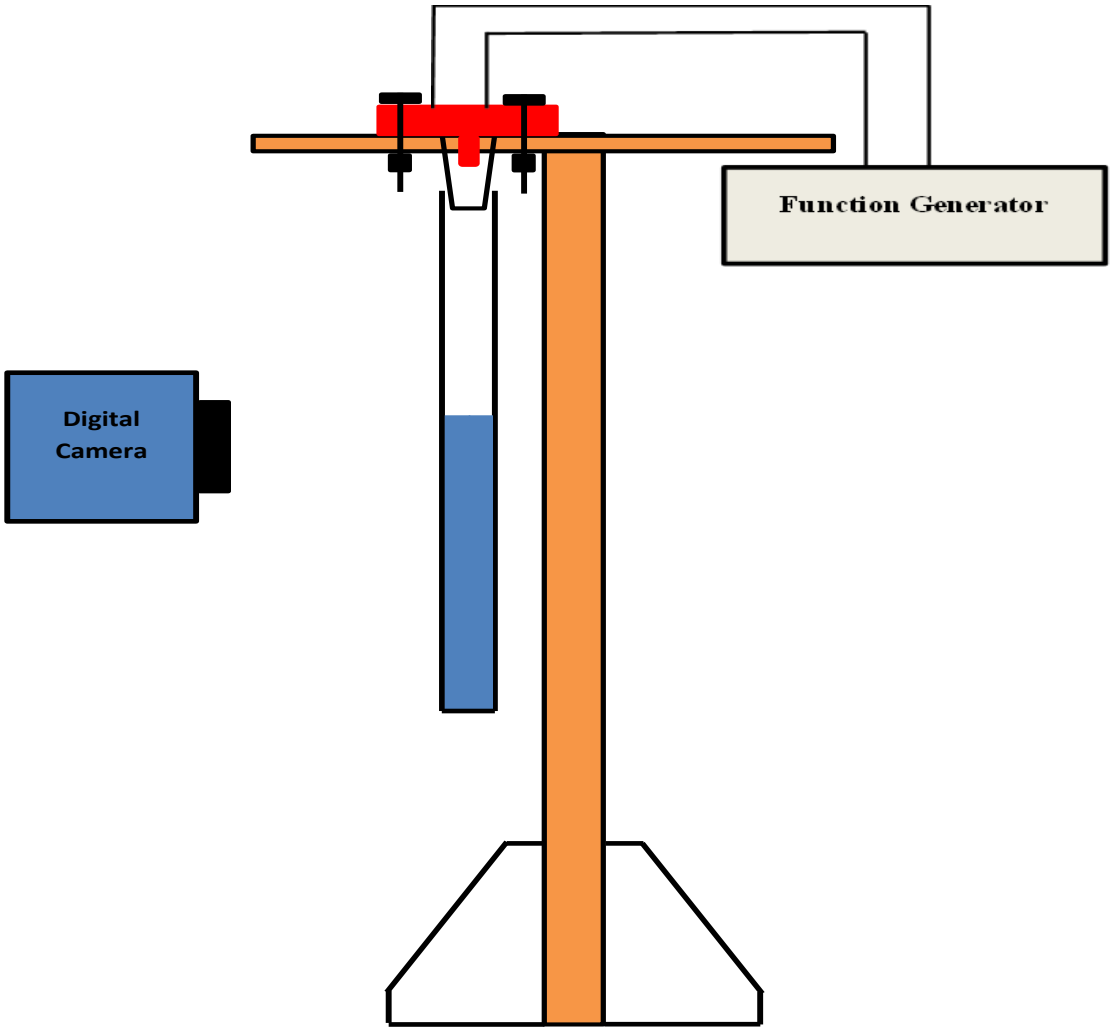

Figure 2: A side view of how the components of the test are oriented

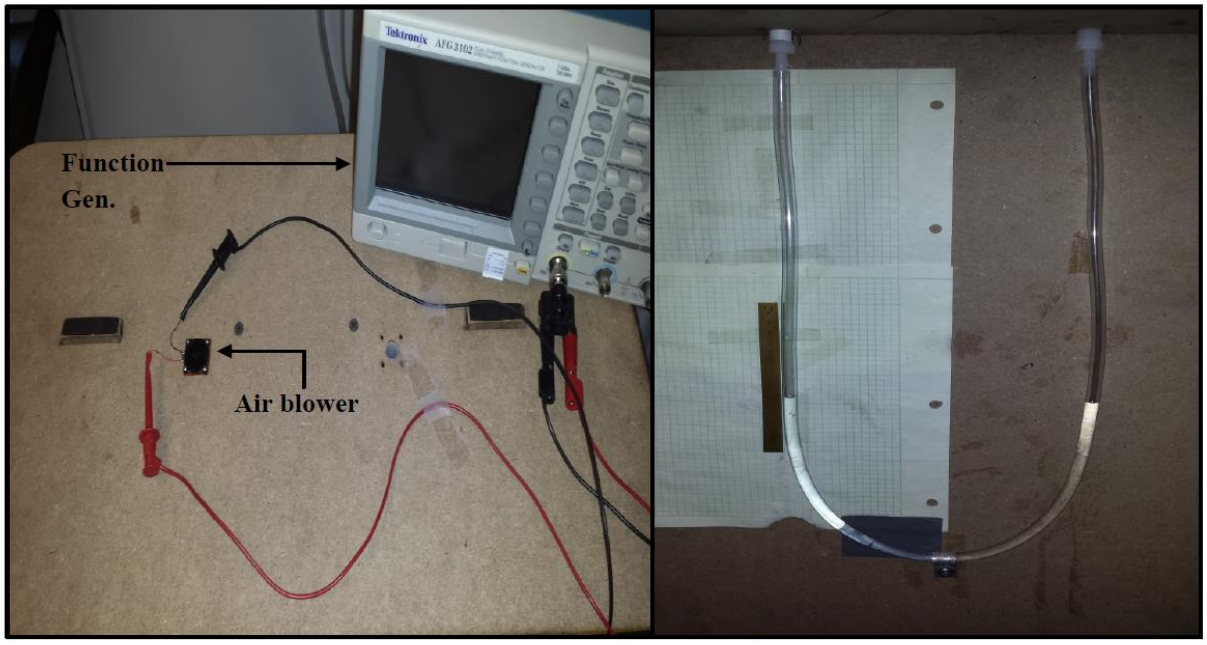

Figure 3: Picture of Actual Setup: (a) Top View (b) Front view

2.2 PROCEDURE FOR FREQUENCY RESPONSE TESTS

For the frequency response testing, a sinusoidal pressure gradient is provided via the blower. The overall goal of the procedure is to quantify the damping of fluid flow under continuous constant oscillation. The standard second order response can be captured under certain conditions for a damped sinusoid oscillation, but it unclear from the literature whether those conditions or any conditions apply when employing a sinusoidal driving force. In addition to quantifying the damping, the tests help to assess the validity of a second order response for sinusoidal loading conditions. The digital camera is mounted on a tripod to capture fluid oscillation. The overall control of the procedure is attained through the function generator. The operating frequency of the air blower is set to 25.1 kHz (the structural resonance frequency of the piezoelectric disk),

which enabled the fluid to achieve the largest displacement from the equilibrium position. It should be noted that this is not the driving frequency of the fluid column. It is simply the resonance frequency of the piezoelectric element inside the air blower. The input voltage is set to a maximum of 10 V. This input voltage yields to a maximum input pressure of 1.078 kPa which is measured based on the maximum displacement of the fluid column. A modulated sinusoidal wave signal is sent to the air blower by the function generator to cause the fluid to oscillate. A modulated square wave is also tested initially, but found to suffer from the flow reversal effect considerably described earlier. The modulated sinusoidal wave helps to minimize these effects since there is no abrupt signal switching between on and off. The frequency range of modulation is between 0.1 Hz and 1.5 Hz for the fluid column oscillation. The modulation sinusoidal wave consists of (i) a carrier frequency and (ii) a modulation frequency. The carrier frequency is the 25.1 kHz of the air blower while the modulation frequency is any single value from 0.1 Hz to 1.5 Hz. For illustration purposes only, Figure 4 represents a modulated sinusoidal wave with carrier frequency of 5 Hz and a modulated frequency of 0.5 Hz. Table 2 summarizes the important operational parameters of the function generator.

Each frequency value (ω) is evaluated separately, and the digital camera records the oscillation of the fluid. The magnitude of fluid displacement is visually measured from the captured video using the precision ruler in the background of the tube column as seen in Figure 1. Fluid displacement values are recorded using a frequency sweep method. The frequency sweep ranges from 0.1 Hz to 1.5 Hz by increments of 0.1 Hz. At each frequency, the fluid oscillates continuously and a video footage is recorded via the digital camera. Since there are several oscillations in each video, an average fluid displacement value is determined for the corresponding frequency using approximately 4-5 amplitude data points. Therefore there are a

total of 15 fluid displacement values for each fluid length/tube size combination. Then these 15 data points are normalized by the corresponded static displacement of the oscillating fluid of that trial, which is quantified by running a group of additional tests between 0.01 Hz and 0.1 Hz, which is well below the U-tube resonance frequency. Plots of magnitude of displacement versus frequency are then generated to detect the trend. The data is then gauged using the normalized magnitude for a second order response [18]:

$$\frac{X}{\delta_{st}} = \frac{1}{\left\{\left[1-\left(\frac{\omega}{\omega_n}\right)^2\right]^2+\left[2\zeta\frac{\omega}{\omega_n}\right]^2\right\}^{1/2}} \; ; \delta_{st} = \frac{F_0}{k} \tag{12}$$

where X is the magnitude of displacement and δ_{st} is the static displacement of the oscillating fluid due to the static force F_0. The static displacement can be measured directly from the raw data therefore the static force is not needed to be measured. According to theoretical analysis, the plots of magnitude versus frequency should follow the expression in Eq. (12). The curve fit tool of MATLAB is used for all the trials to determine the goodness of fit when Eq. (12) is applied. Only the bandwidth range of every trial is supplied to the curve fit tool. Additionally the curve fit tool determines the values of the natural frequency and damping ratio (ζ) that best fit the experimental data. The experimental values of the natural frequency and damping ratio (ζ) are compared to Eq. (2) and Eq. (3) respectively to gauge the accuracy of the theoretical analysis.

The next phase is to determine the relationship between the damping ratio (ζ) and the Womersley number (W_0). In order to achieve a correlation between the two parameters, the fluid level is varied between 40 cm and 200 cm for each tube size in Table 1. Each fluid length for every tube size corresponds to a Womersley number (W_0) value found from Eq. (1). Then, empirical results are compared to the correlations found in Eqs. (6) - (8) [14,16,17] and the analytical solution. It should be noted that Eqs. (6) - (8) are based on the log-decrement

technique. Therefore, the analysis of the forced response data enables a gauge on the validity of these expressions when the driving force is nonzero.

Table 2: Important operational input parameters

Input Voltage (V)	10
Blower Operating Frequency (kHz)	25.1
Waveform	Modulated sinusoidal
Tested frequency Range (Hz)	0.1 – 1.5

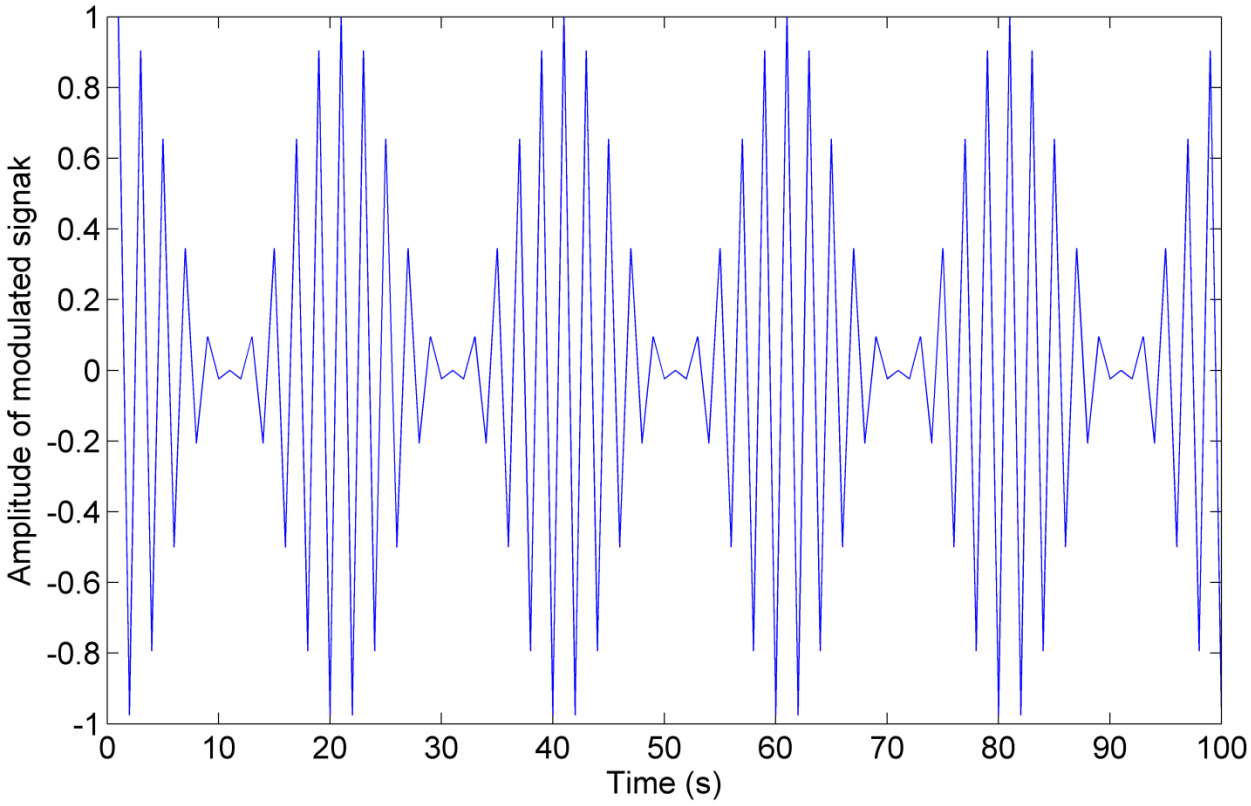

Figure 4: Modulated sinusoidal signal

2.3 PROCEDURE FOR LOG DECREMENT METHOD

For comparison to the frequency response data as well as the expressions developed for U-tube damped oscillations, experiments are conducted to make use of a damped sinusoid response. A continuous pressure is provided for several seconds via the air blower (function generator voltage amplitude is set at 10 V), and causes the fluid to ascend and remain above the equilibrium position. Then the generator is instantly shut off while the digital camera captures the damped response of the oscillating fluid until it comes to a complete stop. Each trial is expected to have about 2 – 4 full cycles of oscillation. The magnitude of fluid displacement for each full cycle is visually measured from the captured video using the precision ruler in the background of the tube column as seen in Figure 1. Once all magnitudes of fluid displacement are determined, the standard logarithmic decrement technique is applied to calculate the damping ratio for each trial.

The rate at which the magnitude of a free damped oscillation decreases is represented by the logarithmic decrement. It is defined as the natural logarithmic of the ratio of any two magnitudes, and is a reliable method to determine the damping ratio for an underdamped ($\zeta < 1$) oscillating or vibrating system. The damping ratio (ζ) is defined according to the logarithmic decrement method as the following [18]:

$$\zeta = \frac{\delta}{2\pi\sqrt{1 + \left(\frac{\delta}{2\pi}\right)^2}} \tag{13}$$

where

$$\delta = \frac{1}{N}\ln\left(\frac{X_1}{X_{N+1}}\right) \tag{14}$$

where N is the number of cycles between the amplitudes X_1 and X_{N+1}. The number of cycles N varies based on the fluid lengths and tube sizes, but the general trend is more cycles exist for large tube diameters ($D \geq 6.35$ mm) with short fluid lengths ($L \leq 70$ cm). Table 3 provides a summary of number of cycles for each trial. It must be noted that the first cycle of each trial is not included in the determination of the damping ratio due to the initial excessive pressure build up by the air blower. The effect of the first value artificially inflated the damping (in some cases 19% higher).

Table 3: Summary of number of cycles for each trial

	D = 4.318 mm	D = 4.762 mm	D = 6.35 mm	D = 9.525 mm
L (cm)	N	N	N	N
40	2.5	3	3.5	4
45	2.5	3	3.5	4
50	2.5	3	3.5	4
55	2.5	2.5	3.5	3.5
60	2.5	2.5	3	3.5
65	2	2.5	N/A	N/A
70	2	2	3	3
80	2	2	3	3
90	2	2	2.5	3
100	1.5	2	2.5	2
110	1.5	2	2	2.5
120	N/A	N/A	2	2.5
165	1.5	1.5	N/A	N/A
200	N/A	N/A	2	2.5

2.4 UNCERTAINTY ANALYSIS

All the variables that are involved in determining the natural frequency (ω_n), the damping ratio (ζ), and the Womersley number (W_0) such as the tube inside diameter, fluid length, or the magnitudes of displacements of oscillating fluid are measured directly. All uncertainty analysis included in the experimental trials are due to digital caliper and precision ruler measurements. The surrounding effects are apparent when comparing different runs of the same diameter size and fluid length collected on different days.

First, an uncertainty analysis is conducted on the natural frequency (ω_n). This parameter is a function of fluid length and the gravitational force. The length of the fluid inside the U-tube manometer is measure via a standard tape measure with an uncertainty of ±0.50 mm. this yields to a maximum uncertainty of 0.44% for the natural frequency (ω_n). The uncertainty of the natural frequency is the same for the two different experimental methods conducted for this research.

The other imperative parameter is the damping ratio (ζ) which is only a function of the parameter (δ) defined in Eq. (14) when considering the log decrement method. The main source of uncertainty for this method comes from the measurements of the amplitudes X_1 and X_{N+1} in Eq. (14). The high precision ruler (see Figure 1) that is used for measuring the amplitudes in Eq. (14) has an error in of ±0.25 mm. Thus the damping ratio has an uncertainty of approximately 2.68% to 6.93% for a tube diameter of 9.525 mm. The overall uncertainty in damping for a tube size of 6.35 mm ranges from 1.87% to 3.70%. The total uncertainty in damping for a tube size of 4.762 mm is between 1.34% and 2.55%, while the uncertainty ranges from 1.35% to 2.10% for a tube size of 4.318 mm. For the smallest tube size ($D = 3.175$ mm), uncertainty is not calculated

since the oscillations die down to unmeasurable levels within a few cycles, thereby preventing experimental trials to be conducted. Overall, the average uncertainty value for all tube sizes for log decrement damping is 2.37%

The uncertainty in the damping ratio analysis based on the continuous oscillation method is determined via the curve fit tool in MATLAB using a confidence level of 95%. This results in damping ratios with uncertainties between 0.71% and 2.50% for a tube size of 9.525 mm, 0.85% and 1.53% for a tube size of 6.35 mm, 0.76% and 1.25% for a tube size of 4.762 mm, 1.04% and 1.54% for a tube size of 4.318 mm, and between 0.76% and 1.43% for the smallest tube size ($D = 3.175$ mm). Overall, the average uncertainty value for all tube sizes for damping under continuous oscillation is 1.24%

3.0 RESULTS AND DISCUSSION

Numerous trials of varying tube sizes and fluid lengths are conducted in order to assess the behavior of damping when forcing the oscillation with a sinusoidal pressure gradient as well as a flow driven solely by gravity (damped oscillation). The results are compared with each other and with theoretical solutions, where applicable.

3.1 FREQUENCY RESPONSE SWEEP DAMPED OSCILLATION

For each frequency considered, the steady state amplitude of oscillation is captured via video footage as previously discussed. Figure 5 through Figure 7 provide the magnitude response curves for these experimental runs for different tube sizes of 3.175 mm, 4.318 mm, and 4.762 mm, respectively. All three have the same length of fluid (65 cm), and therefore have near identical resonance frequencies. Applying Eq. (12) through curve fitting tool, the empirical natural frequency (ω_n) and damping ratio (ζ) are determined. This curve fit is also provided in this set of figures for visual reference of the quality of the fit. Table 4 summarizes the comparison between the analytical and empirical solutions for the natural frequency (ω_n) and damping ratio (ζ), where the analytical values are found from Eqs. (3) and (11). Although empirical values of the natural frequency are comparable to predictions from the analytical

solution (less than 2% difference for each case in Table 4), much larger discrepancies exist between experimental and analytical results for the damping ratio. For example, while experimental damping is 5.5% higher than the analytical value for a tube size of 3.175 mm, this dramatically increases to 92% and 230% for tube sizes of 4.318 mm and 4.762 mm, respectively.

Similar experimental trials are conducted for the remaining tube sizes with different fluid lengths in order cover a wide range of W_o. The natural frequencies for all these cases again are found to mimic the expectations for the analytical solution. The percent deviation for this parameter ranges from 0.22% to 3.08%, and is therefore considered an adequate model to predict resonance conditions. For the damping ratio, we seek to quantify a possible trend. Figure 8 shows the relationship between the damping ratio (ζ) and the Womersley number (W_0), where each set of data is collected from a different tube size. The smallest tube size (3.175 mm) results are the most comparable to the analytical solution. But even then, the curve seems to exhibit a different slope, suggesting that perhaps the theoretical solution does not capture the damping behavior accurately. This is not entirely unexpected since one could argue the forces at play for forced oscillations are different than those for a damped sinusoid response, upon which the available analytical expressions are based.

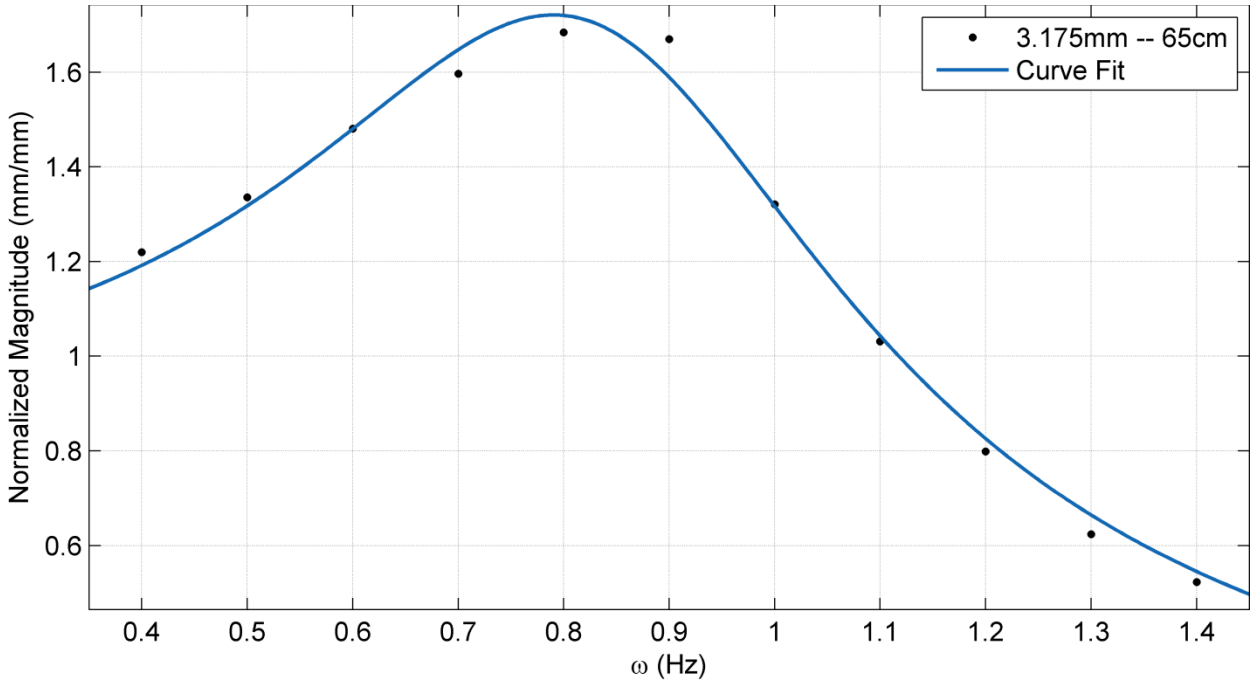

Figure 5: Trial for 3.175 mm with 65 cm in fluid length

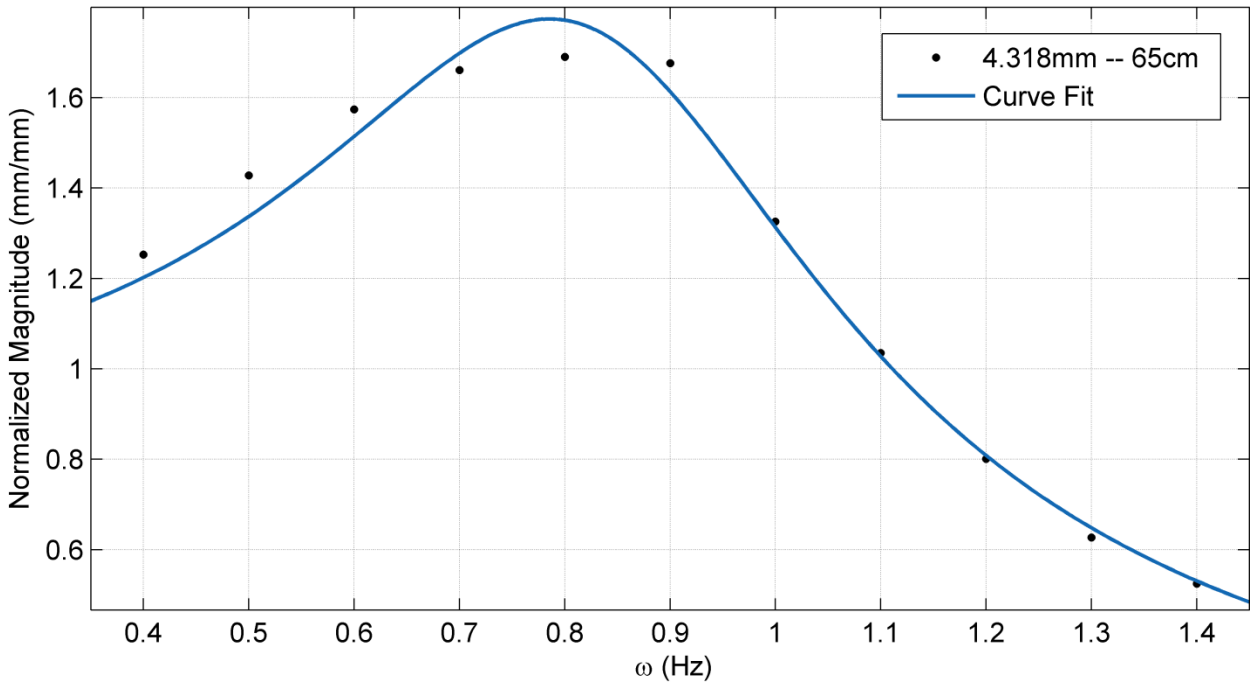

Figure 6: Trial for 4.318 mm with 65 cm in fluid length

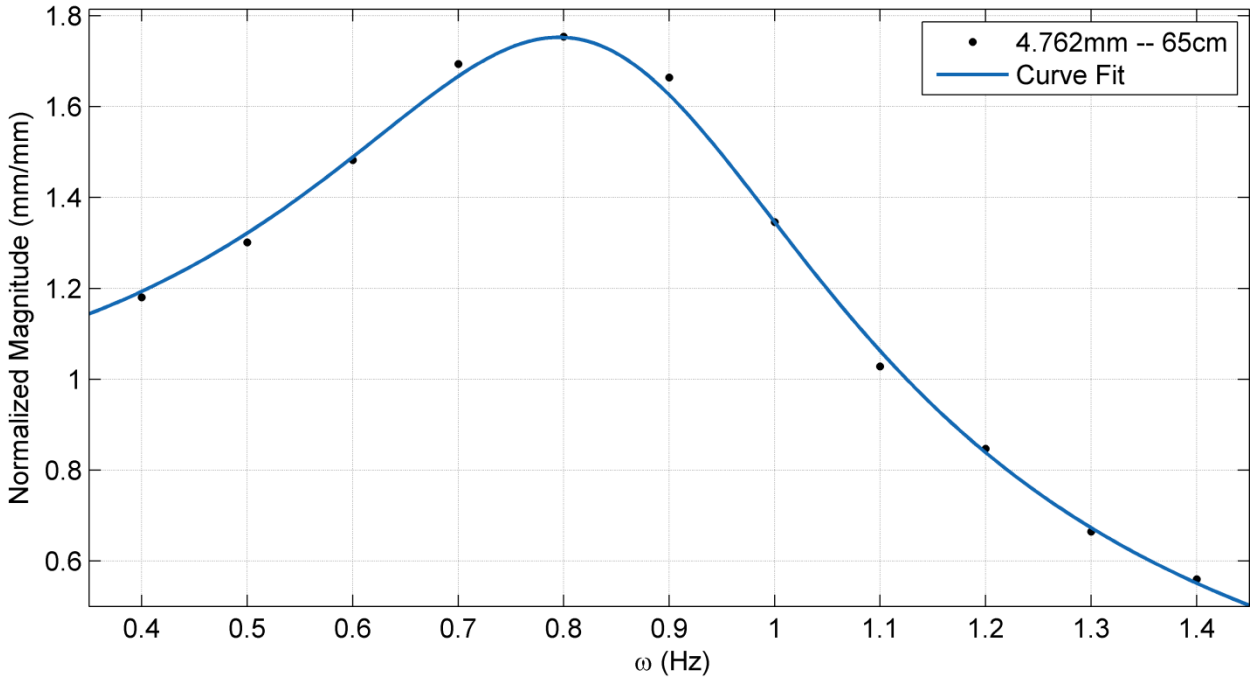

Figure 7: Trial for 4.762 mm with 65 cm in fluid length

Table 4: Theoretical-Experimental $\boldsymbol{\zeta}$ & $\boldsymbol{\omega_n}$ comparison

Tube Size (mm)	Length (m)	Theoretical ζ Eq. (11)	Empirical ζ	Theoretical ω_n (Hz)	Empirical ω_n (Hz)
3.175	0.65	0.289	0.305	0.874	0.876
4.318		0.156	0.299		0.864
4.762		0.128	0.295		0.879

Another potential source of discrepancy is the assumption of parabolic flow for the analytical solution. The velocity profile is known to deviate from this for W_o near unity, which could result in additional damping as W_o increases. This helps to explain the fact that the analytical solution underestimates the damping ratio. Various factors such as the flow reversal effect, and the instantaneous change in the velocity profile would arguably serve as energy dissipaters, thereby impacting the damping ratio. Even for low W_o, the flow, under continuous

oscillation, might not have enough time to become fully developed, even when a parabolic velocity profile is expected. It is possible to verify whether the flow inside the U-tube has become fully developed or not via the hydrodynamic entry length ($x_{fd,h}$) calculation for laminar internal flow [1]. Table 5 represents the summary of hydrodynamic entry length analysis. Since the Reynolds number (Re_D) is less than 2300 for all the combinations of fluid length (L) and tube diameter (D), the flow can be considered as laminar. The maximum change in fluid displacement (ΔZ) that is attained via oscillation for all cases is significantly lower than the necessary entry length for the flow to become fully developed, as determined by well accepted correlations [1]. This confirms that even though the flow is laminar, the velocity cannot achieve the expected steady state profile, thus bringing into question the validity of the parabolic profile assumption. The primary reason for assuming fully developed parabolic flow is because of the simplifications to damping term. Furthermore, there are numerical solutions for internal flow without the fully developed flow assumption, but the friction term that is used to quantify the damping cannot be simplified. As a result this might leads to a complicated numerical solution.

For the current efforts, attempts are made to characterize the behavior such that oscillating flows can be considered in the thermal management toolbox. To predict the natural frequency for forced oscillations, one can simply use the theoretical results, which compare very favorably with experimental values obtained in this study. In order to characterize the damping ratio, standard correlations are not sufficient, and we now apply power law curve fits to each of the data sets in Figure 8 according the following expression:

$$\zeta = C_1 W_0^{C_2} \tag{15}$$

where C_1 and C_2 are coefficients found from a least squares curve fit of the data. It should be noted that for each data set, the diameter is constant, but the length of the water column varies.

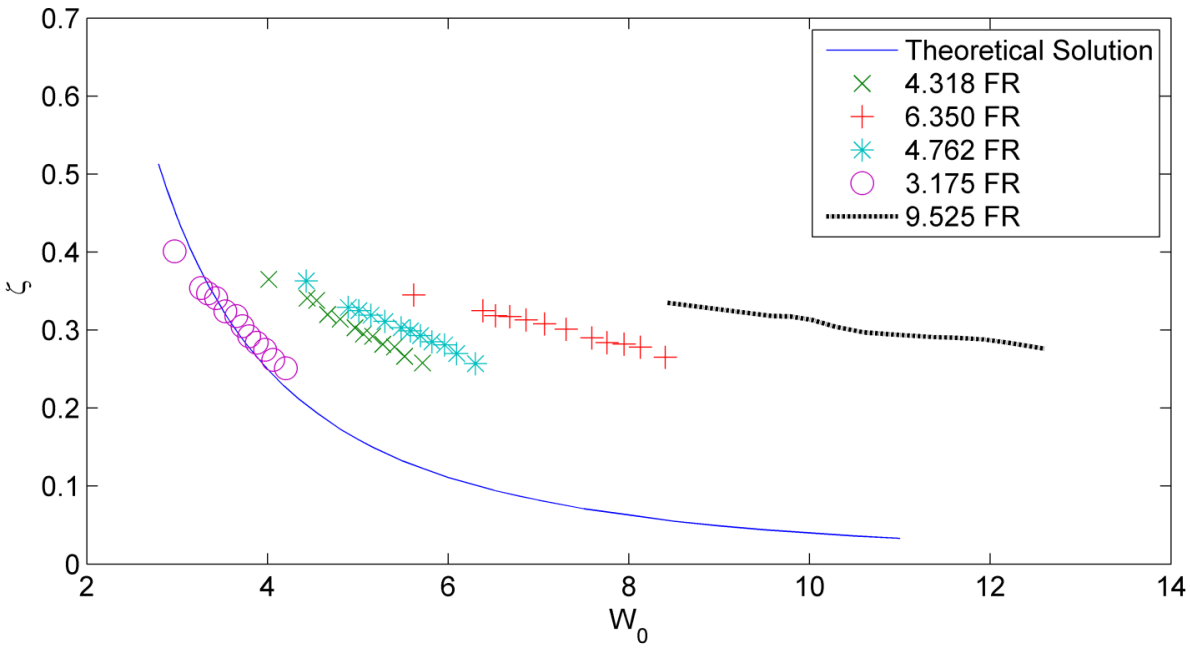

Figure 8: Dependency of damping ratio ($\boldsymbol{\zeta}$) on Womersley number ($\boldsymbol{W_0}$)

Table 5: Hydrodynamic entry length summary

D (mm)	L (cm)	ΔZ (mm)	Re_D	$x_{fd,h}$ (mm)
3.175	40	66	734	116
	65	61	532	84
4.318	40	58	1038	224
	65	68.5	688	149
4.762	40	57	1067	254
	65	64	746	178

Table 6: Summary of frequency response empirical correlations of $\boldsymbol{\zeta}$

Tube Size (mm)	Metric Correlation of Damping Ratio (ζ)
3.175	$\zeta = \frac{1.778}{W_0^{1.35}}$
4.318	$\zeta = \frac{1.56}{W_0^{1.03}}$
4.762	$\zeta = \frac{1.44}{W_0^{0.922}}$
6.350	$\zeta = \frac{1.072}{W_0^{0.645}}$
9.525	$\zeta = \frac{0.9295}{W_0^{0.477}}$

The results in Table 6 indicate the power function relationship between the damping ratio (ζ) and the Womersley number (W_0) for the different tested tube sizes. The constant coefficient decreases as the tube size becomes larger, but more importantly, the exponent also decreases in magnitude, suggesting the curve becomes less and less dependent over a given range of Womersley number. In addition, it is clear that the damping ratio does not follow the analytical model for the forced oscillation experiments. The second order response model seemed to adequately capture the dynamics of the flow, but further investigations are needed to accurately resolve the dependence of the damping on W_0. The set of correlations here provide a first step in achieving that goal. However, it seems possible that the analytical analysis could serve some purpose for extremely small tube sizes, but further work is needed in this area due to the higher pressure drops that result from such small channels. This is not further investigated due to the limitation of the available air blower.

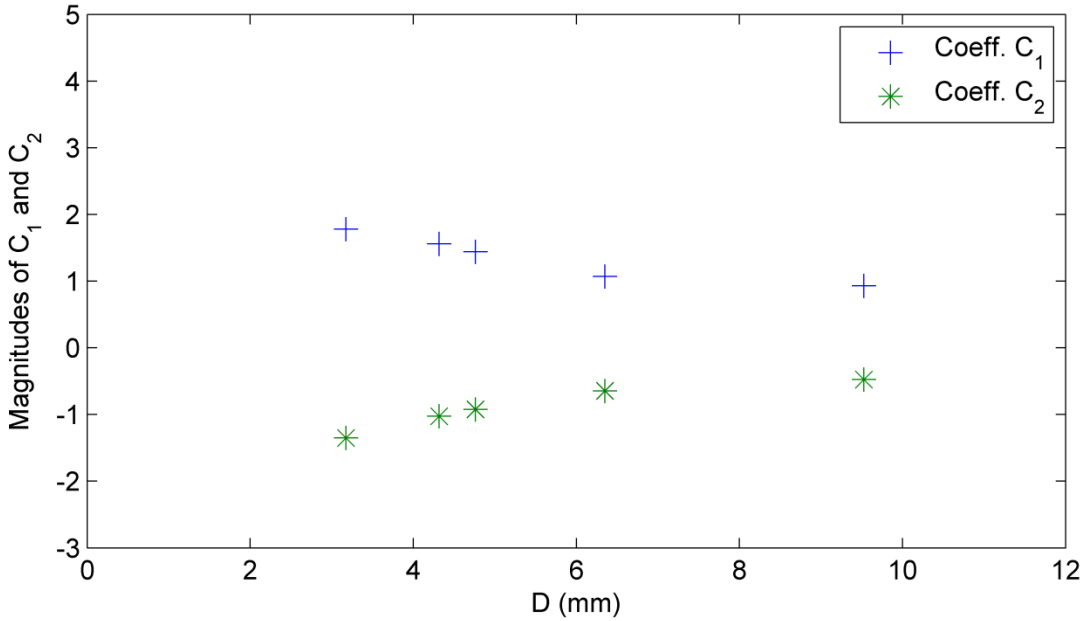

Figure 9: Coefficients $\boldsymbol{C_1}$ and $\boldsymbol{C_2}$ dependency on tube diameter size

The possibility is now explored to quantify the dependency of both coefficients C_1 and C_2 on the tube diameter size in a possible power-law form. For reference, this data points are given in Figure 9. In order to remove the dimensional dependency in this relation, the Keulegan-Carpenter number (KC) is introduced [21]. This dimensionless parameter relates the importance of drag forces to the inertial forces under oscillatory fluid flow conditions and was first developed as a result of analyzing oscillating flows past rigid bluff bodies. The Keulegan-Carpenter number (KC) is defined as:

$$KC = \frac{2\pi\delta_{st}}{D} \tag{16}$$

where the theoretical static displacement (δ_{st}) is defined as:

$$\delta_{st} = \frac{\Delta P}{\rho g} \tag{17}$$

where ρ is the density of the working fluid. The Keulegan-Carpenter number (KC) is now used in place of the diameter from Figure 9 and displayed in Figure 10. It can be shown that C_1 and C_2 can be related to KC based on the following expression:

$$(C_1 \text{or } C_2) = C_3(KC)^{C_4} \quad \textbf{(18)}$$

The correlations for both $C_1$and C_2 are the following:

$$C_1 = 0.1171K_C^{0.6343} \quad \textbf{(19)}$$

$$C_2 = -0.01899K_C^{0.9889} \quad \textbf{(20)}$$

The above correlations for C_1 and C_2 are used to determine a predicted damping model for the five different tube sizes and compared to the experimentally measure values, the result of which is shown in see Figure 11. As can be seen in these results, the predictive tools capture the physical trends that exist in the experiments to a close degree. The mean and maximum absolute errors for this data are 1.27 % and 3.68 %, respectively.

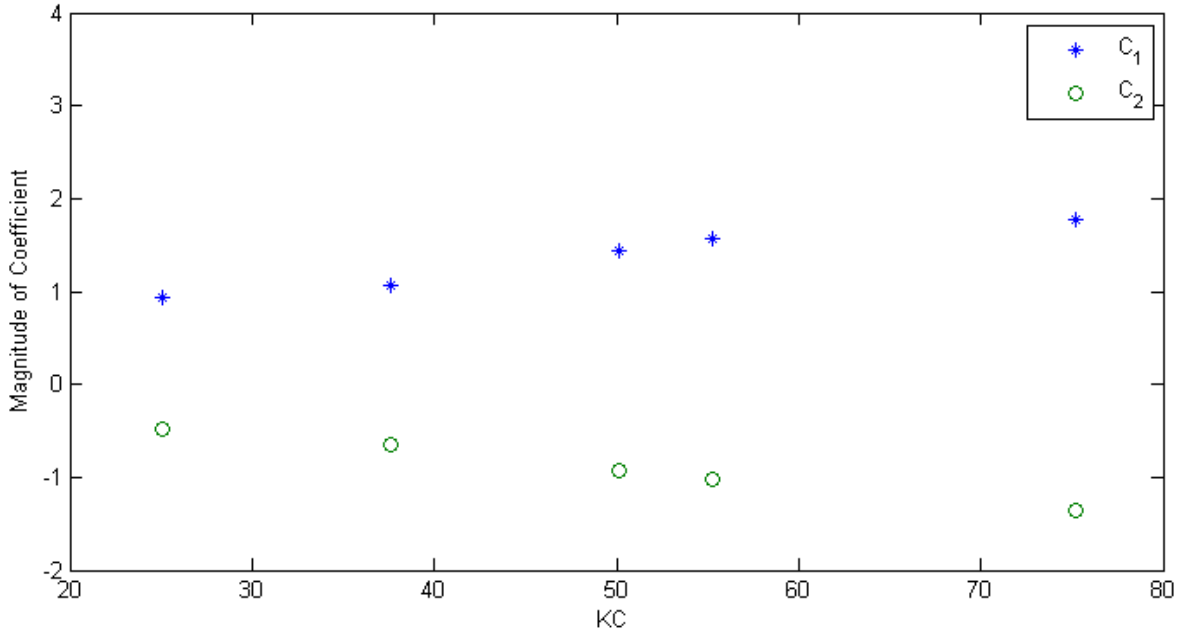

Figure 10: Coefficients $\boldsymbol{C_1}$ and $\boldsymbol{C_2}$ dependency on $\boldsymbol{KC}$

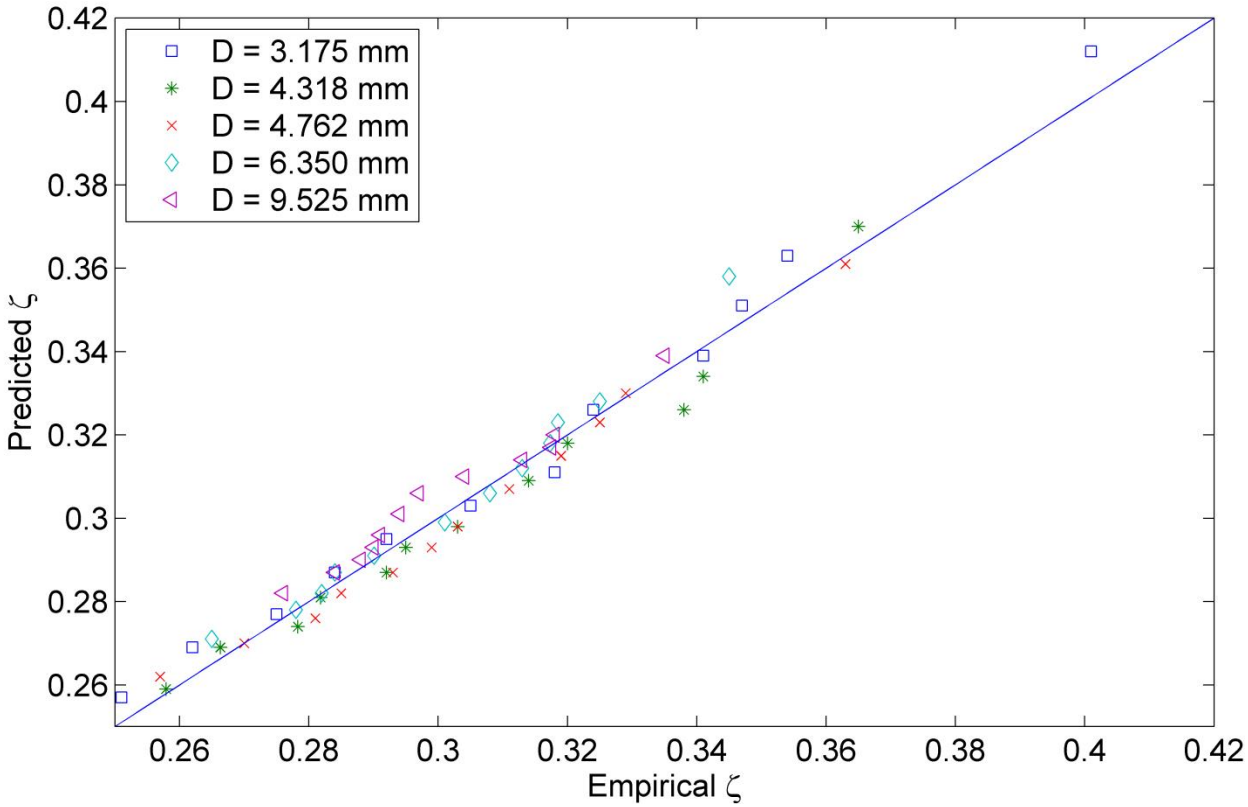

Figure 11: Predicted Damping vs. Empirical Damping

These results, which focus on quantifying the damping from forced oscillations, are the first of their kind. The dependency of the damping on the tube diameter in addition to W_0 is something which has not been reported in the literature. Although the current studies are limited to water as the working fluid and flexible Polyvinyl chloride (PVC) as the tube material, the potential of understanding the flow better is easily recognized from this analysis. Obviously, more comprehensive studies are needed which accommodate different tube materials and working fluids, but the ease of collapsing all data into a set of empirical correlations shows promise and achieving more fundamental insight into internal oscillating flows.

3.2 LOG DECREMENT DAMPED OSCILLATION

A damped sinusoid response is not necessarily applicable to the applications targeted in this study, but repeating the experiments here serves a two-fold purpose. First, it helps to compare and contrast the results with those found from a non-zero forcing function, and second, it helps to more completely understand the current results in the context of previous studies which use the same method for analysis. Results using the log decrement method to extract the damping ratio are provided in Figure 12, where each set of data is again organized according to tube diameter. The findings reveal that as the tube size decreases ($D < 6.35$ mm), the flow inside the U-tube approaches the theoretical solution, both quantitatively and qualitatively (i.e., slope and trend of data is consistent). A summary of empirical correlations are provided in Figure 12 and Table 7. Empirical data is not collected for 3.175 mm tube size because the friction between the fluid and the tube is extremely high that the flow fully damped out after the first half cycle. When $D > 6.350$ mm, the empirical results deviate from the theoretical solution rapidly. It is important to recognize that previous studies do not account for the varying results from different tube diameters. Therefore a new mathematical model is needed to quantify this dependence. The Keulegan-Carpenter number (KC) is again included for this purpose. These results suggest that in order to approach the theoretical solution, both quantitatively and qualitatively, a combination of low Womersley number ($W_0 < 2$) and high Keulegan-Carpenter number ($KC > 50$) is needed. The former is achieved by requiring slow oscillations or a small tube diameter. The latter is achieved when the forcing pressure is high (i.e., a large initial displacement). Maintaining these conditions enables the flow to become fully developed each half cycle. Therefore, this conclusion comes as no surprise. Using Eq. (18) and Table 7, the coefficients of Eq. (15) are the following

$$C_1 = 129K_C^{-0.811} \quad \textbf{(21)}$$

$$C_2 = -0.756K_C^{0.231} \quad \textbf{(22)}$$

The above correlations for C_1 and C_2 are used to determine a predicted damping model for the four different tube sizes. The comparison between predicted and measured values is shown in Figure 13. The mean and maximum absolute errors for this data are 2.87 % and 9.11 %, respectively

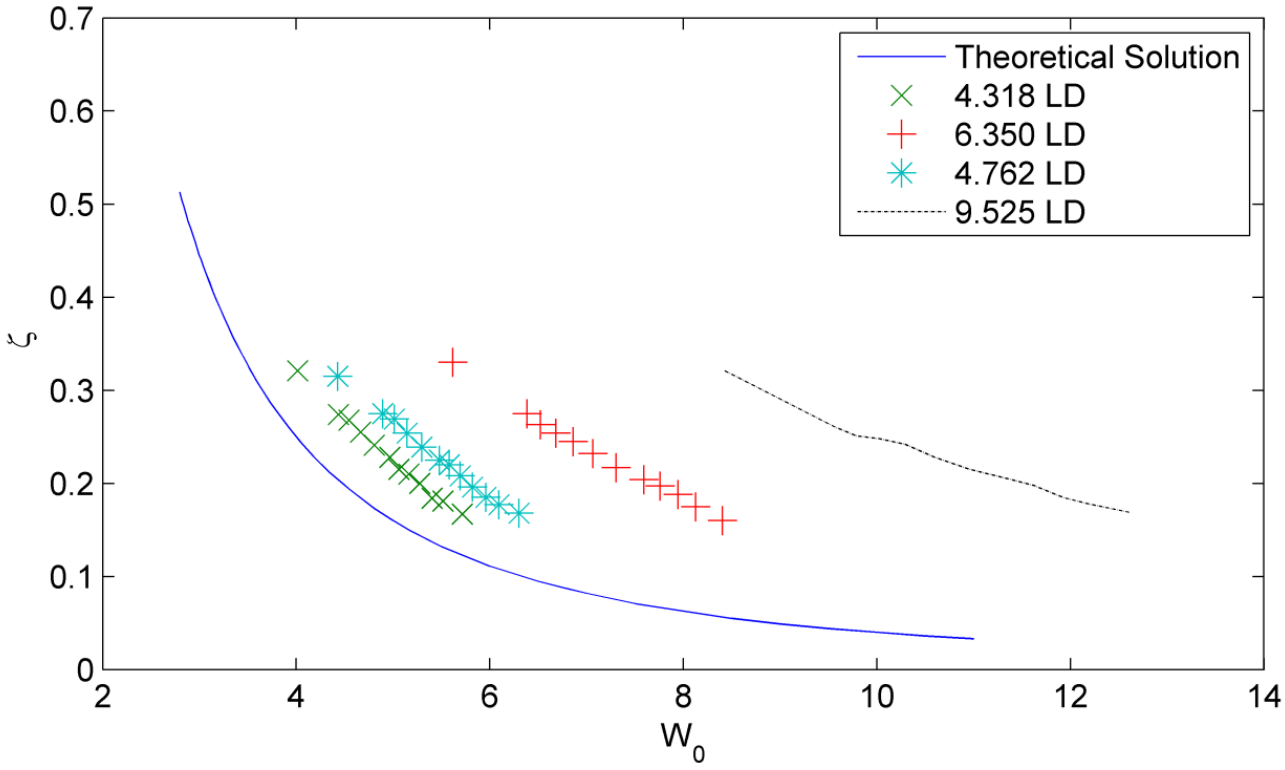

Figure 12: Dependency of $\boldsymbol{\zeta}$ on $\boldsymbol{W_0}$ based on log-decrement method

Table 7: Summary of log-decrement empirical correlations of ζ

Tube Size (mm)	Metric Correlation of Damping Ratio (ζ)
4.318	$\zeta = \frac{4.63}{W_0^{1.894}}$
4.762	$\zeta = \frac{5.44}{W_0^{1.88}}$
6.350	$\zeta = \frac{7.23}{W_0^{1.77}}$
9.525	$\zeta = \frac{9.30}{W_0^{1.58}}$

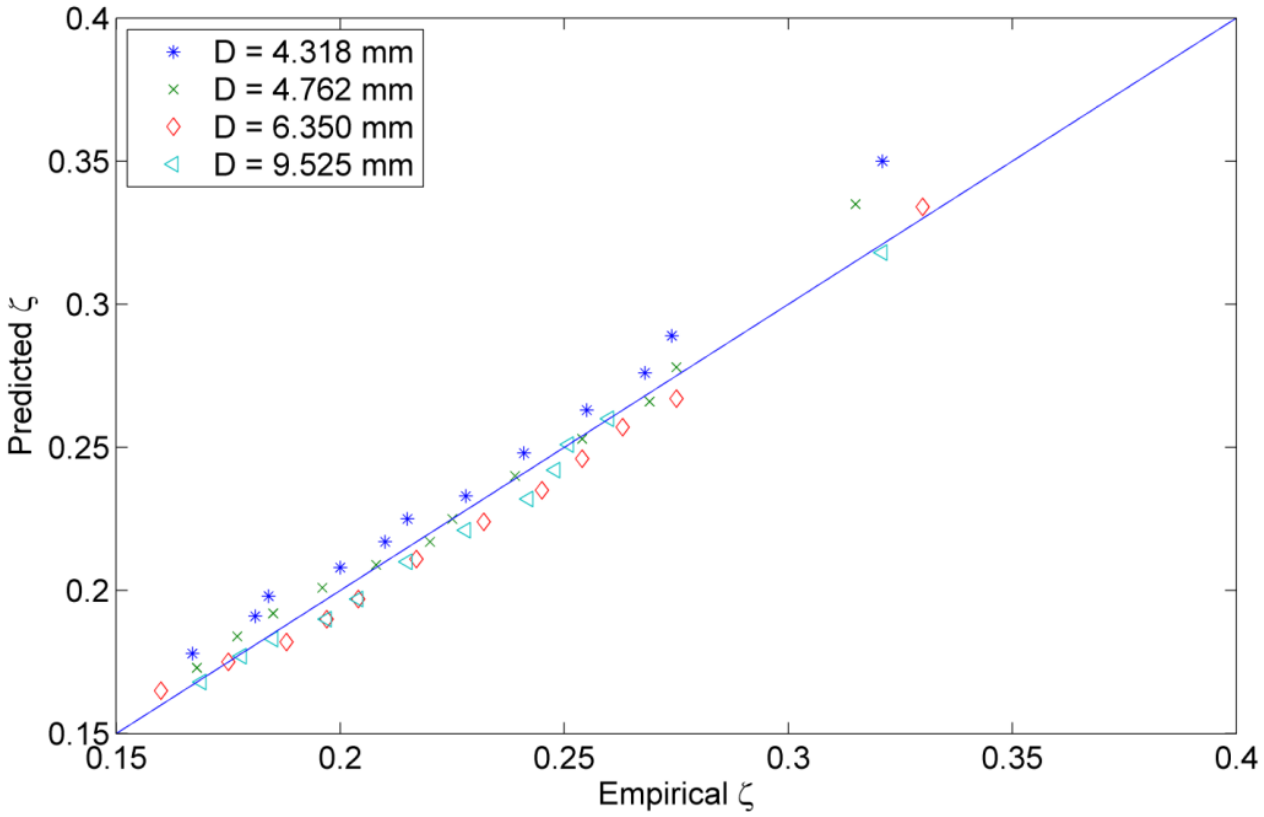

Figure 13: Predicted Damping vs. Empirical Damping

Through introducing another dimensionless parameter, the Keulegan-Carpenter number (KC), along with the Womersley number (W_0), a non-dimensional relation between the damping factor (ζ) and Womersley number (W_0) is established. The new modified analytical solution encompasses the additional forces that causes an increases damping that is not accounted for in the previous standard theoretical solution. The modified analytical solution seems to agree well with experimental damping results according to Figure 13. Table 8 contains a quantitative comparison of the two methods of computing the damping ratio (ζ) for different fluid lengths.

Table 8: Summary of ($\boldsymbol{\zeta}$) for different fluid lengths

	D = 3.175 mm		D = 4.318 mm		D = 4.762 mm		D = 6.35 mm		D = 9.525 mm	
L (cm)	ζ_{FR}	ζ_{LD}	ζ_{FR}	ζ_{LD}	ζ_{FR}	ζ_{LD}	ζ_{FR}	ζ_{LD}	ζ_{FR}	ζ_{LD}
40	0.251	N/A	0.258	0.167	0.257	0.168	0.265	0.160	0.276	0.169
50	0.275	N/A	0.278	0.184	0.281	0.185	0.282	0.188	0.288	0.185
60	0.292	N/A	0.292	0.210	0.293	0.208	0.29	0.204	0.291	0.204
70	0.318	N/A	0.303	0.228	0.303	0.225	0.301	0.217	0.294	0.215
80	0.324	N/A	0.314	0.241	0.311	0.239	0.308	0.232	0.297	0.228
90	0.341	N/A	0.320	0.255	0.319	0.254	0.313	0.245	0.304	0.242
100	0.347	N/A	0.338	0.268	0.325	0.269	0.317	0.254	0.313	0.248

4.0 CONCLUSION

The analytical second order model for U-tube manometer is found to be an insufficient model to characterize the behavior of fluid flow under a continuous oscillation due to unappropriated assumptions such as laminar parabolic flow and the inability to account for additional sources of damping. Most of the deviation between the simulated model and the empirical results is attributed to the flow reversal effect. During the ascending and descending of the fluid at the ends of the tube, the velocity profiles have to adjust to the sudden change of velocity caused by the driving force which results in an increase in the damping ratio (ζ) values. Empirical correlations are determined between the Womersley number and the damping ratio for continuous oscillation flow, and the tube diameter effect is accounted for by including the KC number, a common metric for a variety of oscillating flows. The natural frequency of the system under continuous oscillation is comparable to that of the damped oscillation, both of which agree well with the analytical prediction. The damped oscillation empirical trials indicate that a standard second order response model becomes valid as the tube diameter decreases, or as the driving pressure becomes large, both of which result in an increase in KC number. This work and the predictive correlations developed represent the first step in possibly implementing an oscillating liquid cooled thermal management solution because in forced oscillating flow inside a U-tube manometer, the two most important parameters are the natural frequency (ω_n) and the damping ratio (ζ). According to this study, it is possible to predict the dynamics of forced

oscillating flow where the natural frequency follows the analytical analysis and the damping ratio prediction is established according to the new developed correlations. The next step is to integrate the microchannel heat sink and analyze its impact on the dynamics of forced oscillating flow which will influence the natural frequency and damping.

4.1 FUTURE WORK (ADDITON OF MICROCHANNEL HEAT SINK)

In this section, discussion is made regarding the applicability of oscillating flow as a thermal management solution in the field of electronics cooling with the potential application of microchannels cooling [9]. Also, the additional parameters which should be studied are discussed with their potential impact on the flow behavior when a U-tube manometer is connected to a microchannel heat sink, as shown in Figure 14. Figure 14 does not represent the comprehensive thermal solution because heat carried by the liquid through microchannel will need to be transferred to a radiator so heat is rejected. Microchannel heat sinks with liquid cooling have proven to be an effective and suitable alternative cooling solution to air cooling for high heat-dissipation devices. A microchannel heat sink consists of arrangement of channels and fins. A microchannel heat sink is attached directly to the electronic component via a thermal paste to improve the conduction of heat to the microchannel base. The cooling fluid travels through the channels and transports the heat via forced convection. The thickness of the thermal boundary layer is small in microchannel heat sinks due to microscopic nature of the channel geometry [22]. As a result, microchannel heat sinks have shown significant cooling rates (large convective heat transfer coefficients) from small volumes. To optimize the heat rejection capacity of the system, laminar flow has shown the best ability to achieve high cooling rates. In small confined geometries,

the small flow rate inside the microchannel heat sink results in smooth (laminar) flow. This means that the Nusselt number is constant and the convective heat transfer coefficient becomes inversely proportional to the hydraulic diameter of a single channel. The smaller the channels in the heat sink, the higher the convective heat transfer coefficient [22]. The air blower utilized in the current research can create reasonably high pressure with low flow rates which ideal for microchannel heat sinks, but air within heated microchannels is known to be problematic due to choking of the flow from moderate to extreme density changes within the channel. To mitigate such issues, the working fluid should be a liquid.

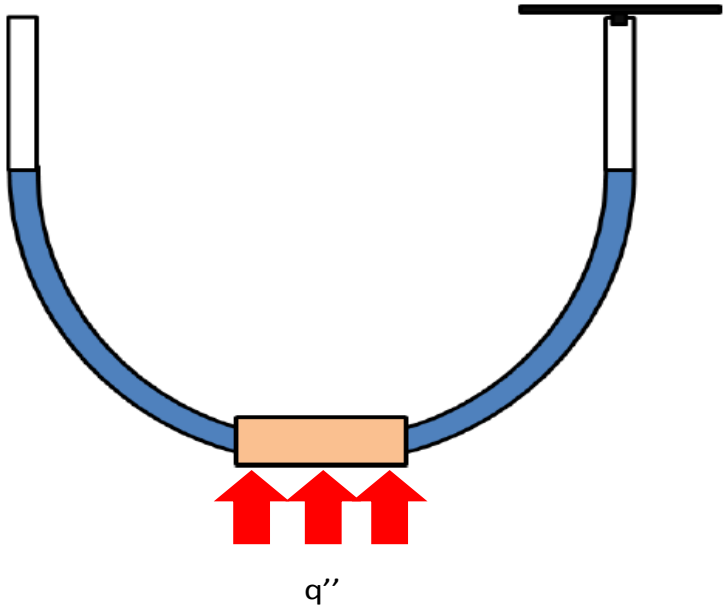

Figure 14: A sketch of a U-tube oscillating flow system connected to a microchannel heat sink [9]

The continuous oscillating flow model is able to predict the natural frequency and damping ratio of the system, but further analysis is needed to couple this with the behavior of microchannel heat sinks in combination with a U-tube manometer. Based on Figure 14, the

addition of the microchannel can have a significant impact on the dynamics of the flow. The presence of the microchannel heat sink introduces additional pressure losses, which show up in the differential equation as added damping terms. This increase in damping ratio, can ultimately affect the natural frequency as well, both of which can affect the overall flow rate, a key metric for electronics cooling applications. It is anticipated that one could accommodate the change in flow cross section from a large tube to multiple microchannels by included standard frictional losses for such geometries. This could be implemented in the governing equations providing the potential to even model this analytically. When properly armed with the dynamic response, one could then easily predict the flow rate through the microchannels, which then provides the metrics needed for designing a thermal management solution based on an oscillating flow.

For the analysis, one would expect some simplifications to be warranted. Considering a set of microchannels that are designed to be used in the water cooling of a computer chip as shown in Figure 15, one could take the hydraulic diameter (D_h) of the channel cross section according to Eq. (23).

$$D_h = \frac{h_c w_c}{2(h_c + w_c)} = 0.179 \times 10^{-3} m \tag{23}$$

Taking the viscosity of water ($1.084 \times 10^{-6}\, m^2/s$) and assuming a fluid column length of 60 cm (suggesting natural frequency of 0.91 Hz or 5.7 rad/s), the Womersley number (W_0), can then easily be calculated according to Eq. (1), W_0 = 0.215. For the experimental data in the previous chapters, the smallest W_o encountered is around 3. For microchannels, the ability to assume a small W_o enables simplifications to be made in the analysis. For example, the velocity profile can be assumed to be parabolic, or at least behave according to a standard steady flow, especially if enough pressure is applied to exchange fluid through the entire microchannel length, which would suggest a high KC number is achieved.

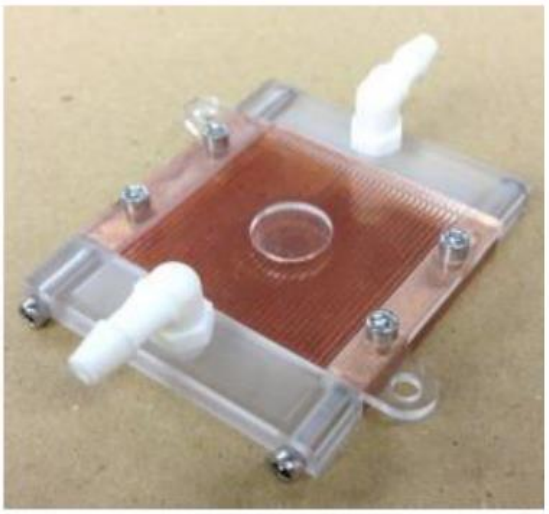

Parameter	Value
Channel Height, h_c	0.787 mm
Channel Width, w_c	0.660 mm
Channel Length, l_c	30.0 mm
Number of Channels, n_c	36

Figure 15: An image of a sample microchannel and the corresponding dimensions [9]

This application should be investigated more thoroughly. This includes developing a solution and validating through detailed experiments. Once a complete set of predictive tools is established for the flow behavior, efforts should turn to characterizing the thermal performance for oscillating flows through the microchannel heat sink.

APPENDIX A

EXPERIMENTAL TRIALS OF FORCED OSCILLATION

The remaining experimental trials for the forced oscillation are listed in this section of the paper. There are a total of five different tube sizes that are utilized to conduct the experimental trials. The tube sizes of 9.525 mm and 6.35 have a fluid length rage from 40 cm to 200 cm (see Figure 16 -Figure 36), while the remaining tube sizes have a fluid length range from 40 cm to 165 cm (see Figure 37 - Figure 67). Also there are tables (see Table 9- Table 13) that summarize the natural frequency and damping ratio results for all the empirical trials based on the second order model input to the curve fit tool in MATLAB.

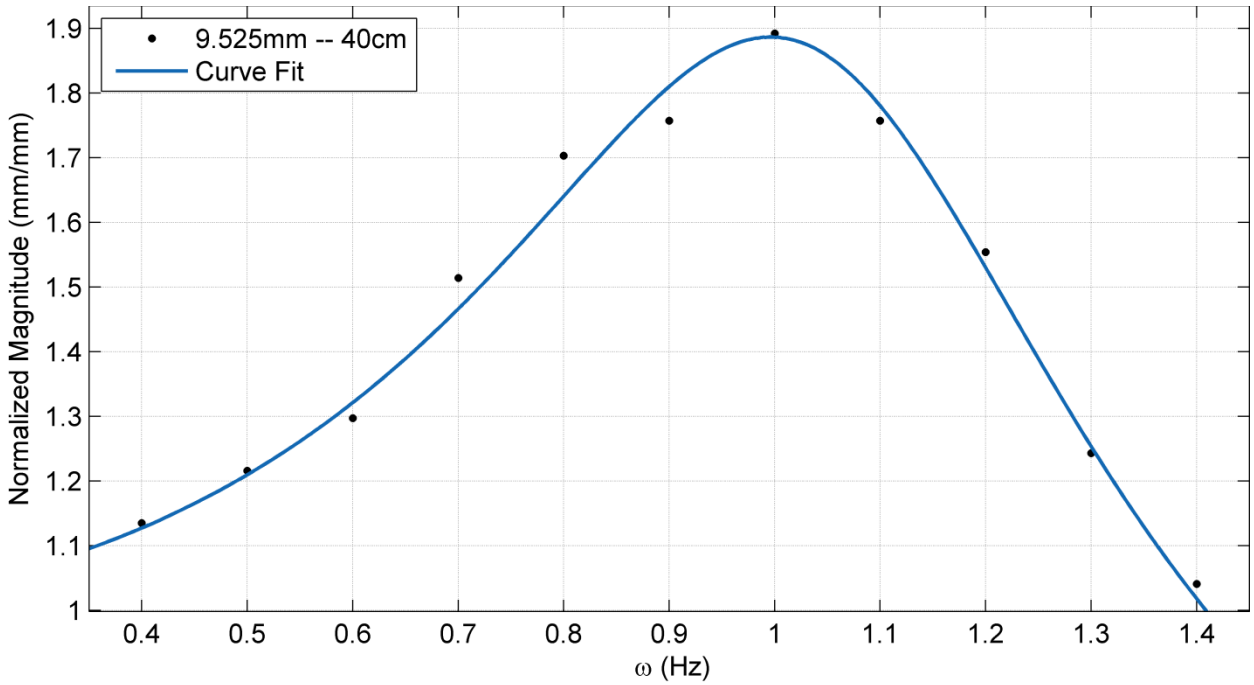

Figure 16: Trial for 9.525 mm with 40 cm in fluid length

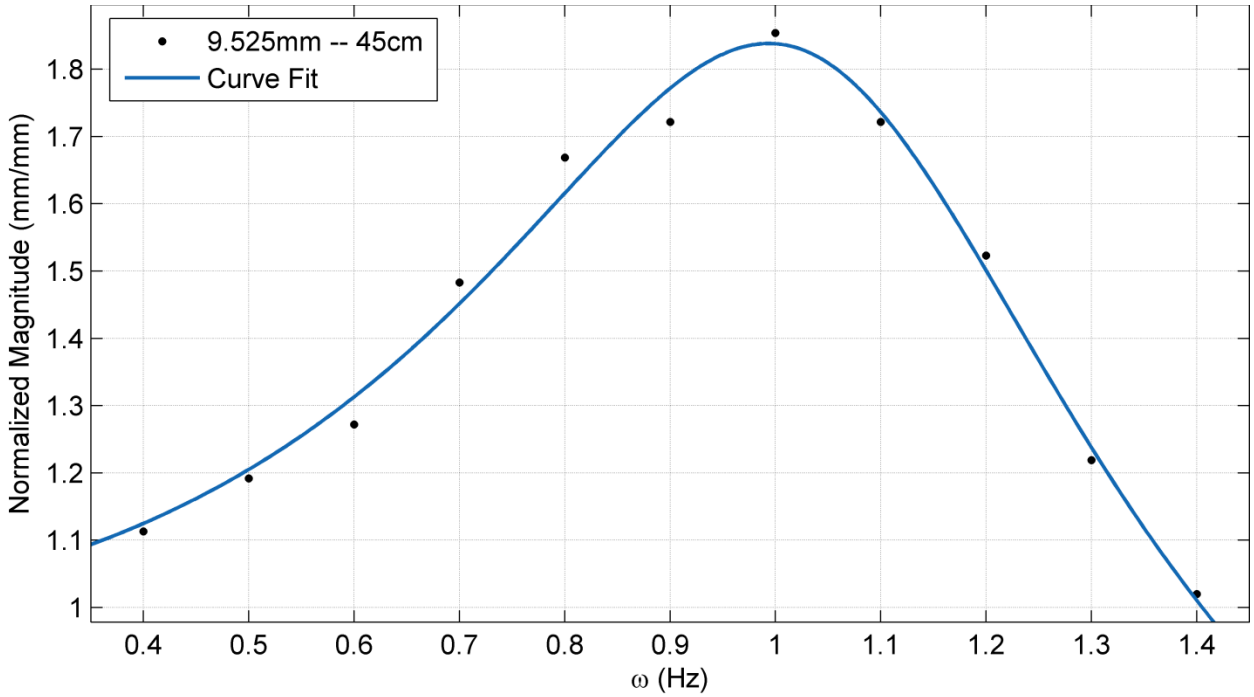

Figure 17: Trial for 9.525 mm with 45 cm in fluid length

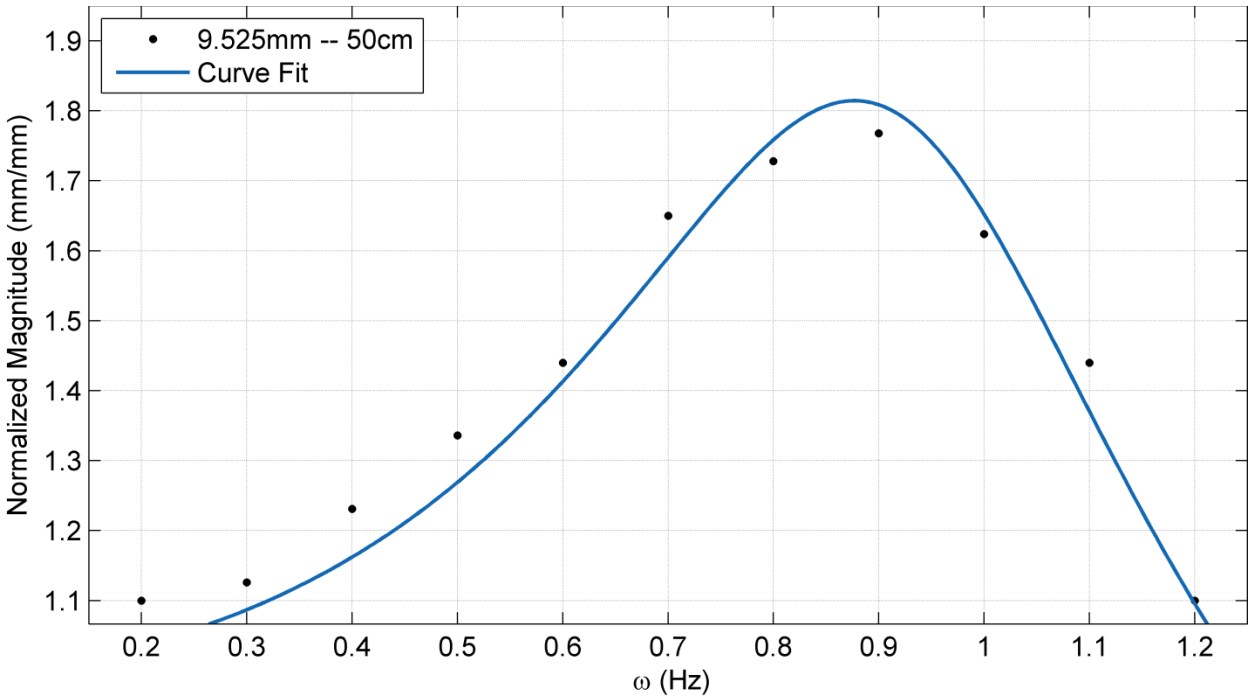

Figure 18: Trial for 9.525 mm with 50 cm in fluid length

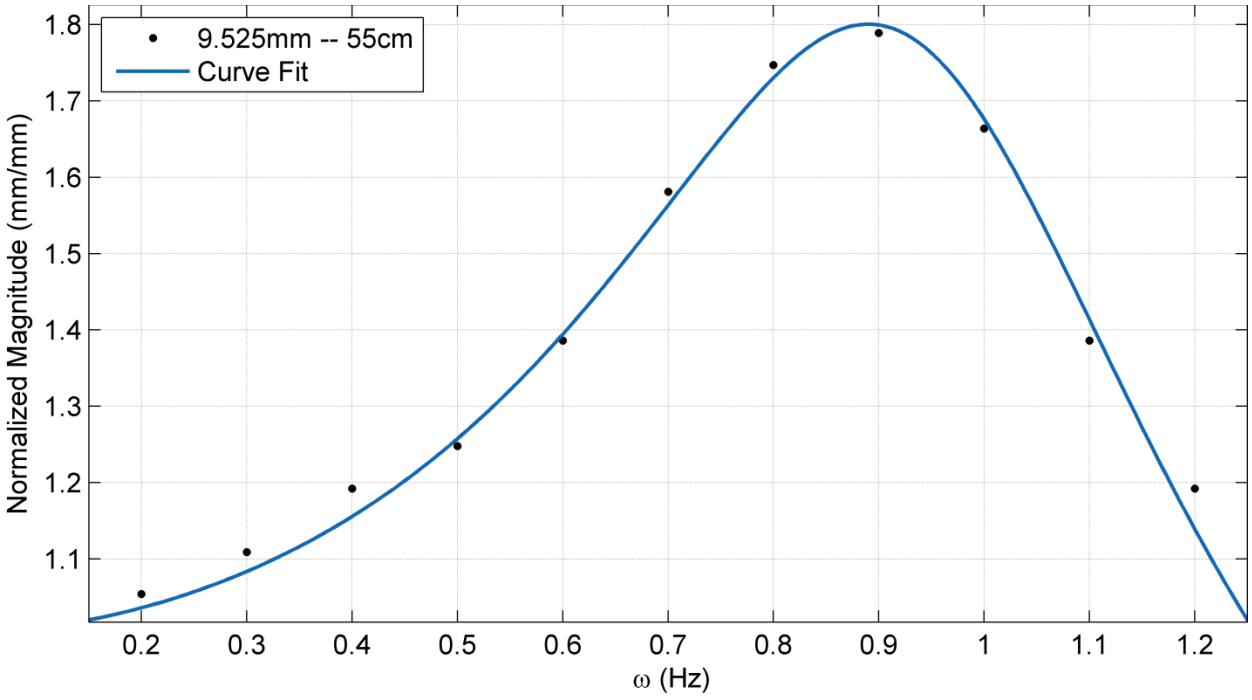

Figure 19: Trial for 9.525 mm with 55 cm in fluid length

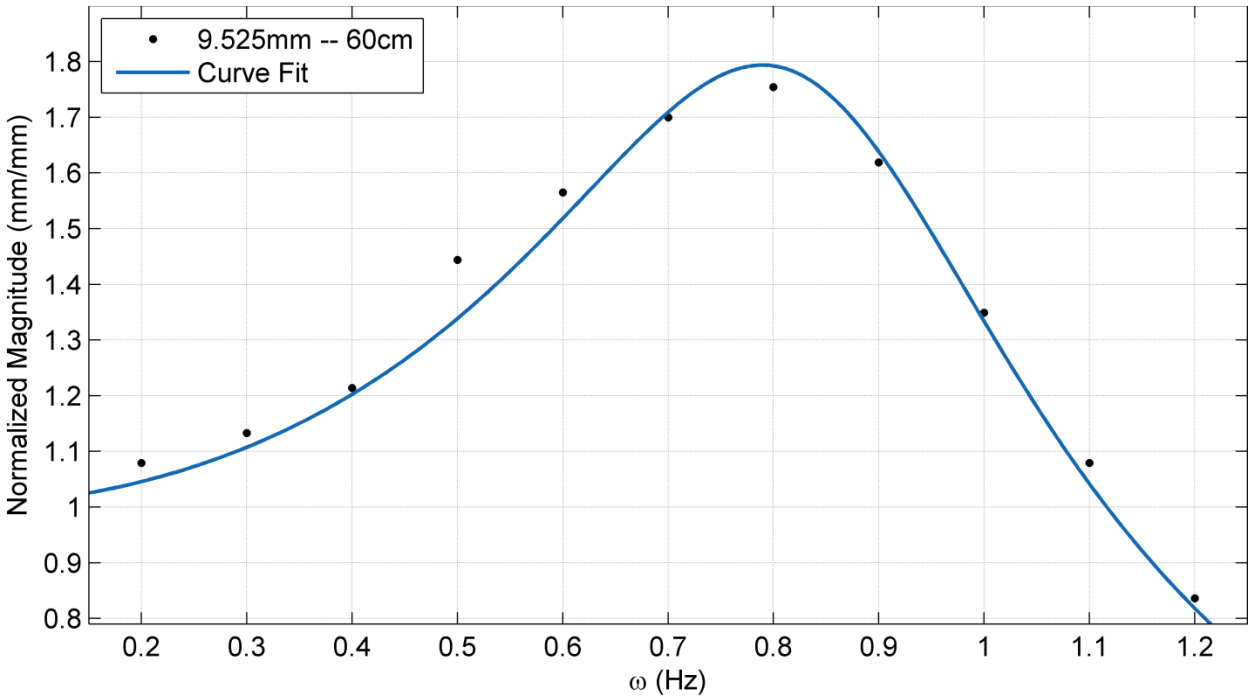

Figure 20: Trial for 9.525 mm with 60 cm in fluid length

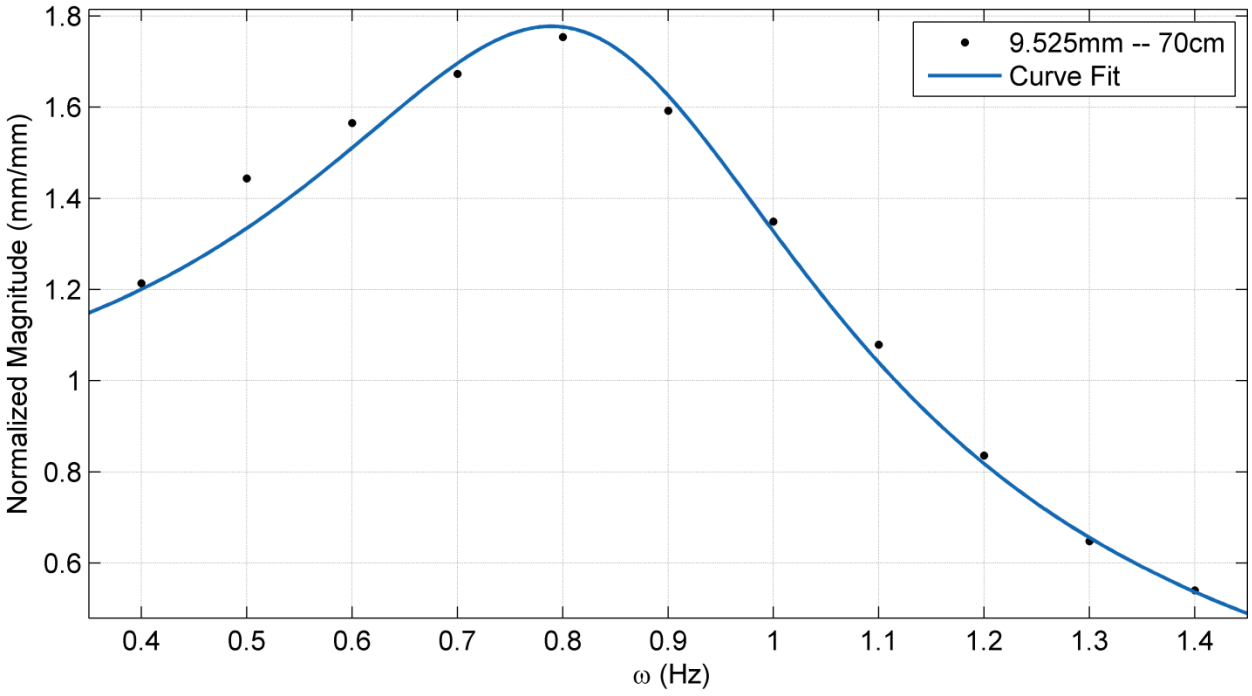

Figure 21: Trial for 9.525 mm with 70 cm in fluid length

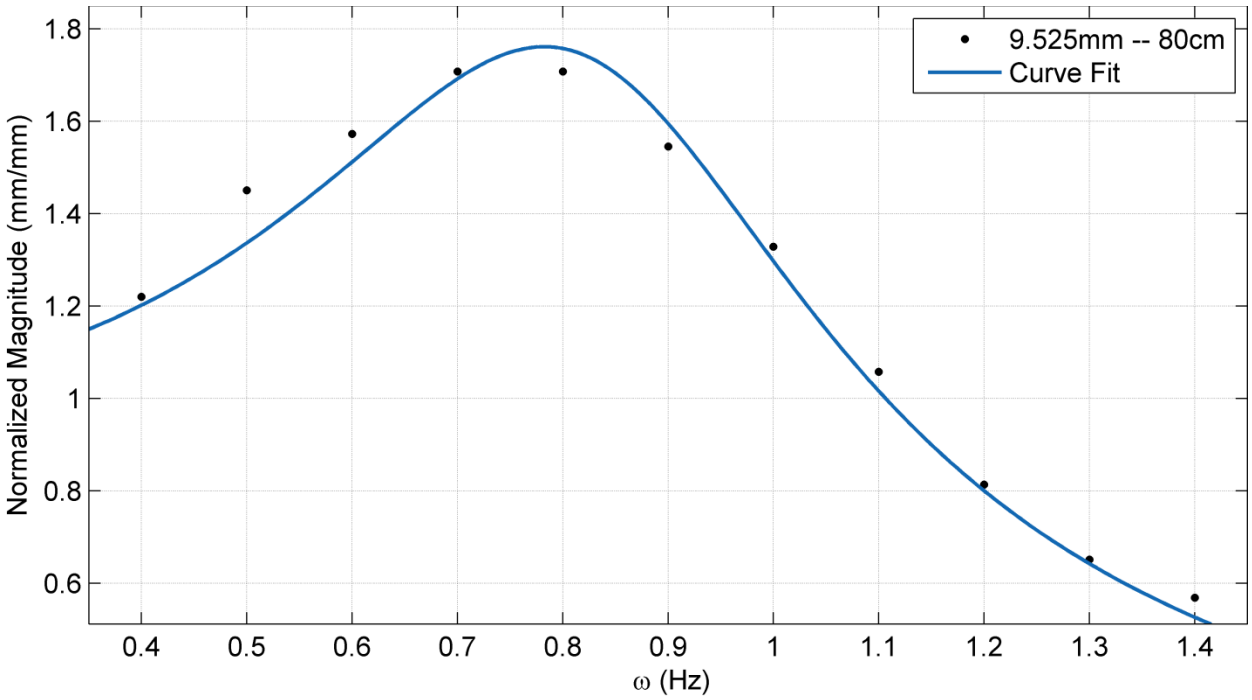

Figure 22: Trial for 9.525 mm with 80 cm in fluid length

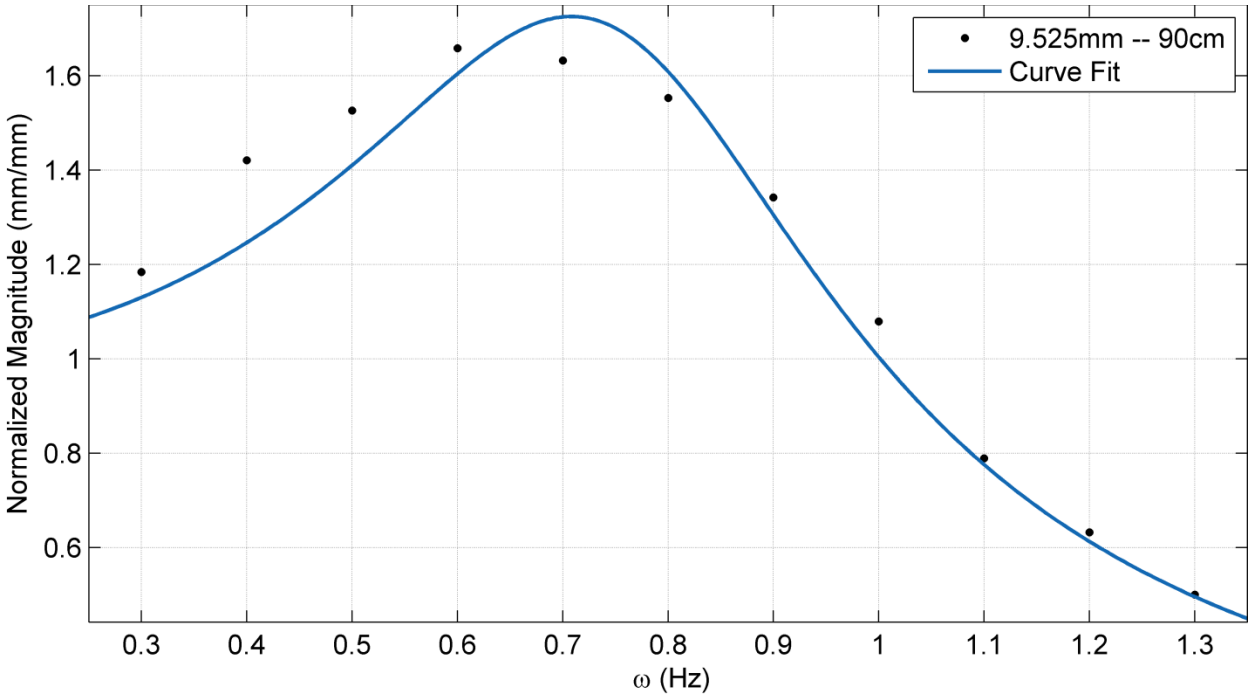

Figure 23: Trial for 9.525 mm with 90 cm in fluid length

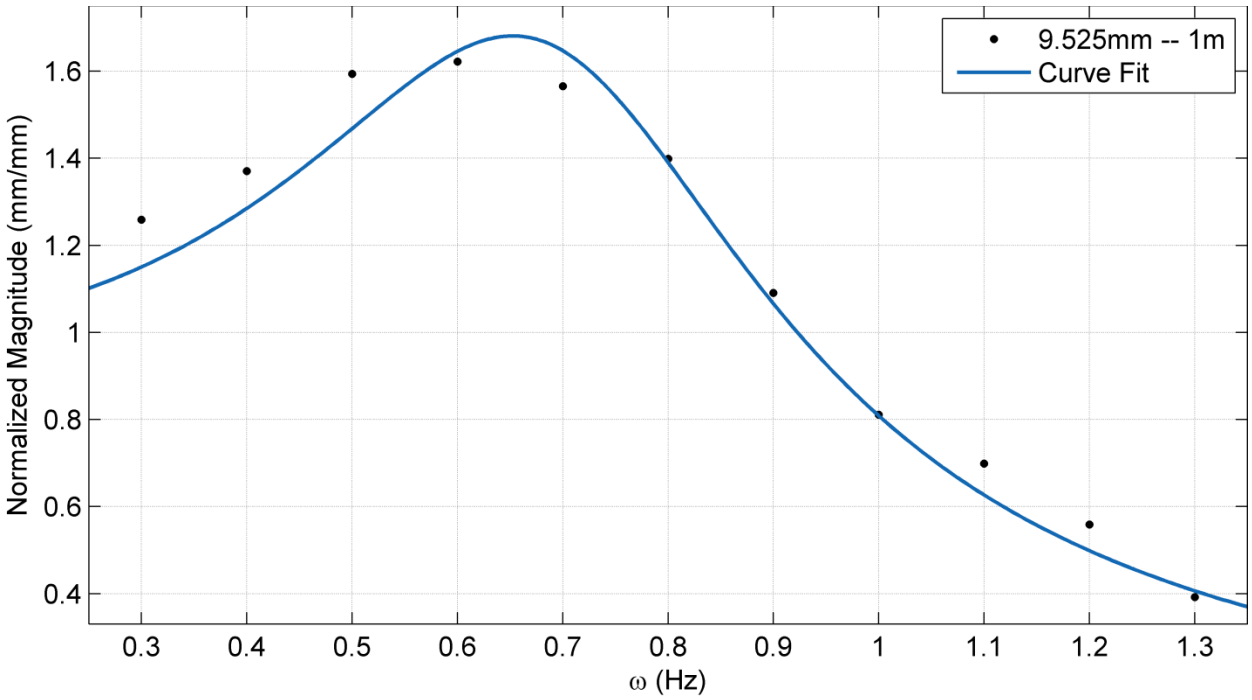

Figure 24: Trial for 9.525 mm with 100 cm in fluid length

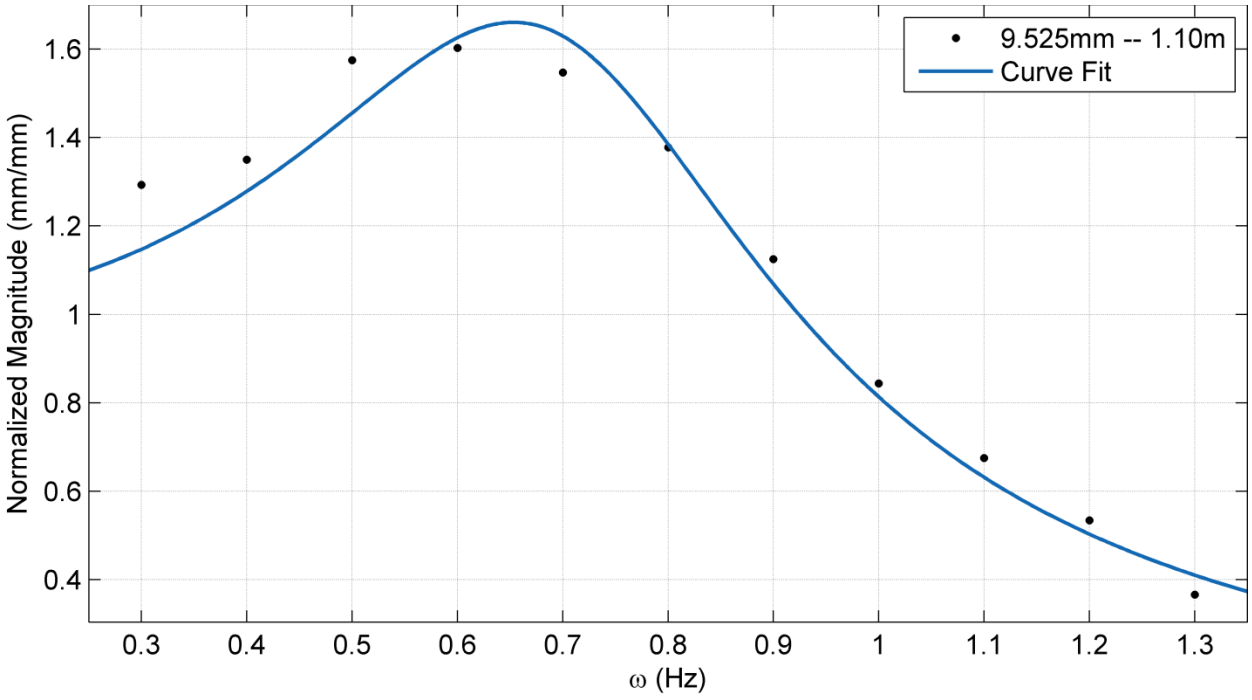

Figure 25: Trial for 9.525 mm with 110 cm in fluid length

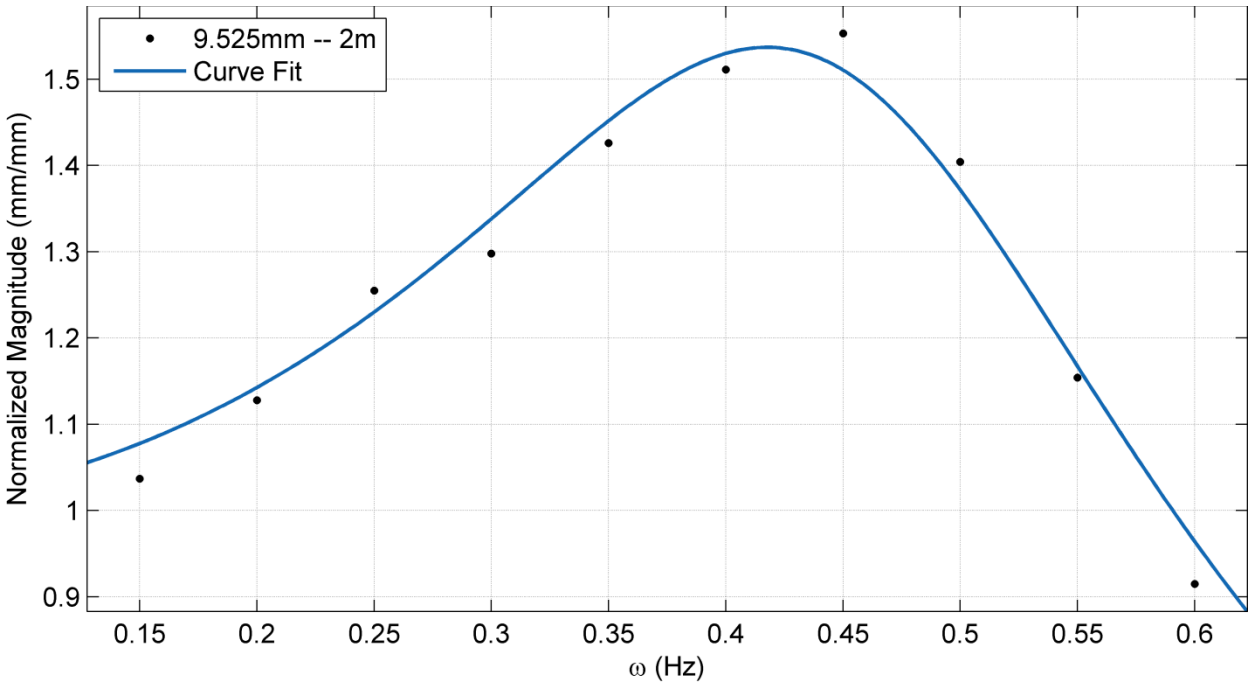

Figure 26: Trial for 9.525 mm with 200 cm in fluid length

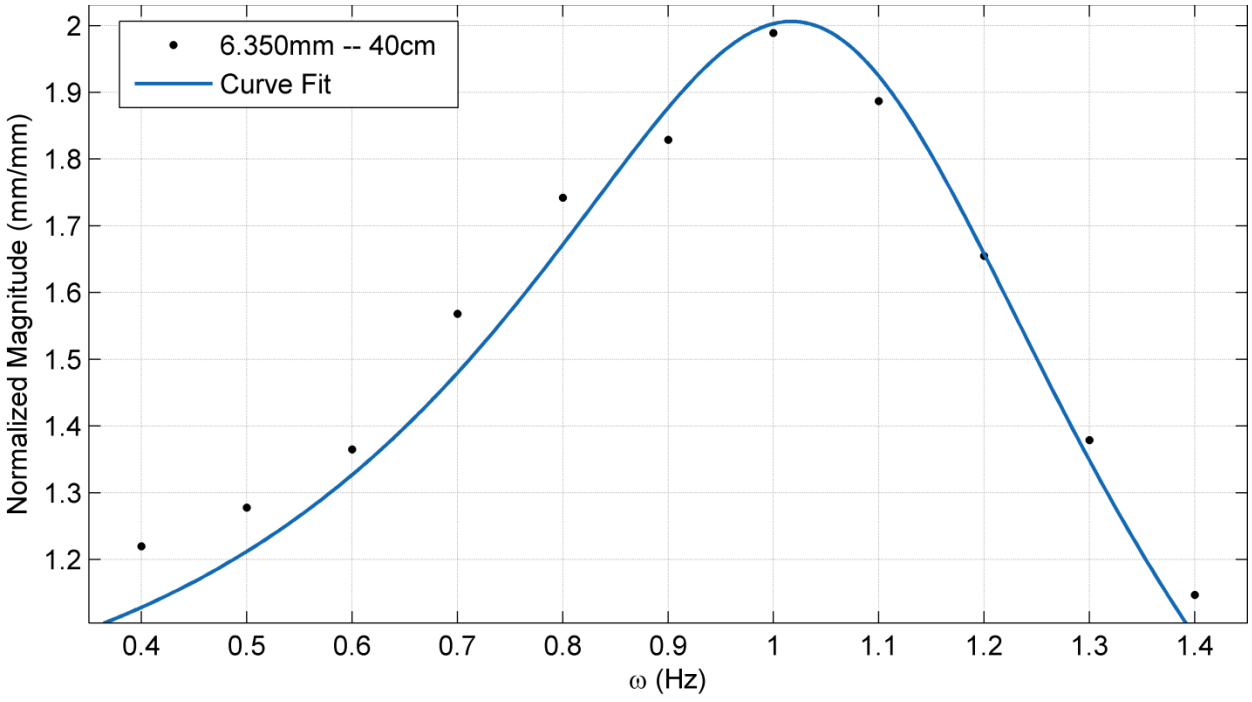

Figure 27: Trial for 6.350 mm with 40 cm in fluid length

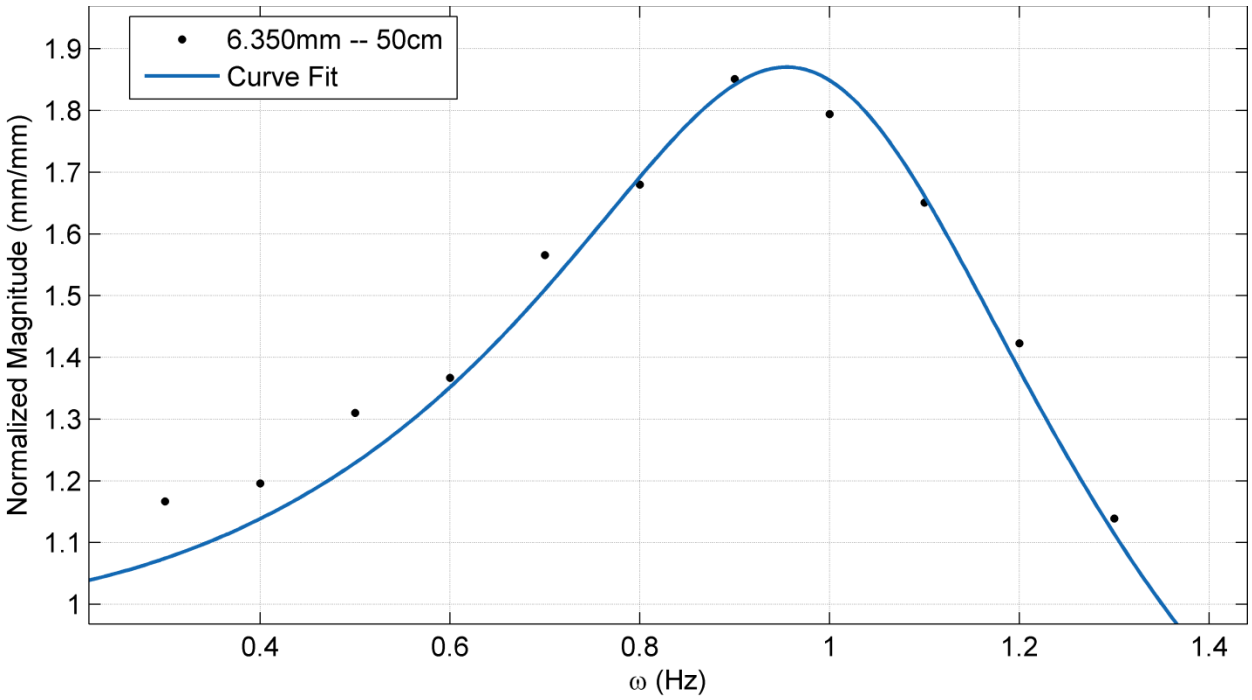

Figure 28: Trial for 6.350 mm with 50 cm in fluid length

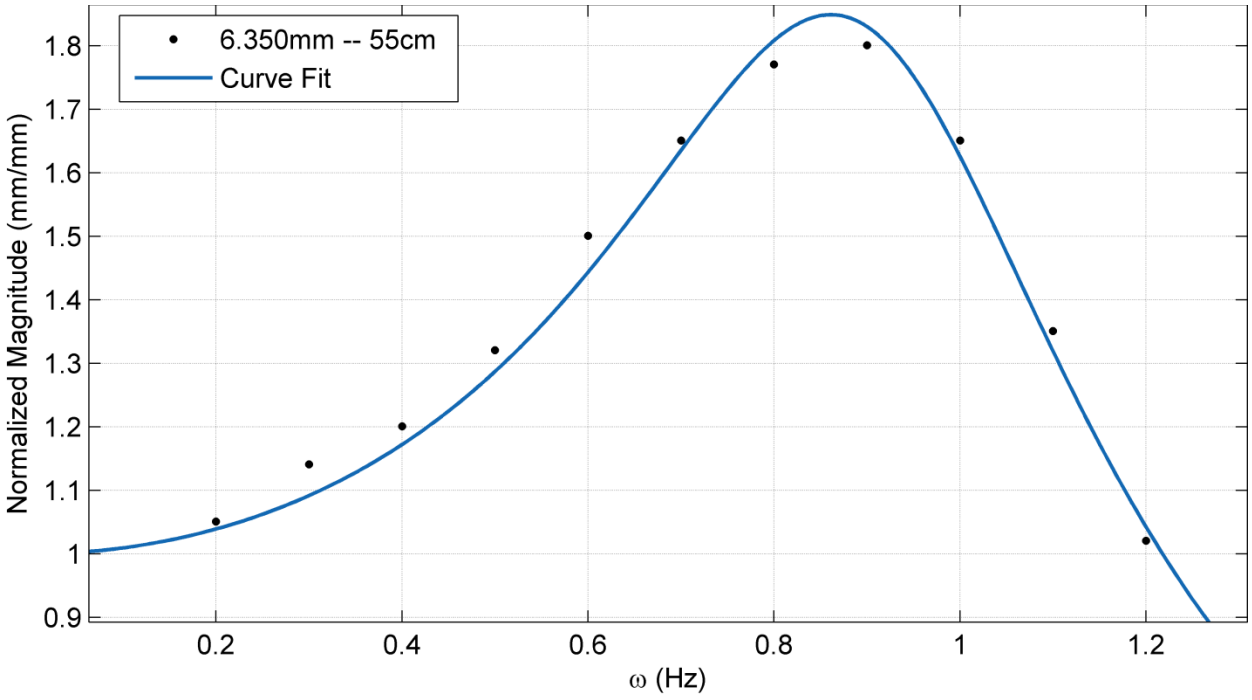

Figure 29: Trial for 6.350 mm with 55 cm in fluid length

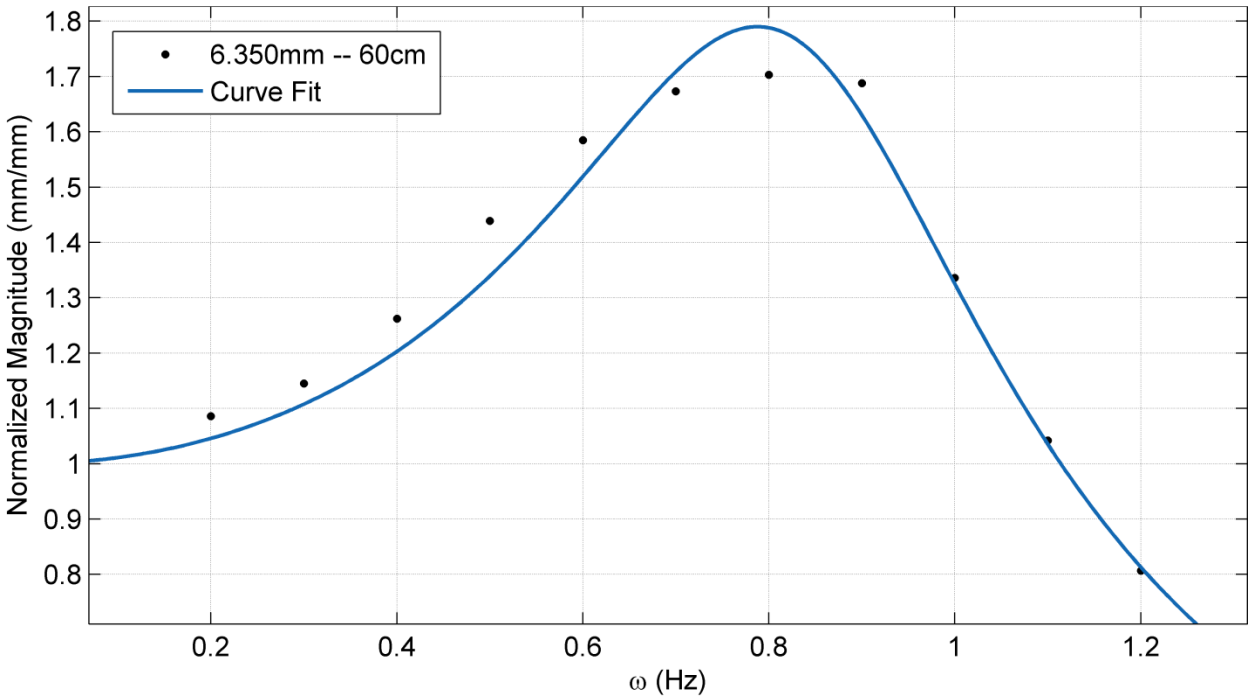

Figure 30: Trial for 6.350 mm with 60 cm in fluid length

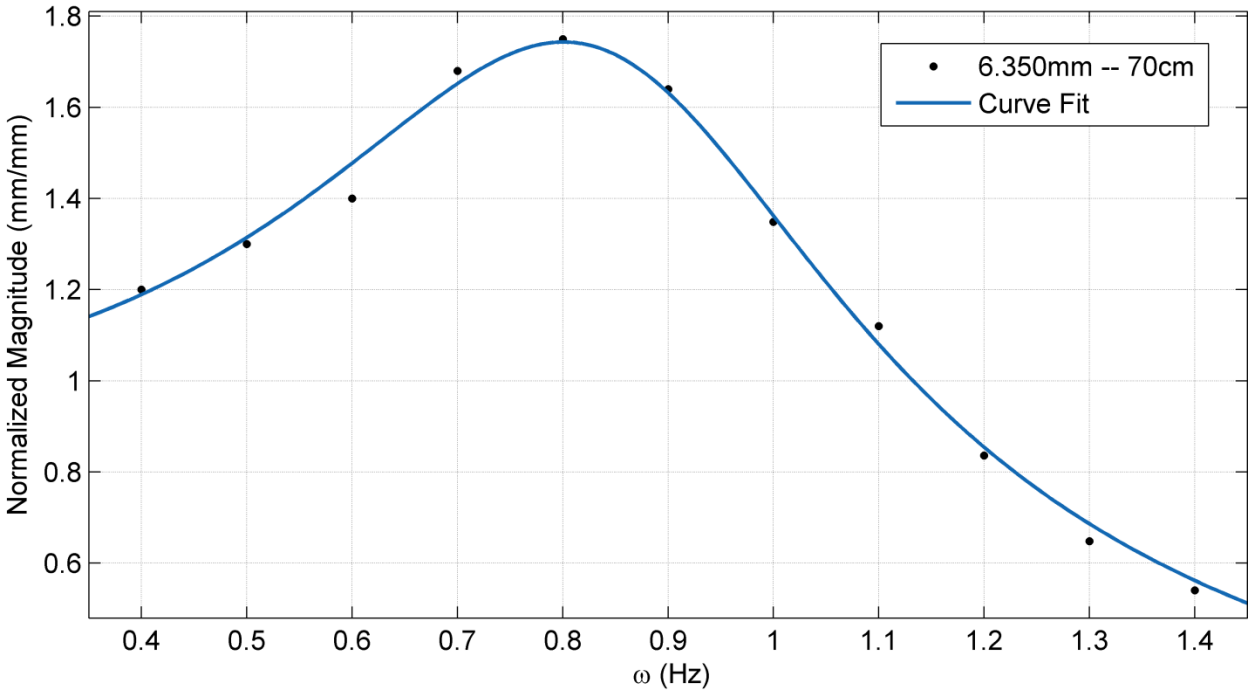

Figure 31: Trial for 6.350 mm with 70 cm in fluid length

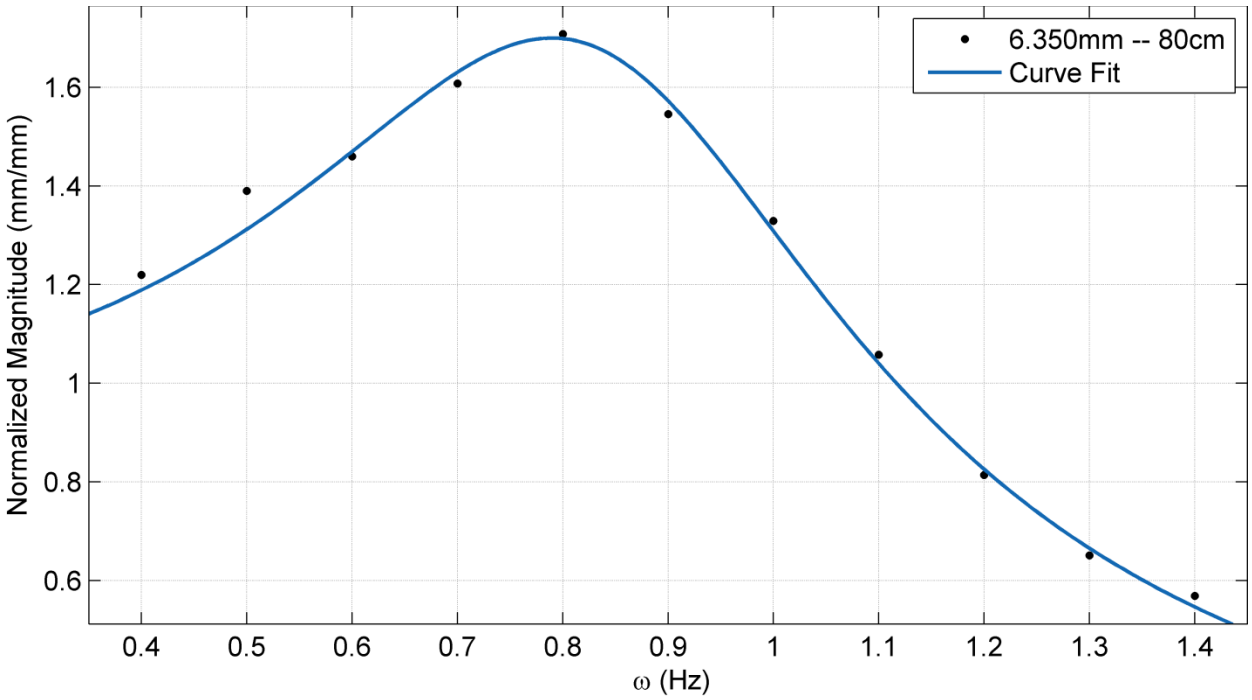

Figure 32: Trial for 6.350 mm with 80 cm in fluid length

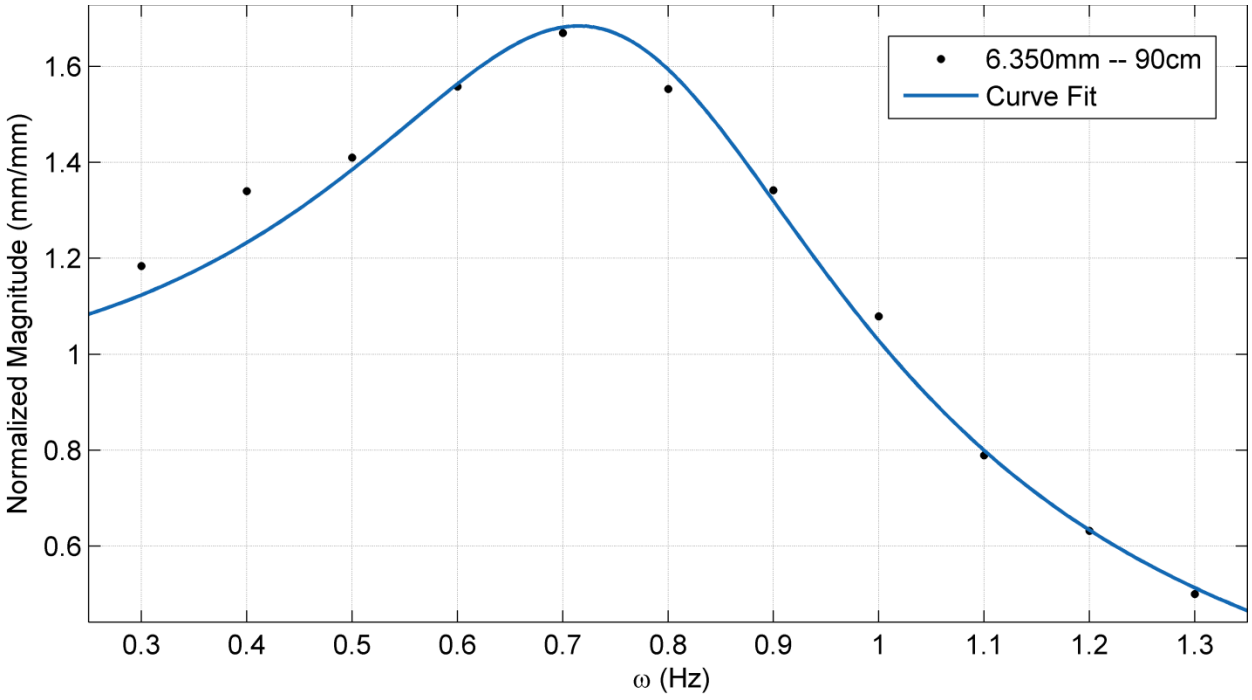

Figure 33: Trial for 6.350 mm with 90 cm in fluid length

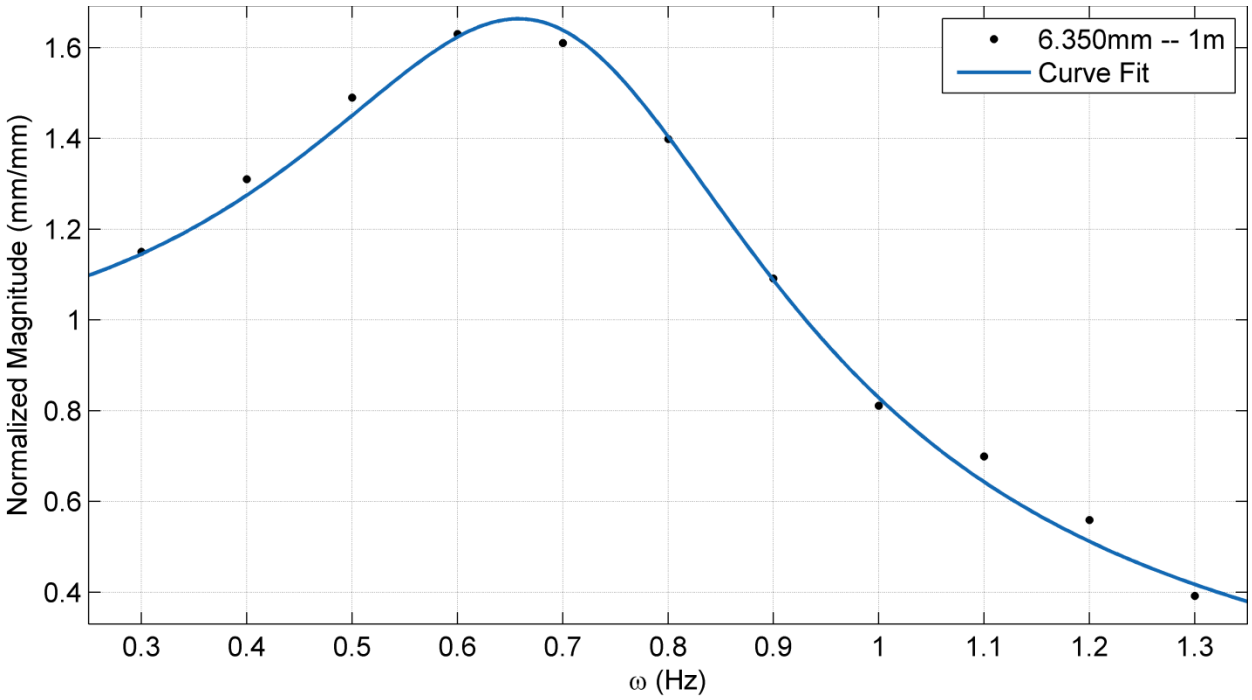

Figure 34: Trial for 6.350 mm with 100 cm in fluid length

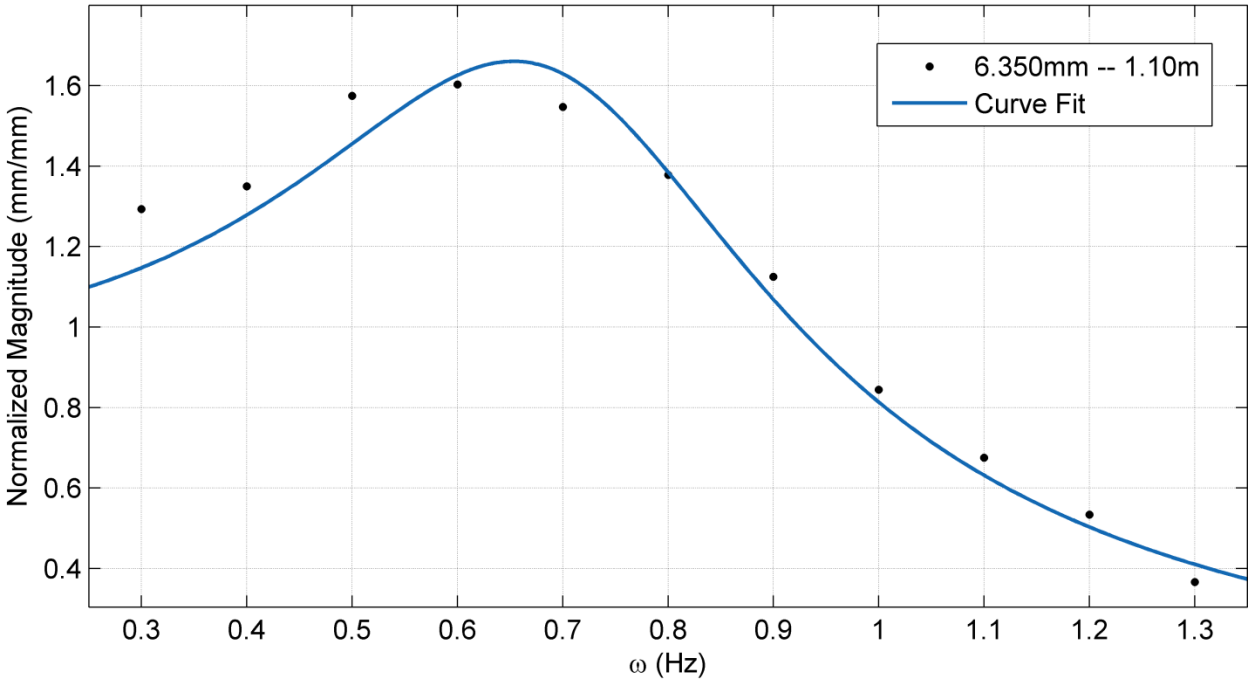

Figure 35: Trial for 6.350 mm with 110 cm in fluid length

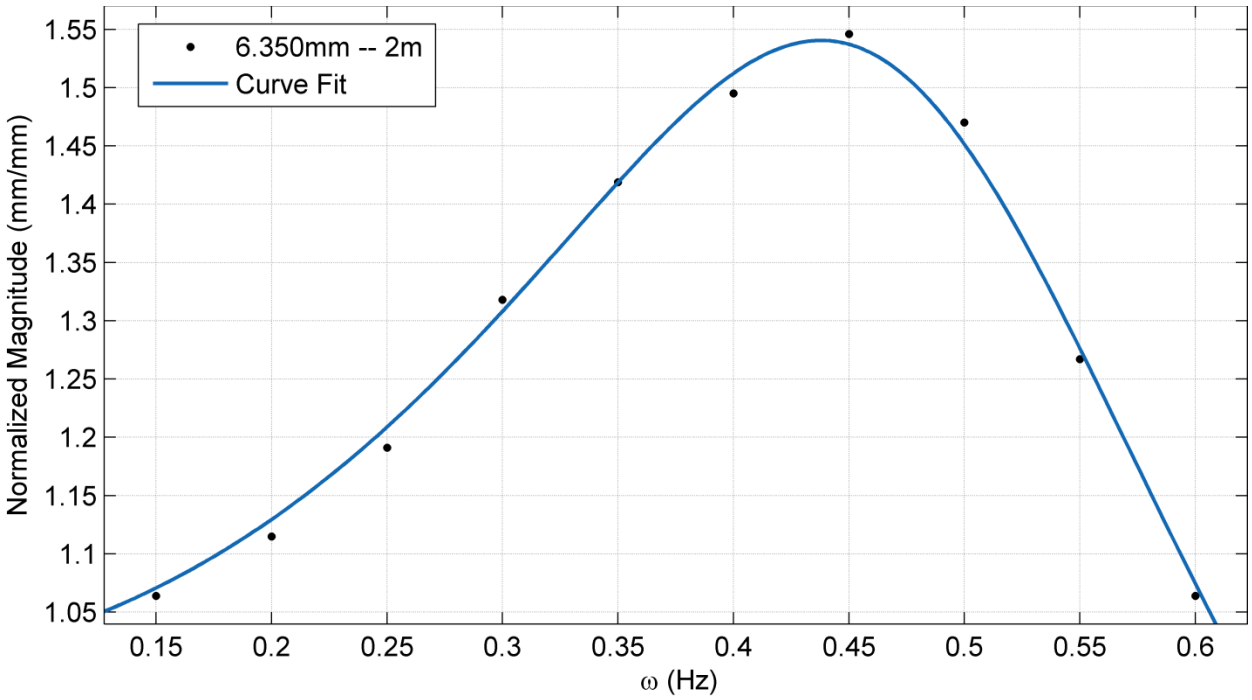

Figure 36: Trial for 6.350 mm with 200 cm in fluid length

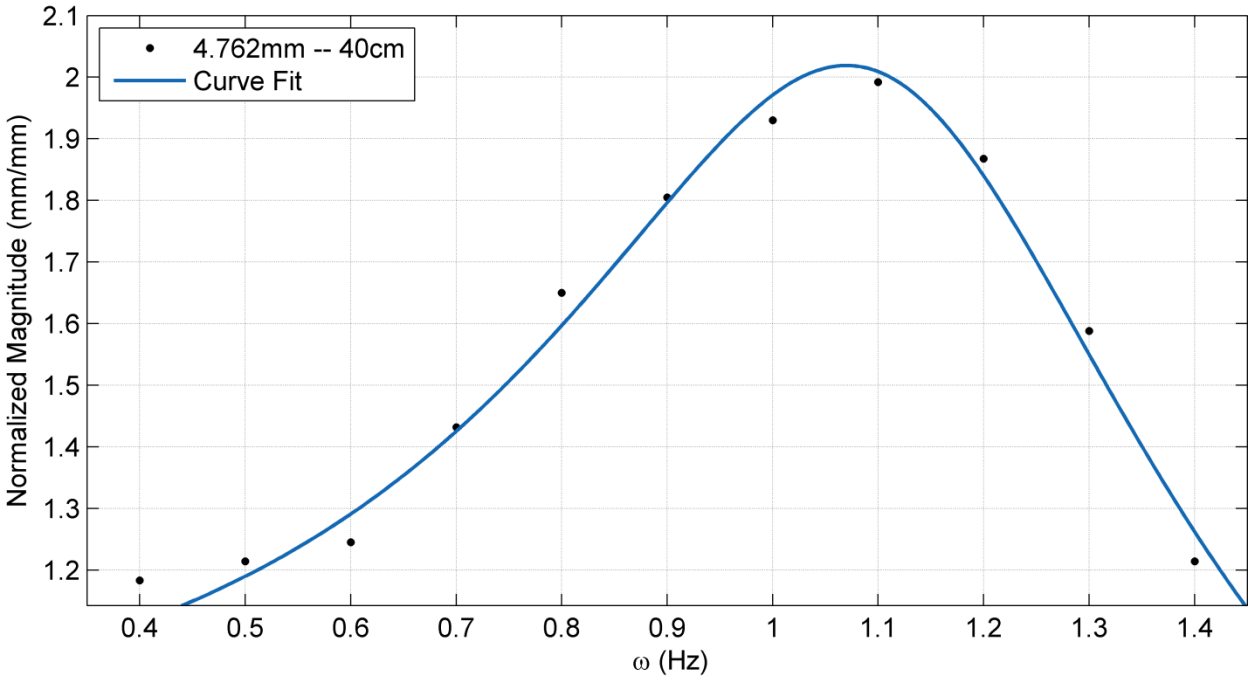

Figure 37: Trial for 4.762 mm with 40 cm in fluid length

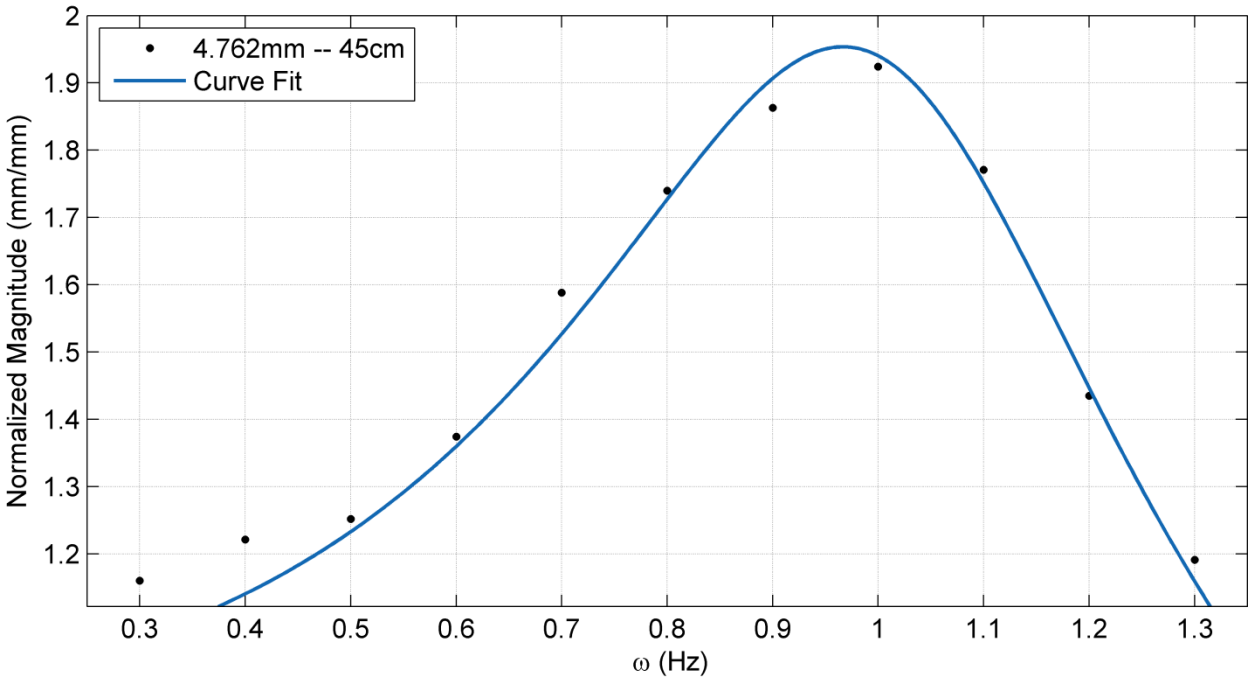

Figure 38: Trial for 4.762 mm with 45 cm in fluid length

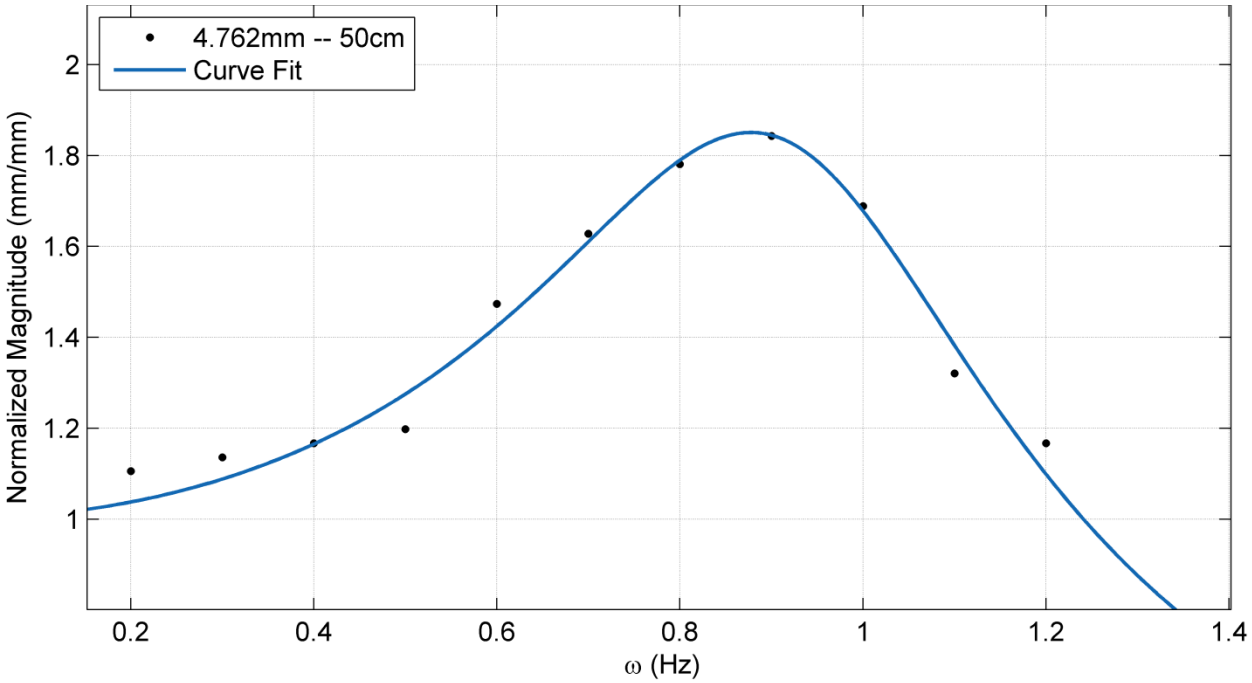

Figure 39: Trial for 4.762 mm with 50 cm in fluid length

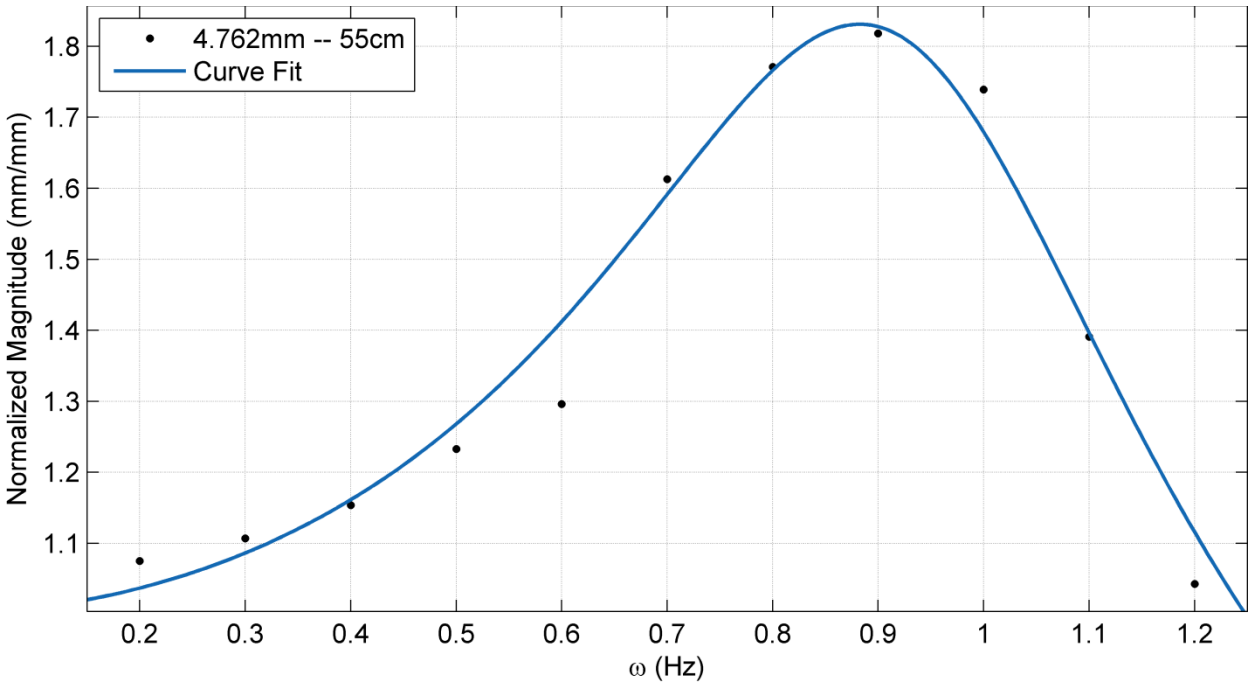

Figure 40: Trial for 4.762 mm with 55 cm in fluid length

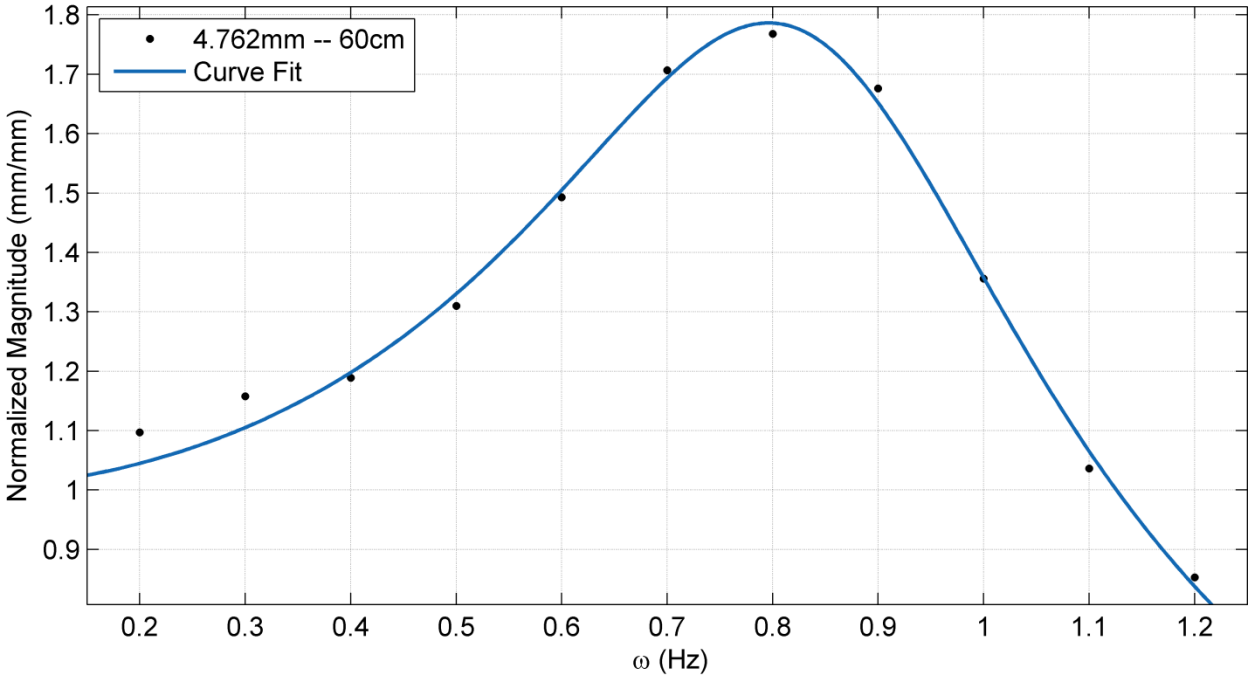

Figure 41: Trial for 4.762 mm with 60 cm in fluid length

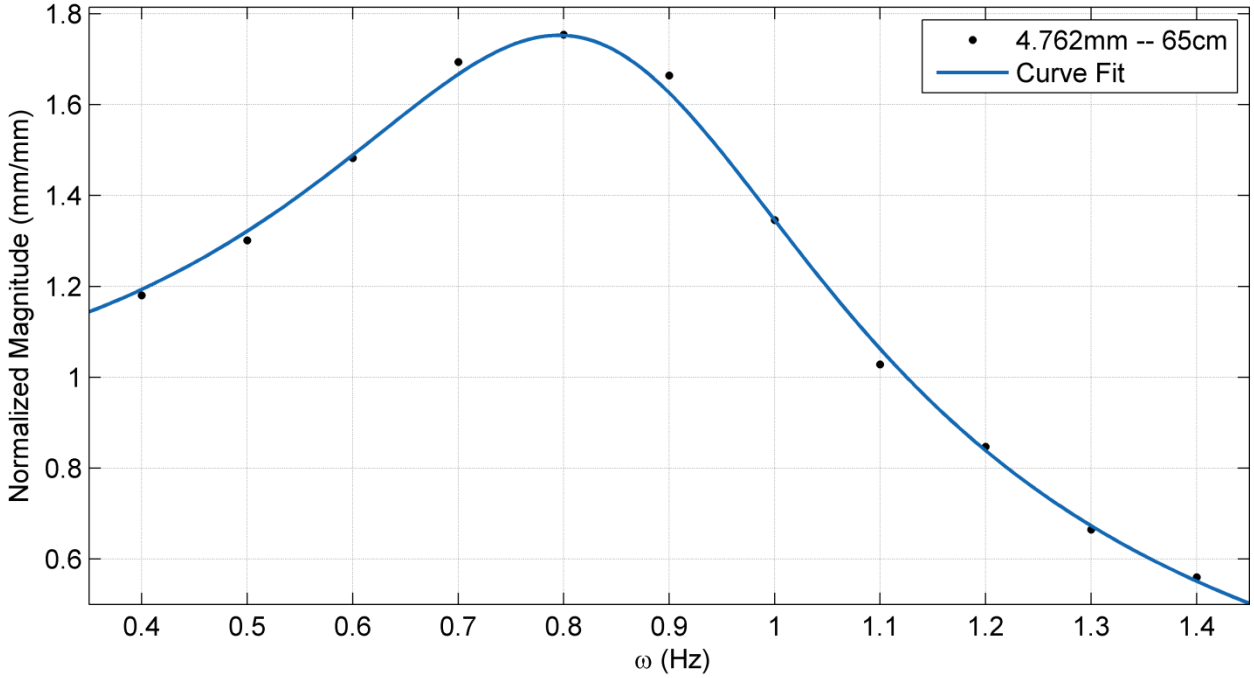

Figure 42: Trial for 4.762 mm with 65 cm in fluid length

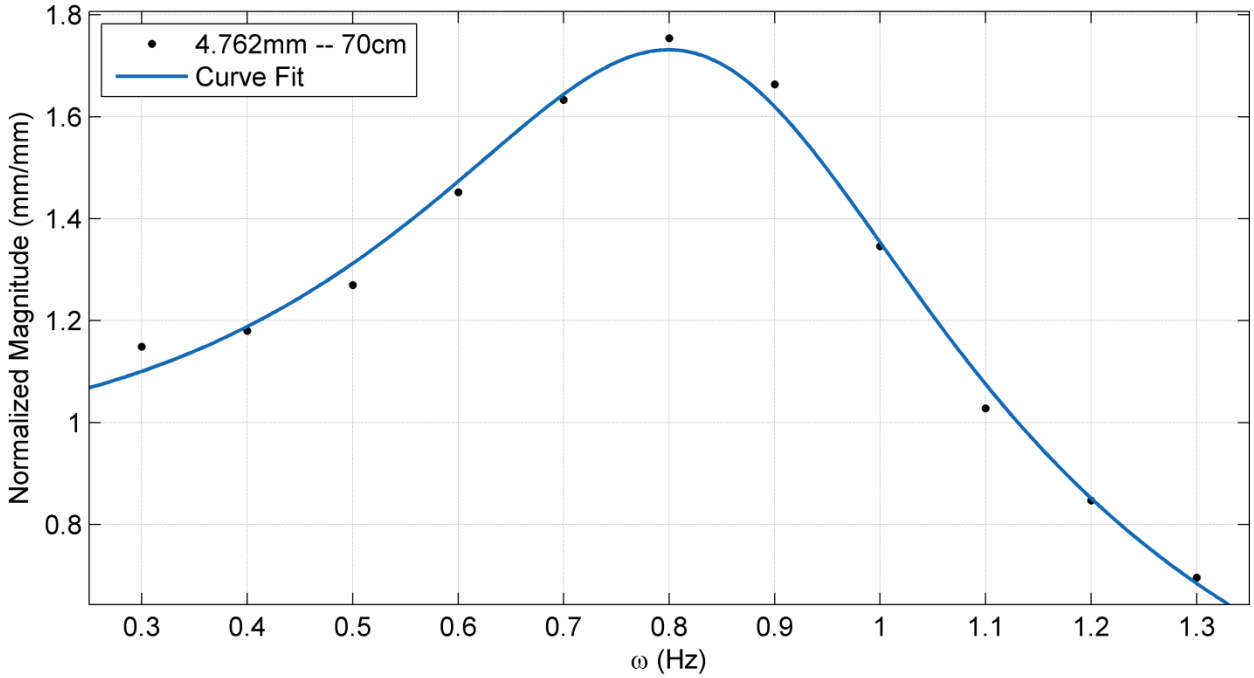

Figure 43: Trial for 4.762 mm with 70 cm in fluid length

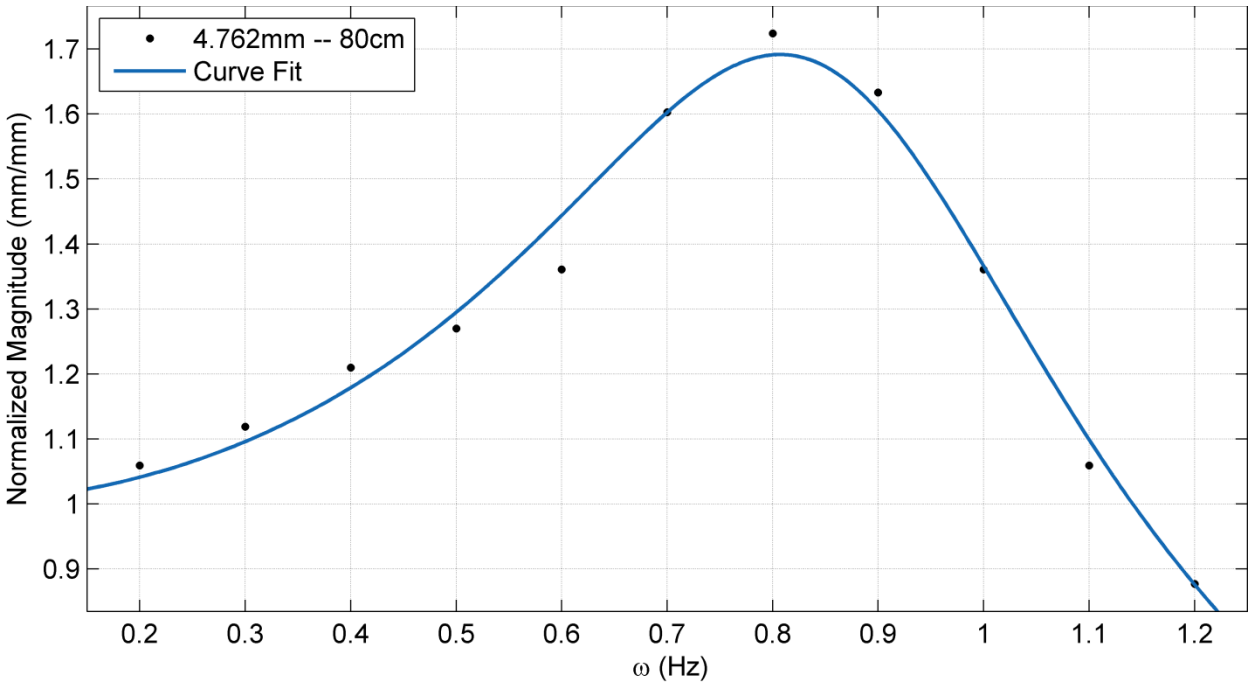

Figure 44: Trial for 4.762 mm with 80 cm in fluid length

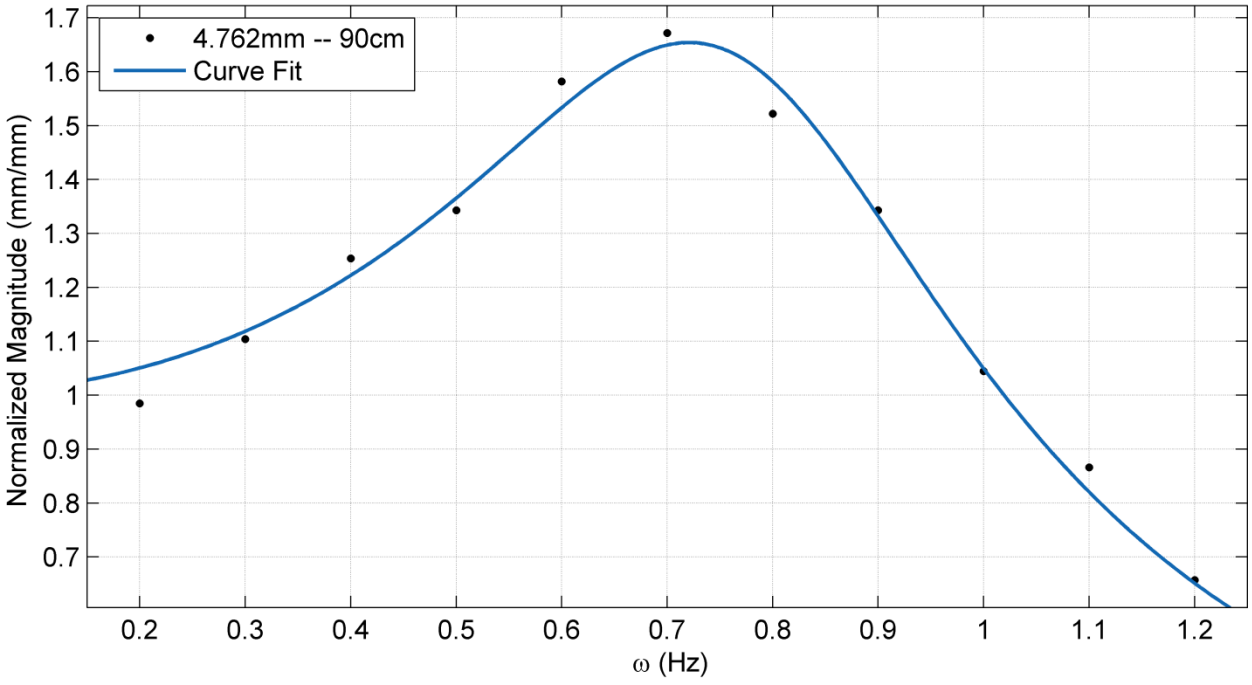

Figure 45: Trial for 4.762 mm with 90 cm in fluid length

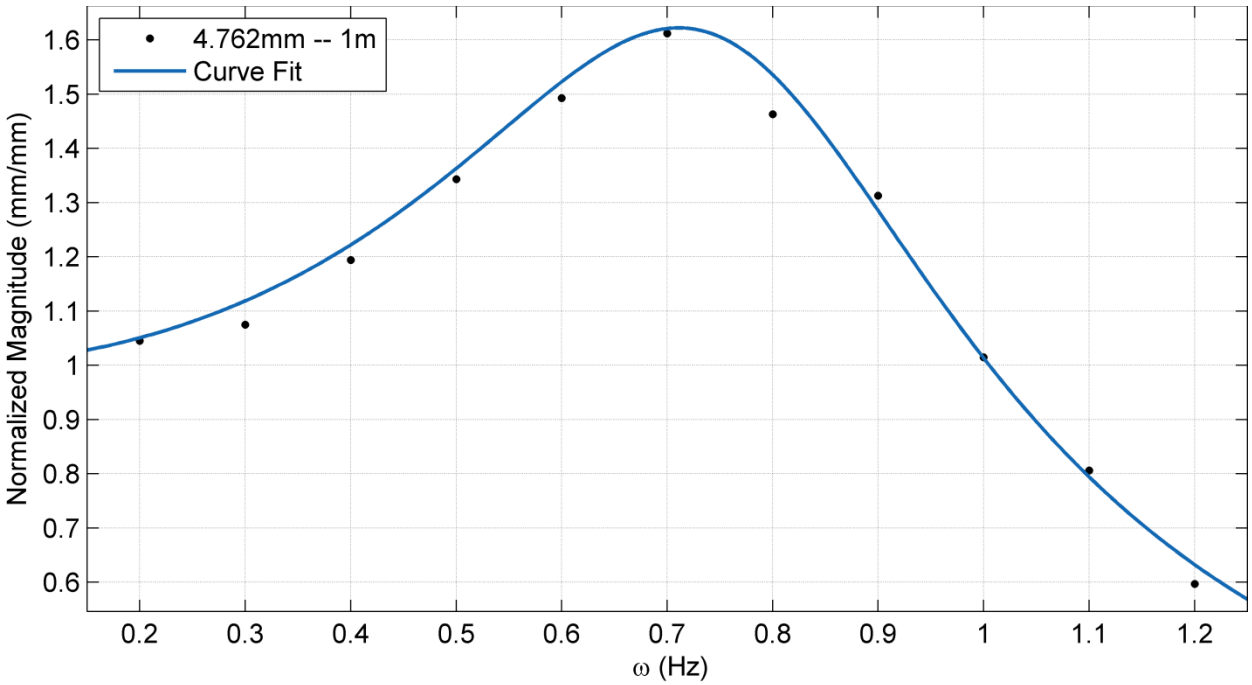

Figure 46: Trial for 4.762 mm with 100 cm in fluid length

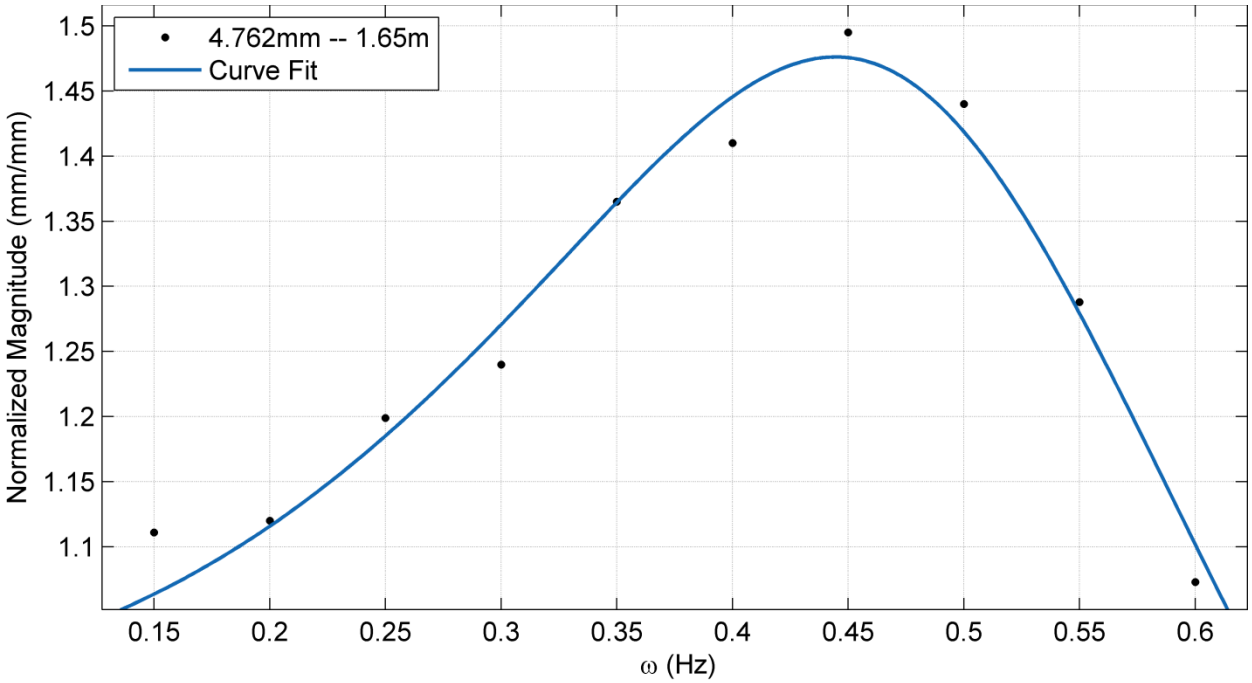

Figure 47: Trial for 4.762 mm with 165 cm in fluid length

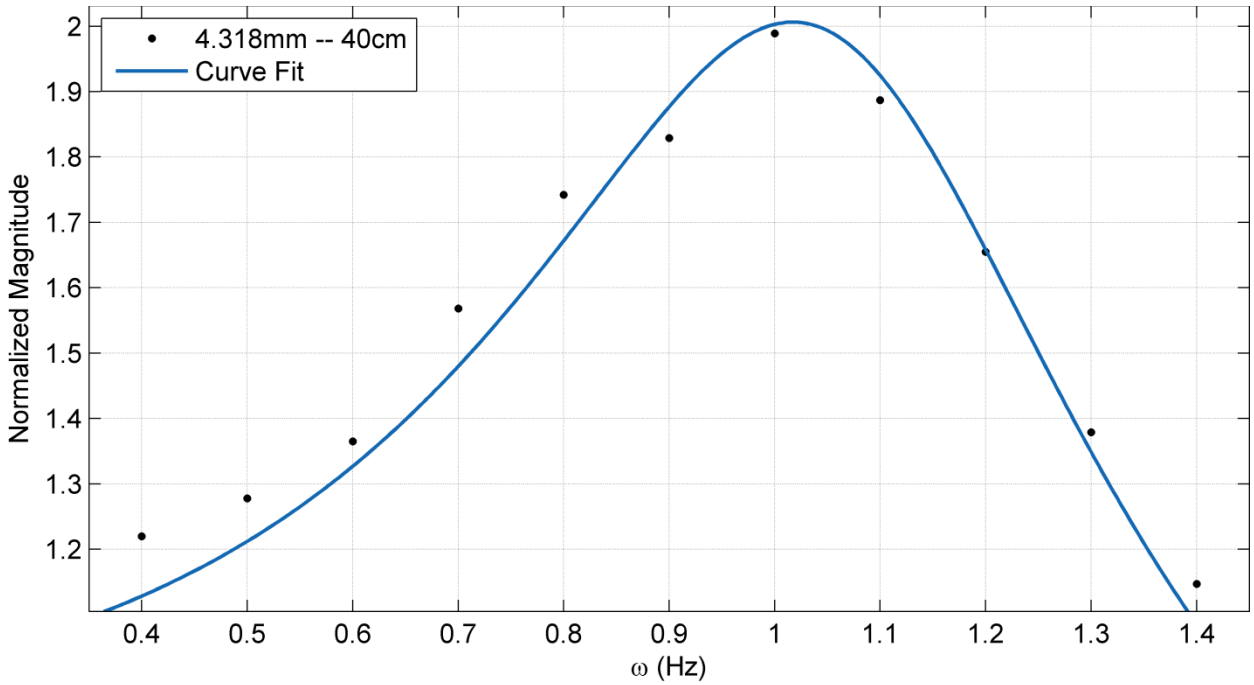

Figure 48: Trial for 4.318 mm with 40 cm in fluid length

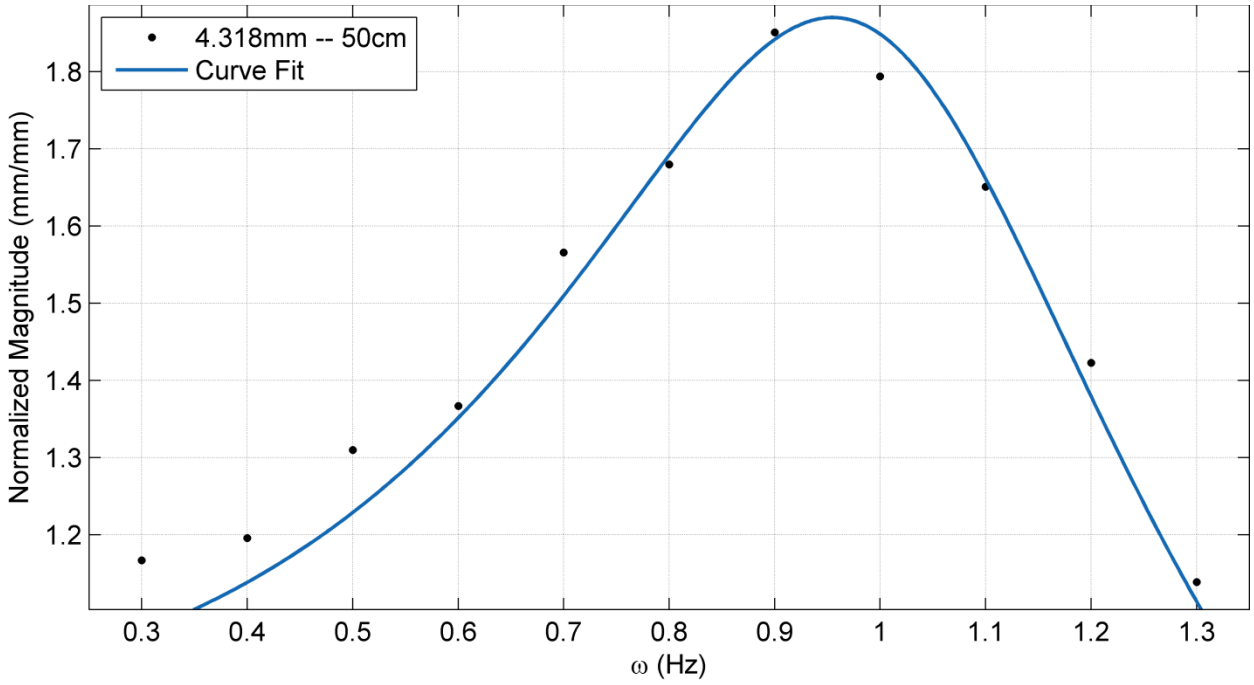

Figure 49: Trial for 4.318 mm with 50 cm in fluid length

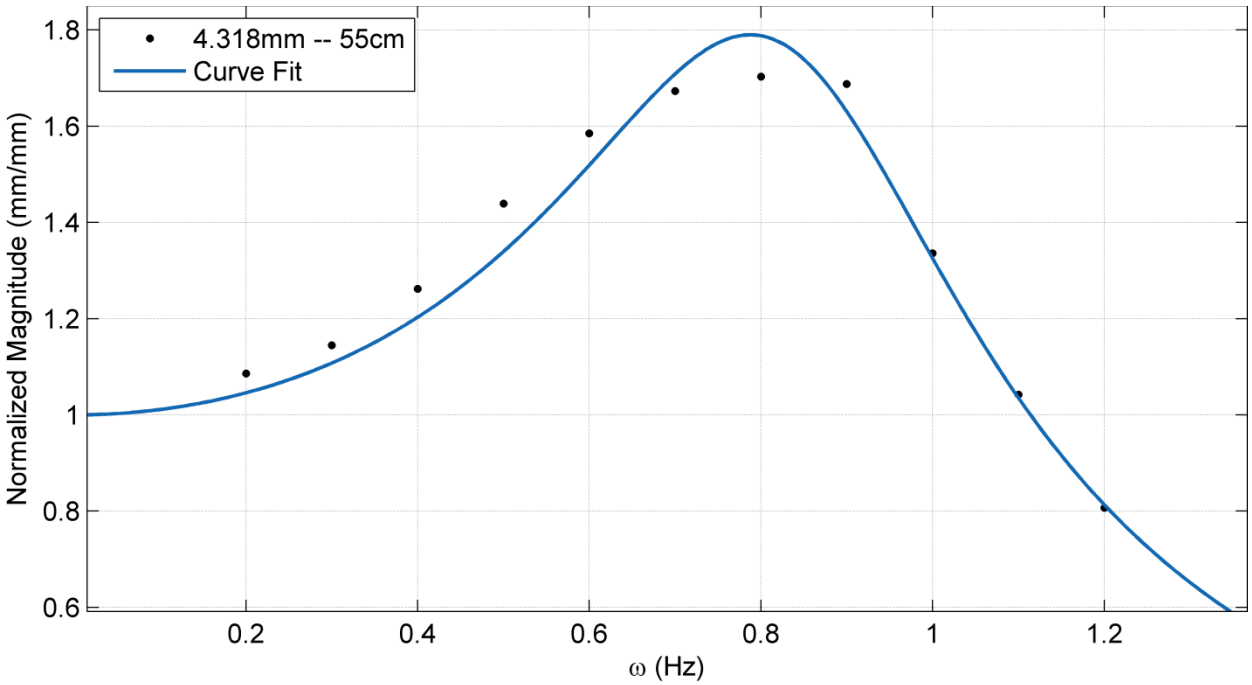

Figure 50: Trial for 4.318 mm with 55 cm in fluid length

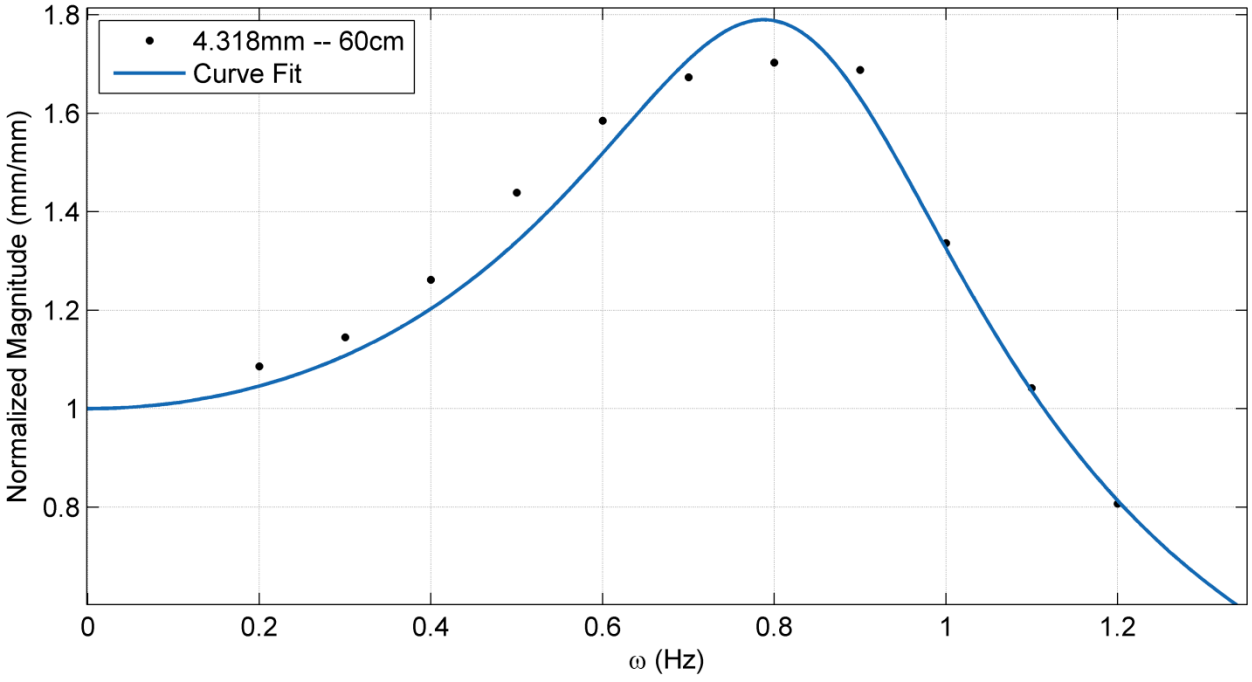

Figure 51: Trial for 4.318 mm with 60 cm in fluid length

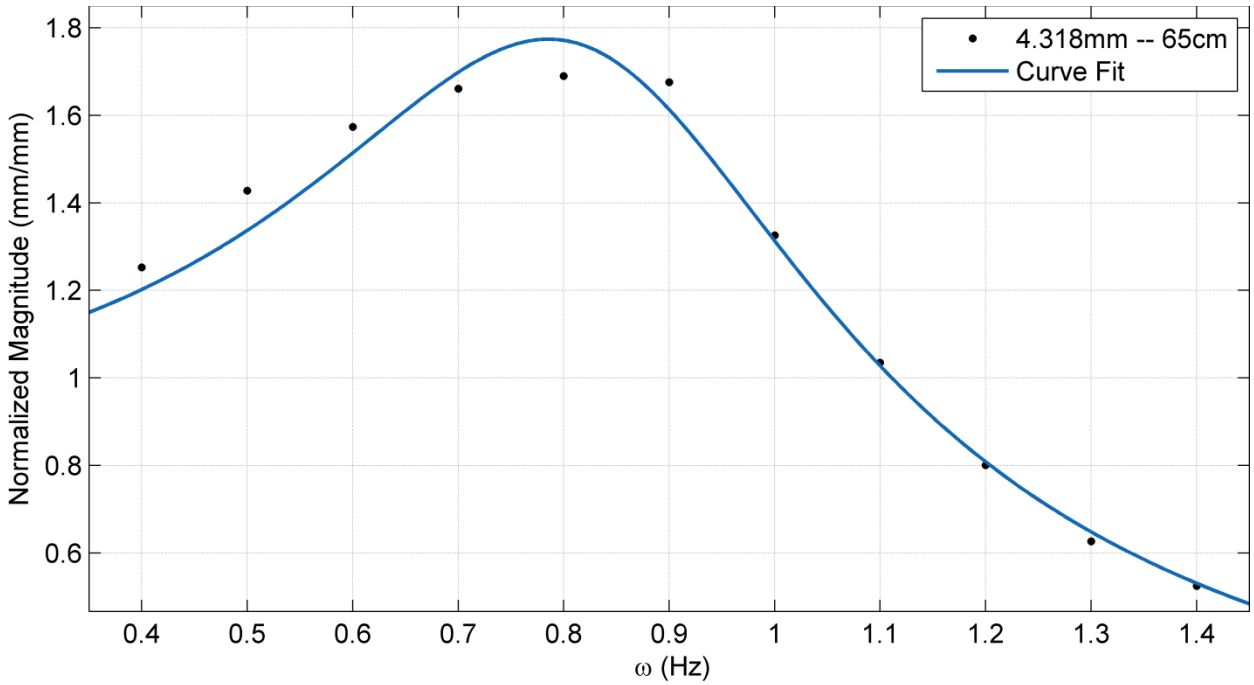

Figure 52: Trial for 4.318 mm with 65 cm in fluid length

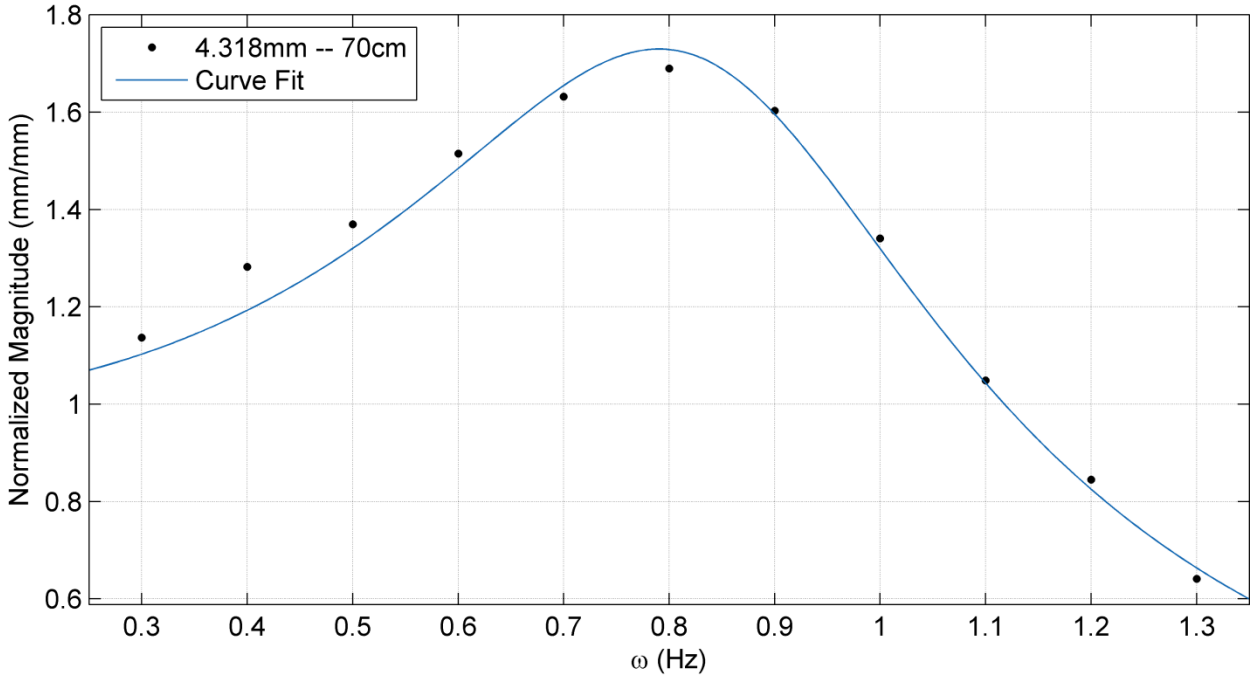

Figure 53: Trial for 4.318 mm with 70 cm in fluid length

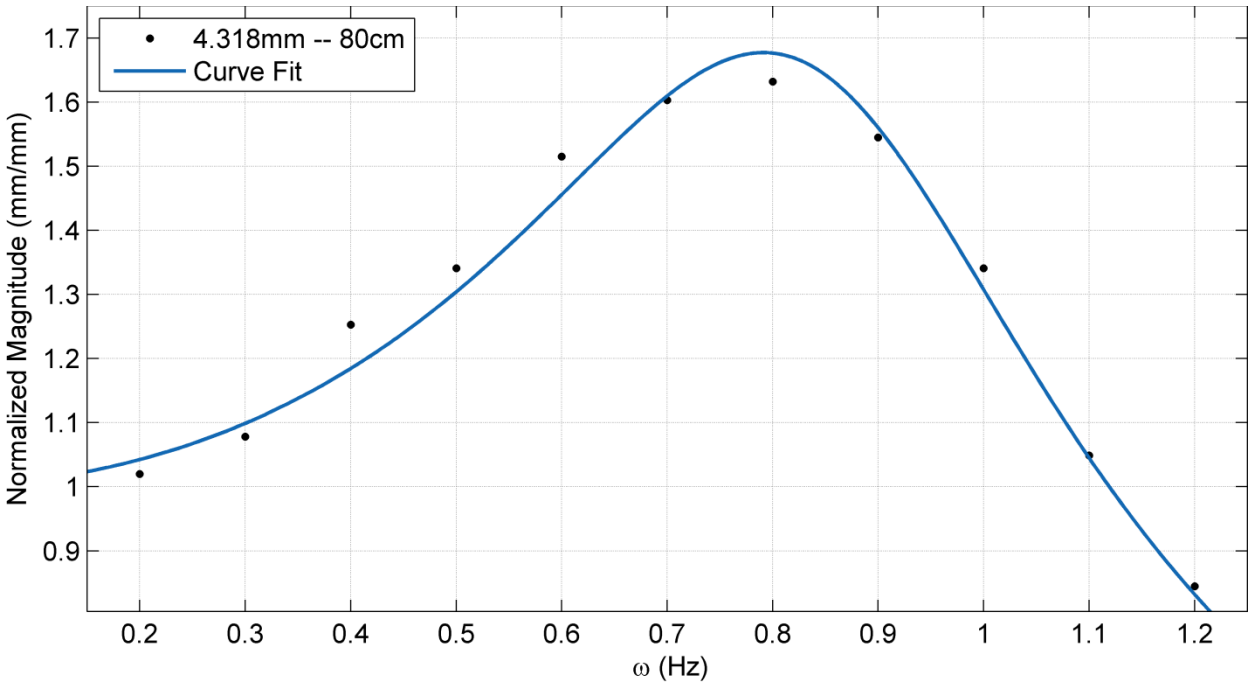

Figure 54: Trial for 4.318 mm with 80 cm in fluid length

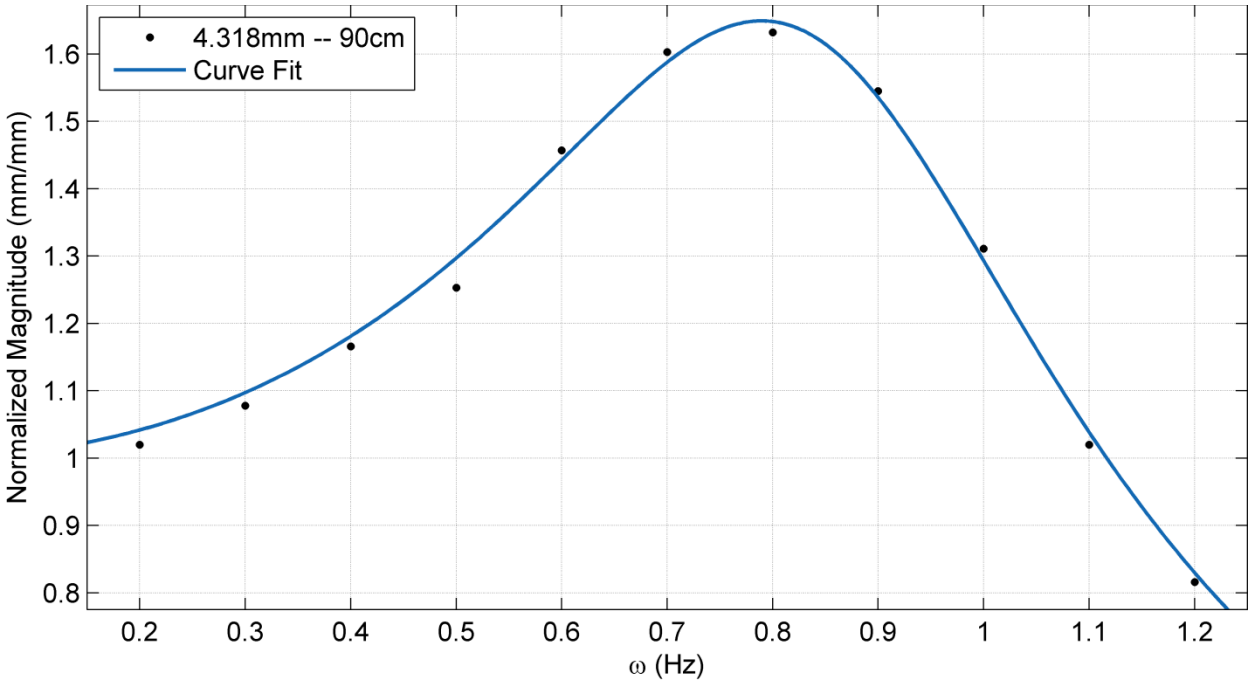

Figure 55: Trial for 4.318 mm with 90 cm in fluid length

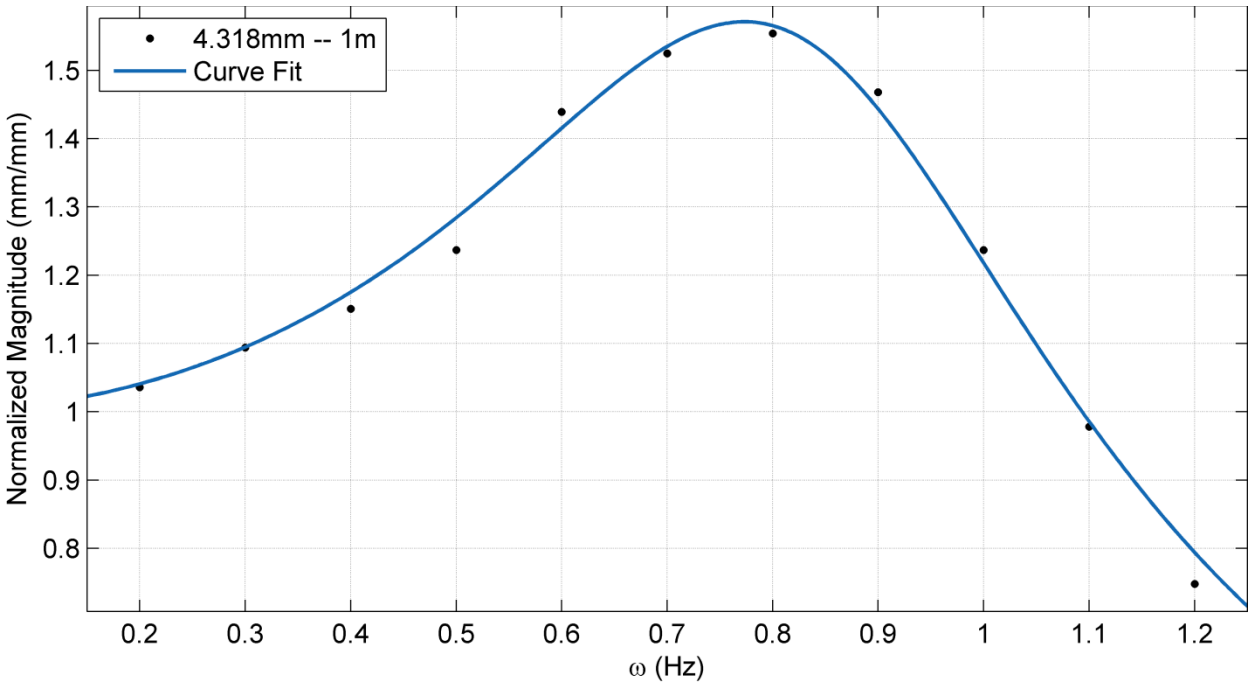

Figure 56: Trial for 4.318 mm with 100 cm in fluid length

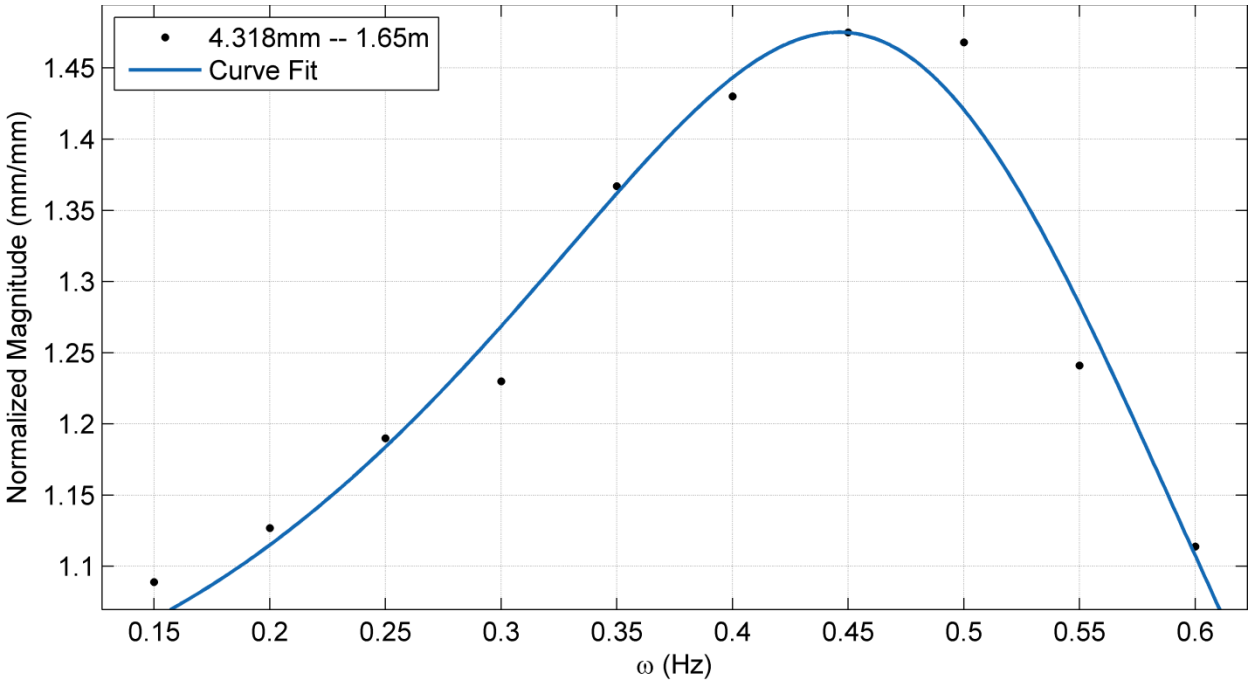

Figure 57: Trial for 4.318 mm with 165 cm in fluid length

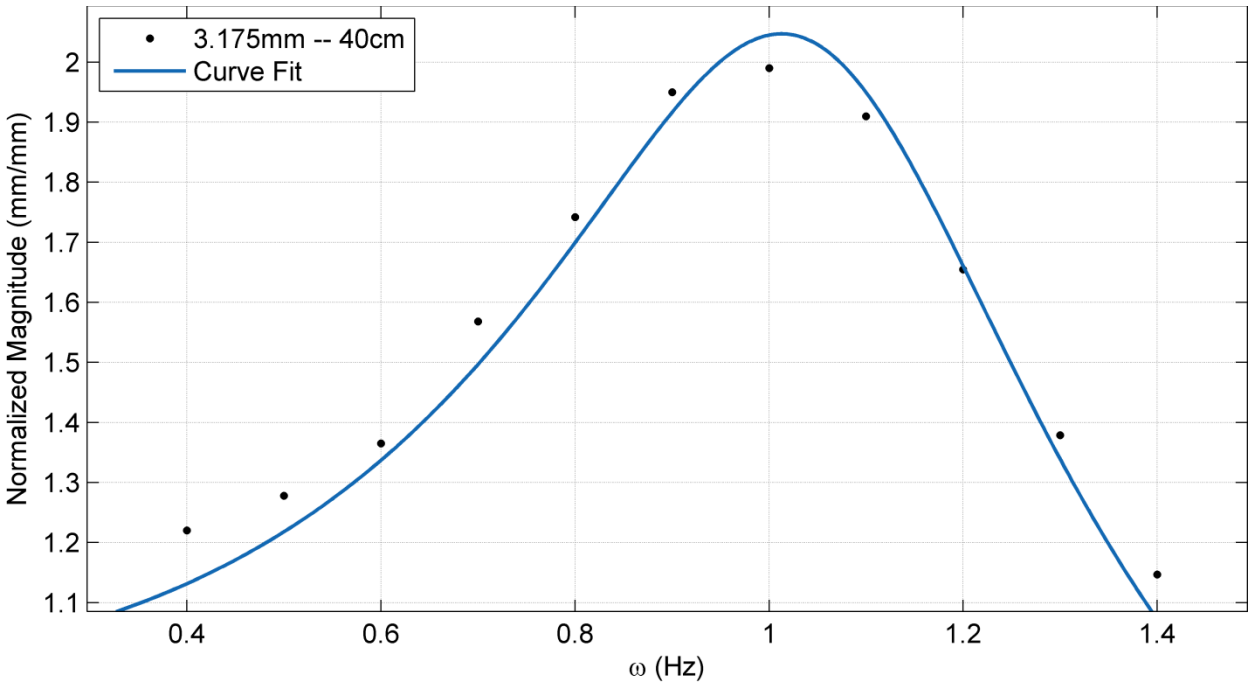

Figure 58: Trial for 3.175 mm with 40 cm in fluid length

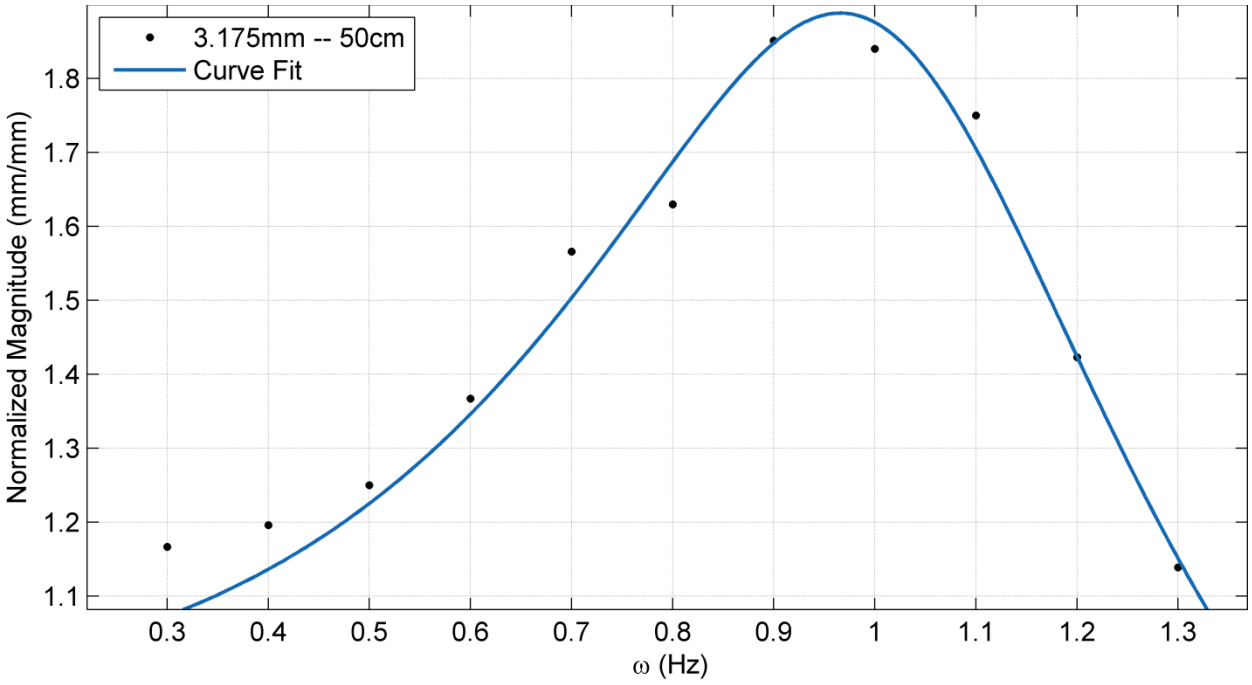

Figure 59: Trial for 3.175 mm with 50 cm in fluid length

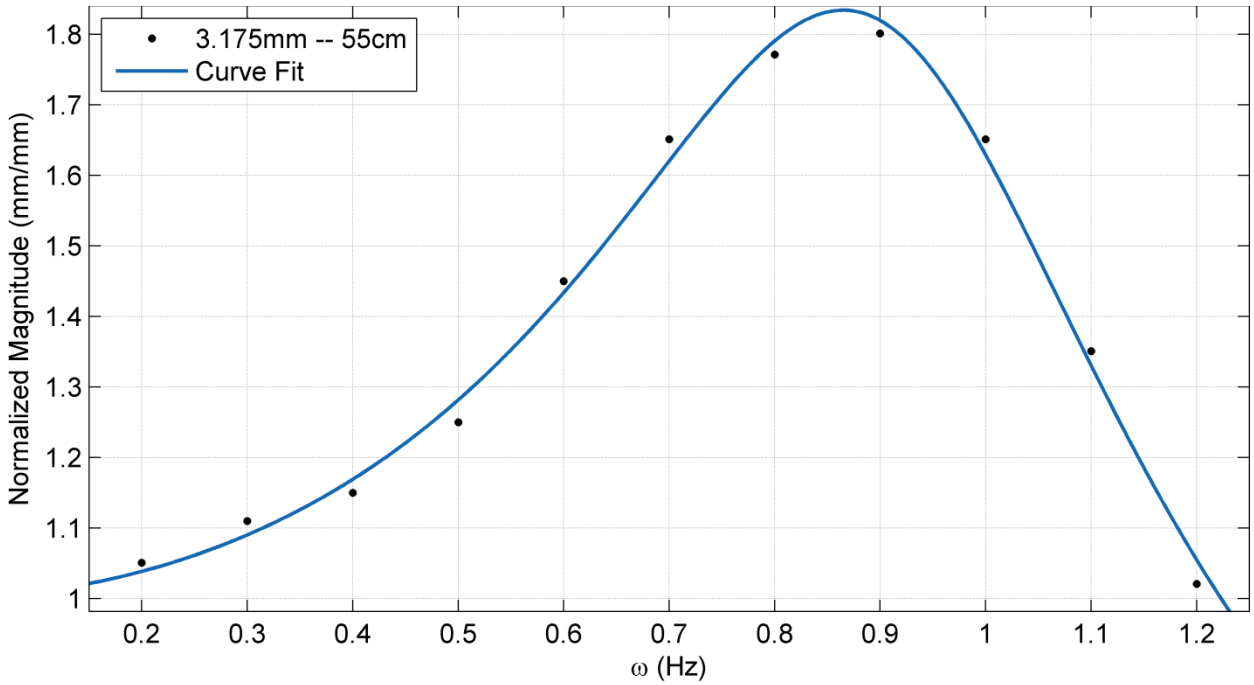

Figure 60: Trial for 3.175 mm with 55 cm in fluid length

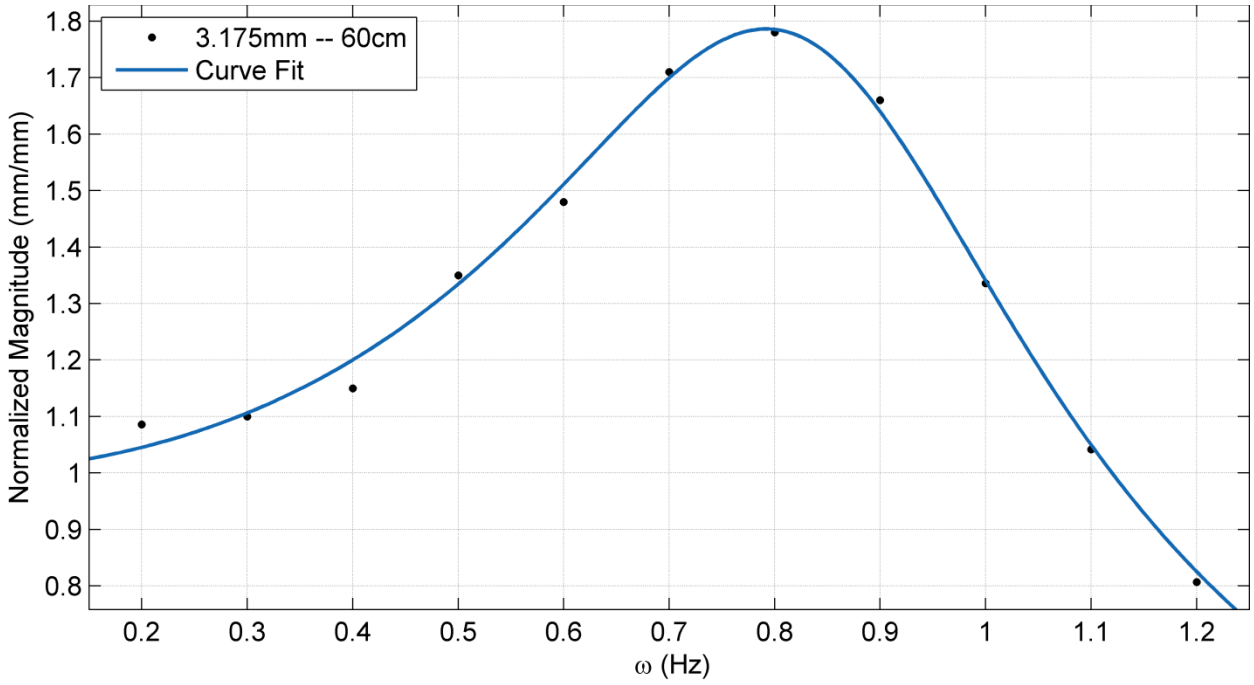

Figure 61: Trial for 3.175 mm with 60 cm in fluid length

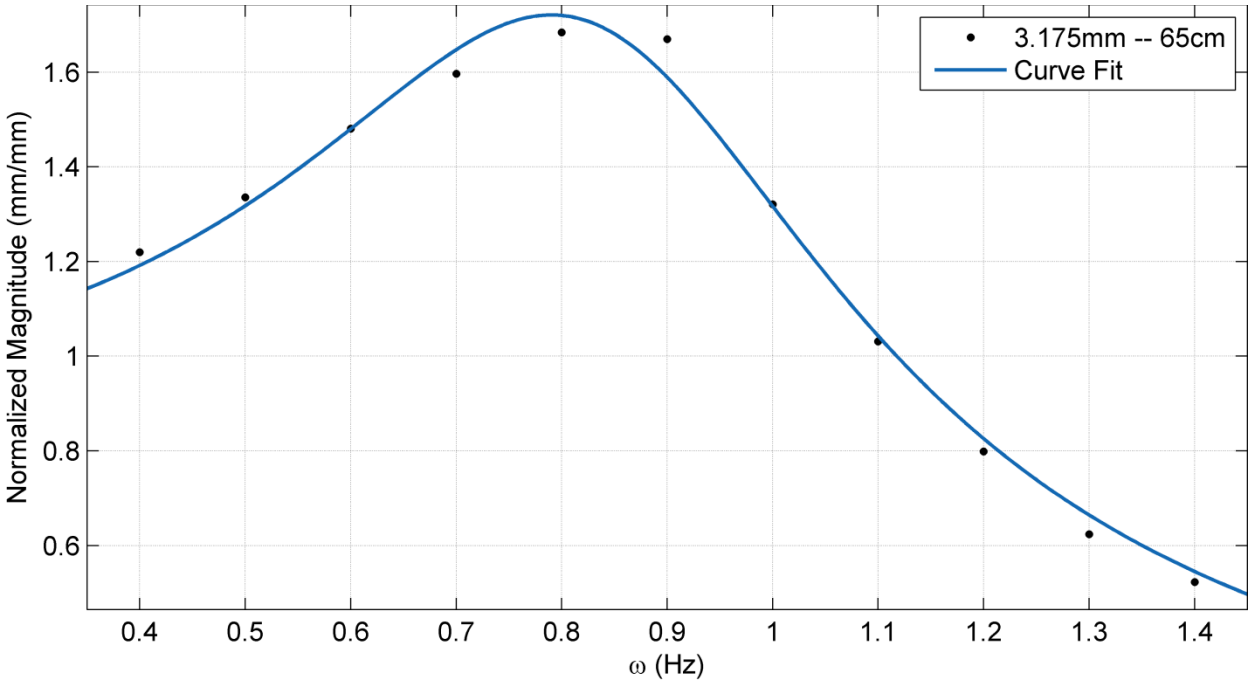

Figure 62: Trial for 3.175 mm with 65 cm in fluid length

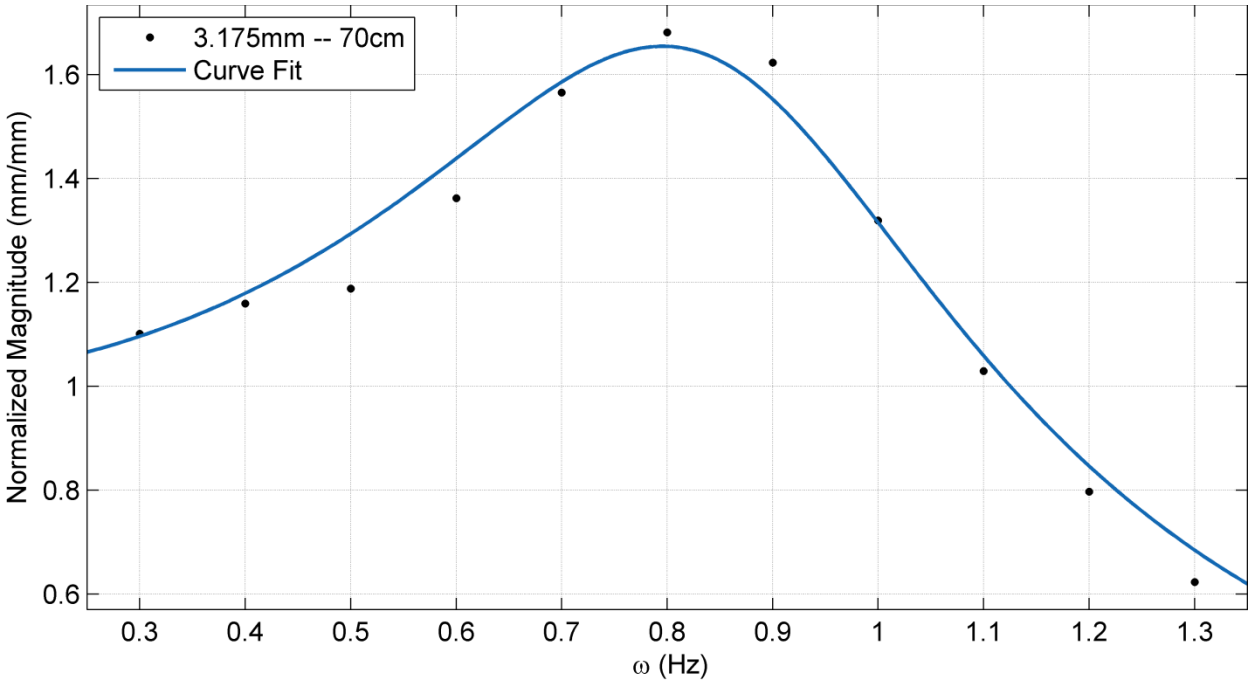

Figure 63: Trial for 3.175 mm with 70 cm in fluid length

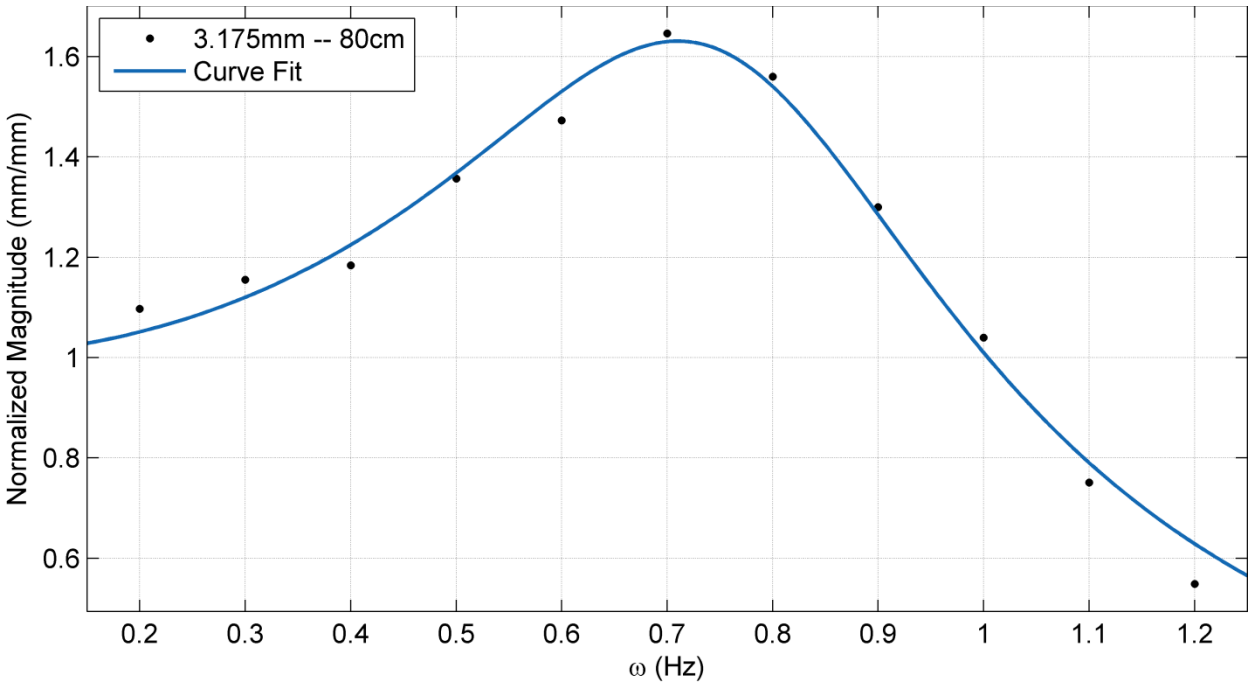

Figure 64: Trial for 3.175 mm with 80 cm in fluid length

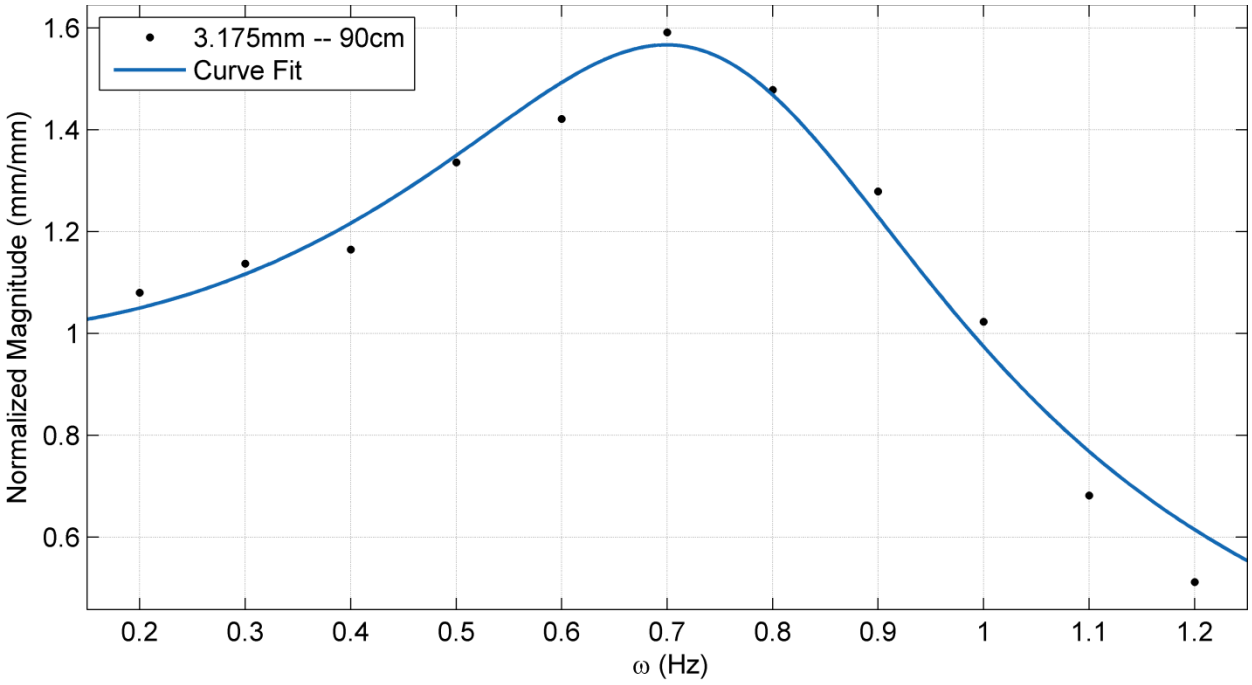

Figure 65: Trial for 3.175 mm with 90 cm in fluid length

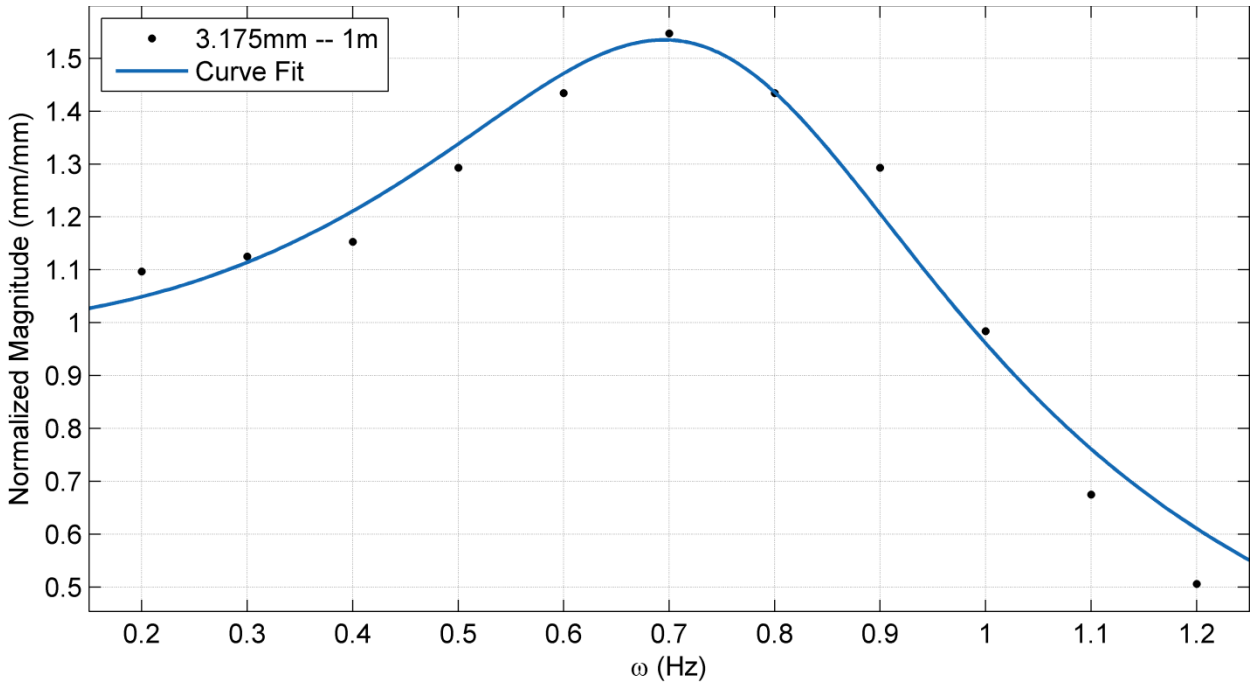

Figure 66: Trial for 3.175 mm with 100 cm in fluid length

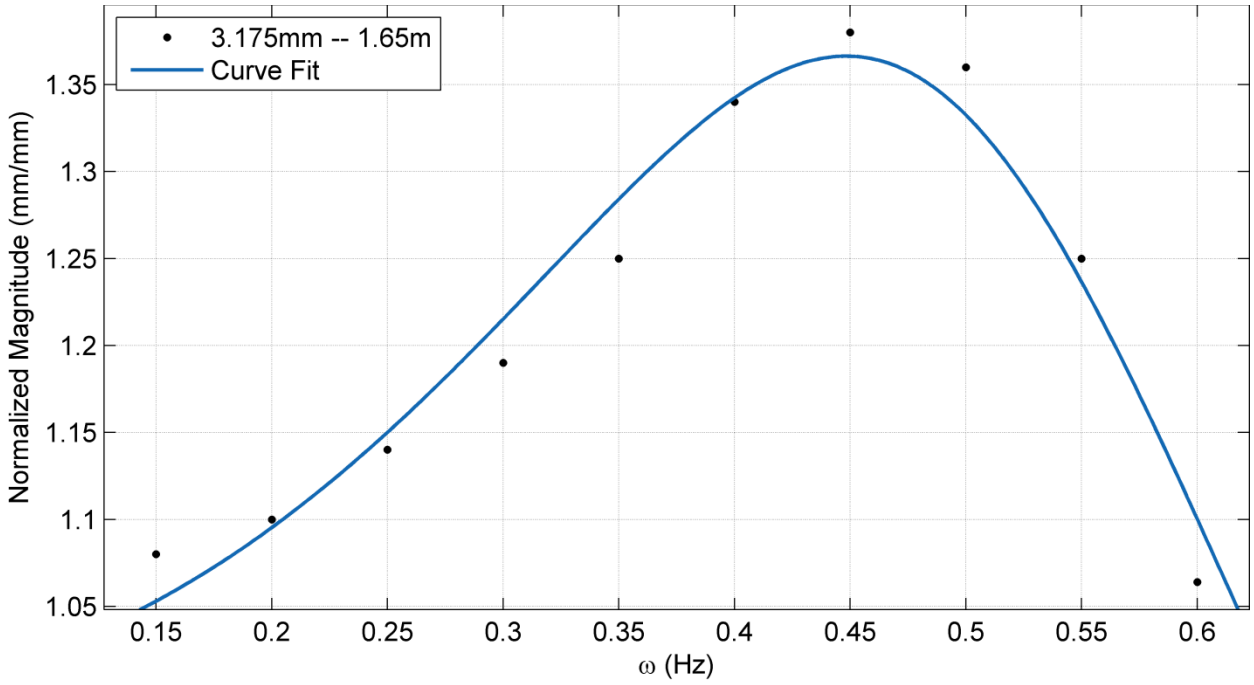

Figure 67: Trial for 3.175 mm with 165 cm in fluid length

Table 9: Summary of $\boldsymbol{\zeta}$ and $\boldsymbol{\omega_n}$ for $\boldsymbol{D} = 9.525$ mm

Tube Size (mm)			**9.525**		
Number of Samples	L (cm)	ζ	Uncertainty of ζ (%)	ω_n (Hz)	Uncertainty of ω_n (%)
3	40	0.276	2.50	1.08	0.44
3	45	0.284	2.47	1.08	0.37
3	50	0.288	2.38	0.976	0.31
3	55	0.290	2.25	0.960	0.27
3	60	0.291	2.20	0.867	0.24
3	70	0.294	1.85	0.866	0.19
3	80	0.297	1.45	0.862	0.15
3	90	0.304	1.38	0.784	0.13
3	100	0.313	1.21	0.731	0.11
3	110	0.318	1.11	0.728	0.10
3	200	0.335	0.71	0.480	0.04

Table 10: Summary of $\boldsymbol{\zeta}$ and $\boldsymbol{\omega_n}$ for $\boldsymbol{D}$ = 6.350 mm

Tube Size (mm)			**6.350**		
Number of Samples	L (cm)	ζ	Uncertainty of ζ (%)	ω_n (Hz)	Uncertainty of ω_n (%)
3	40	0.265	1.53	1.09	0.42
3	50	0.282	1.53	1.04	0.41
3	55	0.284	1.44	0.939	0.38
3	60	0.290	1.43	0.885	0.34
3	70	0.301	1.31	0.878	0.29
3	80	0.308	1.27	0.865	0.25
3	90	0.313	1.17	0.797	0.23
3	100	0.317	0.95	0.736	0.21
3	110	0.319	0.91	0.731	0.20
3	200	0.345	0.85	0.502	0.14

Table 11: Summary of $\boldsymbol{\zeta}$ and $\boldsymbol{\omega_n}$ for $\boldsymbol{D}$ = 4.762 mm

Tube Size (mm)			**4.762**		
Number of Samples	L (cm)	ζ	Uncertainty of ζ (%)	ω_n (Hz)	Uncertainty of ω_n (%)
3	40	0.257	1.25	1.148	0.39
3	45	0.270	1.21	1.043	0.36
3	50	0.281	1.17	0.964	0.33
3	55	0.285	1.16	0.957	0.29
3	60	0.293	1.16	0.899	0.27
3	65	0.299	1.14	0.885	0.25
3	70	0.303	1.10	0.878	0.22
3	80	0.311	0.98	0.875	0.19
3	90	0.319	0.91	0.808	0.17
3	100	0.325	0.83	0.801	0.10
3	165	0.363	0.76	0.518	0.05

Table 12: Summary of $\boldsymbol{\zeta}$ and $\boldsymbol{\omega_n}$ for $\boldsymbol{D}$ = 4.318 mm

Tube Size (mm)			**4.318**		
Number of Samples	L (cm)	ζ	Uncertainty of ζ (%)	ω_n (Hz)	Uncertainty of ω_n (%)
3	40	0.258	1.54	1.092	0.44
3	50	0.278	1.50	1.039	0.31
3	55	0.282	1.47	0.885	0.28
3	60	0.292	1.43	0.883	0.26
3	65	0.295	1.35	0.880	0.21
3	70	0.303	1.35	0.875	0.18
3	80	0.314	1.24	0.865	0.15
3	90	0.320	1.18	0.864	0.13
3	100	0.338	1.11	0.864	0.11
3	165	0.365	1.04	0.520	0.07

Table 13: Summary of $\boldsymbol{\zeta}$ and $\boldsymbol{\omega_n}$ for $\boldsymbol{D}$ = 3.175 mm

Tube Size (mm)			**3.175**		
Number of Samples	L (cm)	ζ	Uncertainty of ζ (%)	ω_n (Hz)	Uncertainty of ω_n (%)
3	40	0.251	1.43	1.084	0.40
3	50	0.275	1.38	1.049	0.33
3	55	0.284	1.31	0.945	0.31
3	60	0.292	1.25	0.891	0.27
3	65	0.305	1.24	0.876	0.25
3	70	0.318	1.19	0.870	0.24
3	80	0.324	1.10	0.799	0.19
3	90	0.341	0.98	0.798	0.13
3	100	0.347	0.83	0.797	0.11
3	165	0.401	0.76	0.543	0.05

BIBLIOGRAPHY

[1] Incropera, Frank P., and Frank P. Incropera. "Thermophysical Properties of Matter." *Fundamentals of Heat and Mass Transfer*. Hoboken, NJ: John Wiley, 2007. 949-50. Print.

[2] Kimber, Mark, et al. "Quantification of piezoelectric fan flow rate performance and experimental identification of installation effects." *Thermal and Thermomechanical Phenomena in Electronic Systems, 2008. ITHERM 2008. 11th Intersociety Conference on*. IEEE, 2008.

[3] Kimber, Mark, and Suresh V. Garimella. "Measurement and prediction of the cooling characteristics of a generalized vibrating piezoelectric fan."*International Journal of Heat and Mass Transfer* 52.19 (2009): 4470-4478.

[4] Kimber, Mark, et al. "Pressure and flow rate performance of piezoelectric fans."*Components and Packaging Technologies, IEEE Transactions on* 32.4 (2009): 766-775.

[5] Silva, Luis, and Alfonso Ortega. "Numerical Simulation of Local Heat Transfer and Scaling of a Synthetic Impinging Jet in a Canonical Geometry." *ASME 2011 Pacific Rim Technical Conference and Exhibition on Packaging and Integration of Electronic and Photonic Systems*. American Society of Mechanical Engineers, 2011.

[6] Silva, Luis A., and Alfonso Ortega. "Convective Heat Transfer in an Impinging Synthetic Jet: A Numerical Investigation of a Canonical Geometry." *Journal of Heat Transfer* 135.8 (2013): 082201.

[7] Go, David B., et al. "Ionic winds for locally enhanced cooling." *Journal of Applied Physics* 102.5 (2007): 053302.

[8] Go, David B., et al. "Enhancement of external forced convection by ionic wind."*International Journal of Heat and Mass Transfer* 51.25 (2008): 6047-6053.

[9] Eastman, Andrew S. *Heat Transfer and Flow Analysis of a Novel Low Flow Piezoelectric Air Pump*. Diss. University of Pittsburgh, 2013.

[10] Womersley, John R. "Method for the calculation of velocity, rate of flow and viscous drag in arteries when the pressure gradient is known." *The Journal of physiology* 127.3 (1955): 553-563.

[11] Loudon, Catherine, and Antoinette Tordesillas. "The use of the dimensionless Womersley number to characterize the unsteady nature of internal flow."*Journal of theoretical biology* 191.1 (1998): 63-78.

[12] Ogawa, Akira, et al. "Damped oscillation of liquid column in vertical U-tube for Newtonian and non-Newtonian liquids." *Journal of Thermal Science* 16.4 (2007): 289-300.

[13] Zahariea, D. "Dynamic response of the U-tube liquid manometer with equal diameter columns." *IOP Conference Series: Earth and Environmental Science*. Vol. 12. No. 1. IOP Publishing, 2010.

[14] Biery, John C. "The oscillating manometer: A review of experimental, theoretical, and computational results." *AIChE Journal* 15.4 (1969): 631-634.

[15] Biery, John C. "Numerical and experimental study of damped oscillating manometers: I. Newtonian fluids." *AIChE Journal* 9.5 (1963): 606-614.

[16] Chan, K. W., and M. H. I. Baird. "Wall friction in oscillating liquid columns."*Chemical Engineering Science* 29.10 (1974): 2093-2099.

[17] Ury, J. F. "Viscous damping in oscillating liquid columns, its magnitude and limits." *International Journal of Mechanical Sciences* 4.5 (1962): 349-369.

[18] Rao, Singiresu S. Mechanical Vibrations. Upper Saddle River, NJ: Prentice Hall, 2011. Print.

[19] McCabe, Warren Lee, Julian Cleveland Smith, and Peter Harriott. Unit operations of chemical engineering. Vol. 5. New York: McGraw-Hill, 2004.

[20] Bird, R. B., W. E. Stewart, and E. N. Lightfoot "Transport Phenomena" 1st Ed., John Wiley, New York (1960).

[21] Eastman, Andrew, Jacob Kiefer, and Mark Kimber. "Thrust measurements and flow field analysis of a piezoelectrically actuated oscillating cantilever."Experiments in fluids 53.5 (2012): 1533-1543.

[22] Hassan, I., Phutthavong, P., and Abdelgawad, M., 2004, "Microchannel Heat Sinks: An Overview of the State of the Art," Microscale Thermophysical Engineering, 8(3), pp. 183-205.